FINITE ELEMENT ANALYSES OF A WAVE LOADED PILE :

DETERMINISTIC AND PROBABILISTIC

C.L. GRANT

BSc (Mech Eng), Witwatersrand

A dissertation submitted to the Department of Civil Engineering, University of Cape Town, in partial fulfilment of the requirements for the degree of Master of Science in Engineering.

February 1991

ABSTRACT

The problem of pile stick-up, where the pile has been stabbed into the pile guide of the platform to be fixed to the sea-bed and is loaded by the current and waves of the ocean, was recently of concern when the fixation of the first local offshore production platform took place. A previous investigation[13] considered the resonant behaviour of the undriven pile subjected to various predicted sea states and various methods were examined to limit the large displacements anticipated. In the present work, a refined model of the problem is developed using the ABAQUS finite element program.

Of particular interest is the applicability of the probabilistic finite element method (PFEM). It is important to appreciate that a mere deterministic dynamic analysis — however accurate analytically — may be of limited value when applied to structures in the ocean. The response achieved thus will either be unelegantly conservative or very unreliable due to the many uncertain parameters that pervade the field of structural dynamics in the ocean. Traditionally, statistical methods are reverted to with uncertainty analyses, but they seldom have much appeal because of the computational effort involved.

The PFEM was found quite attractive with a formulation where the uncertainty of the drag coefficient and the inertia coefficient were investigated. It was concluded that the uncertainty in these coefficients should be limited to a coefficient of variation of approximately 20% and that the simplified model on which the formulation was based should be refined if acceptable results for the purposes of design were required.

ACKNOWLEDGEMENTS

The kind and constant assistance of my supervisor Dr H.T. Pearce of the Mechanical Engineering Department is greatly appreciated. A word of thanks to everybody who contributed to facilitate my studies, especially the library staff, the computer operators and the Foundation for Research Development, whose financial aid was indispensable. My gratitude is also extended to the people who provided the wizardry to get the document in this form.

DECLARATION

I declare that the work contained in this document is essentially my own work unless specifically acknowledged, and that it has not been presented at another academic institution. Any errors are entirely my fault.

C. Lotz Grant, 22 February 1991

To my mother, who supplied the ten percent inspiration

TABLE OF CONTENTS

NOMENCLATURE

Latin symbols:

$\mathbf{a}$	vector of structure accelerations
a_0	amplitude of ocean wave
$\Delta\mathbf{a}$	second order component of the mean response
$\mathbf{b}$	vector of random variables
b_j	j-th component of the vector of random variables
$\mathbf{C}$	global damping matrix of the structure
C_D	drag coefficient
C_M	inertia coefficient
C_A	added mass coefficient
$\mathbf{d}$	vector of structure displacements
$\Delta\mathbf{d}$	second order component of the mean response
D_O	outside diameter of cylinder
D_I	inside diameter of cylinder
E	modulus of elasticity
$E[\ ]$	expectancy operator
e	length of element
$\mathbf{f}$	global load vector
$\mathbf{f}_e$	element load vector
g	gravitational constant
$\mathbf{I}_x$	identity matrix
I	second moment of area of section
i	iteration counter
$\mathbf{K}$	global stiffness matrix of structure
$\mathbf{k}$	element stiffness matrix
K_c	Keulegan-Carpenter number
k	wave number of wave
ℓ	depth of the sea
$\mathbf{M}$	global mass matrix of structure
$\mathbf{m}$	element mass matrix

N	number of simulations
q	dimension of the random vector
R_e	Reynolds number
s	the sign of a value
T	period of wave
t	time
u	velocity of the free stream
V	relative velocity
v	vector of structure velocities
Δv	second order component of the mean response
y	elevation in the sea from the sea-bed

Greek symbols:

α	parameter for numerical damping
β	Newmark coefficient
χ	ratio of stiffness-proportional damping
γ	Newmark coefficient (to control numerical damping)
λ	wavelength of wave
μ	mean (expectancy) of a value (1^{st} statistical moment)
ν	kinematic viscosity
ρ	mass density
σ	standard deviation (2^{nd} statistical moment)
ω	circular frequency of wave
ξ	ratio of mass-proportional damping

Accents:

$\bar{}$	indicates that a variable is evaluated at the mean value of the independent parameter
$\dot{}$	indicates a derivative with time

Subscripts:

f	pertaining to the fluid
s	pertaining to the structure
x	in the direction parallel to the free stream velocity
c	pertaining to the current
w	pertaining to the wave

Superscripts:

T	transpose of a matrix

GLOSSARY

Cov	co-variance
c.o.v.	coefficient of variation
eqn	equation
MCS	Monte Carlo simulation
PDF	probability density function
PFEM	probabilistic finite element method
ref.	reference
Var	variance
$0\cdot\dot{3}$	0·333...

LIST OF FIGURES

LIST OF TABLES

1. INTRODUCTION

Fixed offshore structures are normally erected in shallow water (the tallest to date being 385 m) and are normally production platforms. The steel template jacket structures are typically made up of tubular steel legs and cross braces and are fixed to the sea-bed with piles. At the bottom of the legs, a pile guide which consists of hollow steel sections is attached by a mudmat. During the pile installation process, the pile is lifted by a crane on a nearby barge and is stabbed into this pile guide. Clearly, there is a limiting sea state in which this operation can be performed. Once the undriven pile is released, the wave and current loading should also not cause structural failure of the pile.

It is the response to this loading of the pile standing unsupported in the pile guide which is the focus of this study. Two aspects will be investigated:

The first concerns the deterministic dynamics of the non-linear pile system, the objectives being to understand the capabilities of the ABAQUS finite element code to model the response. The difficulties include the use of gap elements in a dynamic analysis in the ocean, the non-linear geometry, and the iterative solution procedure required for the drag loading given by the Morison equation. The non-linear response achieved using the gap elements is compared with that without the gap elements.

The second area of interest is that of computing the response of the pile when uncertainties are present in the system. A probabilistic approach becomes essential. The literature contains many different probabilistic analyses for offshore structures, the harsh reality of wave loading in the ocean being what it is. The objective here is to explore the application of the probabilistic finite element method (PFEM) to the structurally linear pile stick-up problem with uncertainty in the drag coefficient and the inertia coefficient.

2. THE PILE STICK-UP PROBLEM

2.1: INTRODUCTION.

In the extreme environmental conditions of the sea, the analysis of the response of even the simplest structure can become fairly complex. Such a structure is the undriven pile: a pipe inserted in the pile guide of the jacket to be fixed onto the sea-bed (See Figure 2.1.1).

Consideration is now given to the loading on the structure, the primary loading being that due to the waves. There is a wealth of literature on the theory and measurement of forces on solid bodies in dynamic fluid fields (a review can be found in ref.[33]) but the mainstay of equations to calculate the lateral force on slender bodies remains Morison's equation:

$$F = \frac{1}{2}\rho_f C_D D_0 |u| u + C_M \rho_f A_0 \dot{u} \qquad (2.1)$$

Essentially, this force has two components: a drag force which is proportional to the square of the water particle velocity, u, and has a constant of proportionality, the drag coefficient (C_D). This force is mainly due to the effects of viscosity in the medium, and there is controversy about the accuracy of the drag force calculated from the Morison equation: it has been shown[7] by Laird that the drag force may be much larger when the natural vibration frequency of the body approaches that of the eddy shedding frequency. Every *et al* [ref.35] undertook tests during the COGNAC pile installation, and report an increase of as much as 250% in the steady drag force. There are, however, substantial gaps in the understanding of the fundamental mechanisms at work[36] and the phenomenon appears to be considered problematic only with very flexible, deep water structures.

The inertia (virtual mass) force is proportional to the horizontal component of acceleration of the water particles. The constant of proportionality in this force is denoted by C_M and the force can be thought of as being composed of two parts[7]. Firstly, there is an added inertia (a force in opposition to the motion of the member) due to the entrained water moving with the structure. The other part is due to the inertia force on a stationary member in an accelerating fluid.

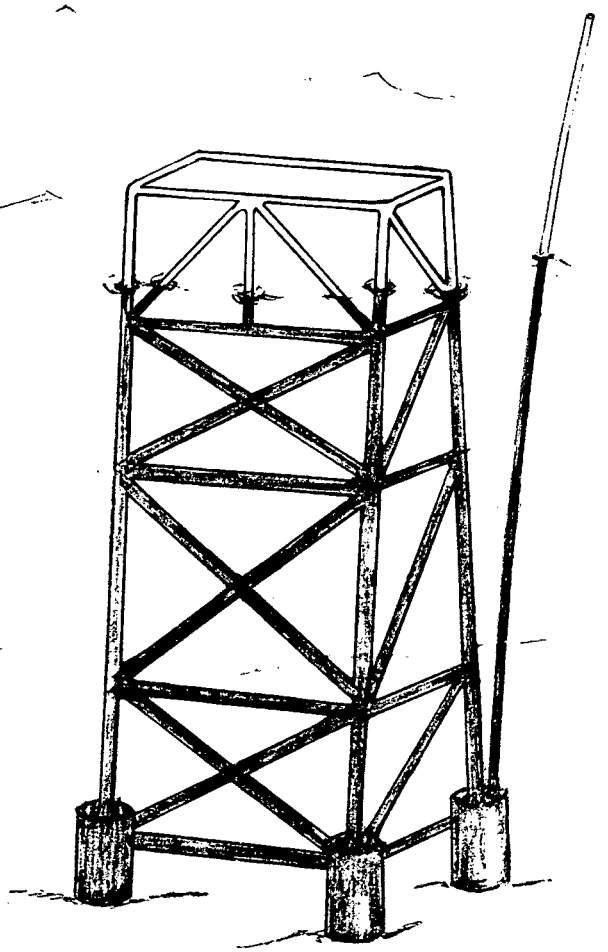

Figure 2.1.1: Sketch showing the pile stabbed into the pile guide of the jacket.

The Morison formula gives drag forces and inertia forces without considering any modification in the shape of the wave or flow field due to the presence of the structure. This assumption is generally made if the ratio of the diameter of the structure to the wavelength of the wave is less than $0{\cdot}2$[7]. When considering a cylinder with such flexibility that its horizontal velocity, v_x, and horizontal acceleration, a_x, are often significantly higher than the corresponding quantities u and $\dot{u}$ for the water [ref.3], Berge and Penzien suggest that eqn (2.1) be modified by replacing u with the velocity of the water particles relative to the structure, $(u - v_x)$, and similarly by

replacing $\dot{u}$ with $(\dot{u} - a_x)$. Assuming that the Froude-Krylov force (per unit length), $C_{M1}\rho_f A_0 \dot{u}$, is independent of the acceleration of the structure[34], the equation is rewritten as:

$$F = \tfrac{1}{2}\rho_f C_D D_0 | u - v_x | (u - v_x) + C_{M1}\rho_f A_0 \dot{u} + C_{M2}\rho_f A_0 (\dot{u} - a_x) \qquad (2.2a)$$

In this way, the explicit effect of the wavelength of the wave on the fluid force coefficients can be shown. The coefficients recommended by Moan *et al* (see ref.[3]) are given by:

$$C_M = C_{M1} + C_{M2} \qquad (2.2b)$$

$$C_{M1} = 1{\cdot}0 - 0{\cdot}12 \frac{\pi D_0}{\lambda} \qquad (2.2c)$$

$$C_{M2} = \begin{cases} 1{\cdot}0 \text{ for } \dfrac{\pi D_0}{\lambda} < 0{\cdot}5 \\ 1{\cdot}54 - 1{\cdot}08 \dfrac{\pi D_0}{\lambda} \text{ for } \dfrac{\pi D_0}{\lambda} > 0{\cdot}5 \end{cases} \qquad (2.2d)$$

Using eqn (2.2*b*), eqn (2.2*a*) is rewritten as:

$$F = \tfrac{1}{2}\rho_f C_D D_0 | u - v_x | (u - v_x) + C_M \rho_f A_0 \dot{u} - (C_M - C_{M1})\rho_f A_0 a_x \qquad (2.3)$$

The values of C_D and C_M to be used in the Morison equation must be chosen mainly on the basis of empirical data. Although there is no shortage of published data for determining the coefficients, serious conflicts and uncertainties regarding the reliability of these methods and associated data exist[27]. The coefficients are functions of three key parameters: the Reynolds number, R_e, serving as a criterion of scale effect on drag; the Keulegan-Carpenter number, K_c, which is a measure of the relative importance of drag and inertia forces; and the ratio of structure diameter to wavelength, which defines limits beyond which Morison's equation is not valid, as discussed earlier.

The available data of C_D and C_M are summarised by Hogben *et al*[27]. Using the particulars of the model (see section 2.3), the suggested value for C_D is 0·6 and that for C_M is 1·5. In these regimes of R_e and K_c, the available data is sparse and errors in calculated wave forces are not really known, but could be between 20% and 50%. Susbielles *et al* measured C_D-values in the range 0·6 - 3·0, and C_M-values in the range 0·8 - 2·1 with their full scale laboratory

model (D_0 = 1 m, ℓ = 20 m) using linear waves, while Reid reported C_D = 0·53 (σ = 0·2) and C_M = 1·47 (σ = 0·36) with tests performed in the Gulf of Mexico. It is evident that these coefficients should be determined using a model and sea conditions appropriate to the problem at hand in order to minimise the error in them. They remain the largest source of uncertainty in the determination of the loading of a structure in the ocean.

The drag term in eqn (2.3) is non-linear and various techniques[7] exist to linearise this equation. It is generally attractive for linear systems and essential for modal analyses. Because the non-linear term contains the drag coefficient (which will be treated as a random variable in Chapter 4), a linearisation of the loading was not considered here lest the effect of this uncertain parameter on the response of the structure is lost in the approximation.

To facilitate the calculation of the free stream velocity and acceleration, a wave theory is necessary. In common use is the linear wave theory (Airy wave theory) which uses a sinusoidal wave of frequency, ω, as model to determine the free stream velocities from the velocity potential function, Φ. The horizontal particle velocity is then given by:

$$u = \frac{\partial \Phi}{\partial x} = \frac{g}{\omega} k a_0 \exp[-i(kx-\omega t)] \frac{\cosh(ky)}{\cosh(k\ell)} \tag{2.4}$$

where k is the wave number;

a_0 is the amplitude of the wave;

ω is the wave frequency;

y is the elevation in the sea from the sea-bed;

ℓ is the depth of the sea.

The popularity of the Airy theory stems partly from the fact that complex waves can be modelled by superimposing several wave trains of differing frequency, amplitude and direction. This is not possible with the non-linear wave theories such as Stokes' third order and fifth order theories, since the 'mode shapes' corresponding to these theories are not orthogonal. Ref.[7] refers to a paper by Hogben and Standing in which a linear and a Stokes' fifth order wave of the same height and period are compared. The main effect of non-linearity is to steepen the waves, the differences becoming less important for deeper water. Their conclusion was that linear theory is adequate except for slender, drag dominated members, and that the error entailed in regarding the immersed length of the structure as constant is larger than the error in using linear rather than a higher order wave theory.

Inherent in the wave motion is the fluctuating buoyancy force in the vertical direction. This effect is ignored in both the analysis with the ABAQUS finite element package (for reasons explained in section 2.3) and the customised linear-geometry program discussed in section 3.2 . For deep water and relatively small waves, this simplification is justified. Also neglected is the possibility of wave slapping, but these horizontal impact forces are more important the nearer the diameter of the member is to the wavelength of the wave.

The gravitational force takes on a new dimension with structures where large horizontal displacements occur. If the member is in a vertical orientation in the undeflected state, the weight of the member will result in an axial force in the member only, but a component of the gravity forces will constitute a distributed load in the lateral direction of the member at large horizontal displacements. These distributed loads will generously contribute to the bending moments and 'additional' displacements of the member.

A careful consideration of the boundary conditions is of vital importance, especially in a dynamic analysis. The way in which a member is restrained plays an important role in the natural frequencies that a structure may possess, and these frequencies may be crucial when the response of the structure to a time dependent load is sought. The bottom end of the pile will penetrate the soil on the sea-bed to a certain extent, and the estimation of this rotational stiffness will call for some expertise. The boundary conditions that the pile guide will impose on the pile can accurately be interpreted as a non-linear spring where the stiffness is zero while the pile is free to flop from one side of the pile guide to the other, becoming infinitely stiff at these extremes when contact is made with the pile guide.

2.2: APPLICABILITY OF THE ABAQUS FINITE ELEMENT PROGRAM.

The model described in the previous section is a fully non-linear one:

1. The drag force calculation (eqn 2.3) involves the velocity of the structure, which is not known yet;
2. The boundary conditions at the pile guide will require the action of a non-linear spring, providing zero stiffness in a small range of deflections from the vertical state, and infinite stiffness at the extremes of this range;
3. The soil conditions may well impose a non-linear boundary condition at the pile end;
4. Large deflections will cause a component of the gravity forces in the lateral direction of the member to develop. Furthermore, they will result in a variation in the stiffness of the member as the displacements change, because the axial and transverse strain components in the cylinder are coupled.

In this section, the applicability of the ABAQUS program (version 4-8) to the pile stick-up problem is investigated. This commercial finite element package has features that make it particularly attractive for non-linear dynamic analyses of a range of beam-type structures used in offshore structures[37].

Elements: The beam-type elements allow both bending and stretching. Special pipe elements (with a hollow circular section) are available if the hoop strains are important due to internal or external pressure forces. The beams using cubic interpolation are based on Euler-Bernoulli beam theory where the transverse shear is ignored, while the linear and quadratic beams use Timoshenko beam theory. When the ratio of section depth to element length becomes smaller, the shear terms dominate the stiffness contribution and could give rise to 'shear locking'[14]. This problem is usually solved by employing reduced integration. All the beam-type elements are written for small strain, large rotation analysis and all changes in length are considered negligible as far as distributed loads are concerned. An exception to this is when a distributed drag force and/or distributed buoyancy force is applied to a linear or quadratic beam element: here, these loads are distributed on the current length of the element.

For very slender structures where the axial stiffness of the member is much higher than the bending stiffness (this critical situation occurs when the

axial stiffness is about five orders of magnitude greater than the bending stiffness[37]), the standard finite element equations become ill-conditioned leading to divergent numerical solutions. McNamara *et al*[45] developed a special hybrid beam element in which the axial force and the strain are interpolated independently of each other, decoupling the bending and axial terms in the finite element equations. A similar approach is adopted in ABAQUS's hybrid elements, for beams where the beam length to cross-section diameter ratio is very large.

To all the beam-type elements, the following distributed loads can be applied:

GRAV : gravity loading in a specified direction;
PX : distributed force per unit length in the global X-direction;
PY : distributed force per unit length in the global Y-direction;
PZ : distributed force per unit length in the global Z-direction;
PB : distributed buoyancy force;
PD : distributed drag force, defined by Morison's equation.

(More will be said later of the PB and PD specifications.)

A flag (NLGEOM) can be set during a stress analysis to account for geometric non-linearity, otherwise one stiffness matrix is used throughout the analysis.

Several spring elements are available to simulate the resistance to rotation of the pile end in the mud. These elements can have either linear or non-linear stiffness ascribed to them.

Gap elements placed between nodes allow for nodes to be in contact (gap closed) or separated (gap open) with respect to particular directions and separation conditions. These elements are ideal to simulate the presence of the pile guide, which limits the degree to which the undriven pile can displace from the vertical.

Morison loads: Central to the offshore capability of the ABAQUS program, is the AQUA subprogram. The PB and PD loading mentioned before is active in this routine and at each point in time, the elements with these loadings prescribed are checked to establish their degree of immersion. To calculate these loadings, the definition of all the parameters in eqn (2.3), excepting the velocity and acceleration of the wave, is specified in this option of the main program. A steady current, whose velocity may vary linearly with elevation, may also be specified. Furthermore, these velocities may be changed as a

function of time.

A major limitation of the applicability of the ABAQUS/AQUA program to offshore problems is its inability to find the eigenvalues of the system. By invoking the *AQUA option, the system matrix becomes unsymmetric and this precludes the extraction of eigenvectors. This fact, together with the absence of a linearised form of the Morison equation, exclude all the modal analysis techniques (for example the response spectrum analyses and random response analyses) present in version 4-8 of the program.

Although greater versatility is lent by the user subroutines, the structure parameters (particularly the velocities) are not passed to these routines, and a linearisation of the drag force is thus not possible.

Wave theories: Two wave theories are supported in the AQUA subprogram: Linear (Airy) wave theory, and Stokes' 5^{th} order wave theory. The latter is usually preferred for deeper water and larger wave applications, but only one wave train is allowed per analysis. For the Airy wave, the wavelength and period of each component are related by[10]:

$$\frac{2\pi}{T^2} = g\,\frac{1}{\lambda}\tanh\frac{2\pi\ell}{\lambda}$$

This relation may be used as an approximation when considering the Stokes' wave. The fluid particle velocities and accelerations needed to calculate the drag and inertia forces are computed from the velocity potential of these theories. The program finds the elevation of the fluid surface and omits the drag and buoyancy loadings for those parts of the structure that are above this surface. Convective acceleration terms are neglected in the Airy theory as part of the linearisation.

Time integration schemes: It is clear from the aforesaid that the integration scheme selected to solve the equilibrium equations will have to be robust. ABAQUS provides three direct integration schemes, of which two can be discarded straight away for this problem: The subspace projection method uses an explicit method projected onto the eigenvectors. As already mentioned, an eigenvalue extraction cannot be performed here. The fully explicit integration scheme is stable on condition that the maximum increment in time is a fraction of the period of oscillation of the highest frequency present in the finite element model. This time can be very small indeed compared to the response time[10]. The remaining scheme is implicit and the non-linear dynamic

equilibrium equations must be solved at each time increment. Like most implicit schemes, it is unconditionally stable for linear systems, and because of the great difficulty to prove this for non-linear equations, it is tacitly assumed. There is, therefore, no limit on the size of the time interval for stability, but the Newton-Raphson method used to iterate the non-linear equations, has a finite radius of convergence beyond which a non-linear solution cannot be found. It is therefore advisable to leave the choice of increment size to the program. The implicit integration scheme is the Newmark method as modified by Hilber, Hughes and Taylor to include the parameter α for introducing numerical damping. An important feature of this integration algorithm is the ability to change the time step size throughout the analysis, certainly vital for a model which contains gap elements.

2.3: DESCRIPTION OF MODELS ON ABAQUS.

Two models of the pile stick-up problem were developed: Model A is an upgraded version of the model by Young[13] which was developed during an investigation of the resonant behaviour of the undriven pile. This problem received attention from a local consulting engineering practice who supplied the details for the problem particular to the installation of piles for the MOSSGAS project. The differences between Model A and that presented in ref.[13] will not be explored here, but they both treat the boundary condition at the pile guide as a pinned joint at the bottom of the pile and a fixation in the horizontal direction at the top of the pile guide. In contrast, Model B utilises the gap elements in the ABAQUS element library to simulate the pile guide, which is essentially the only difference between this model and Model A. The particulars of the pile in question is given in Table 2.3.1.

Length of the pile	145 m
Length of the pile guide	13·5 m
Lack of verticality	0·7°
Depth of the sea	ℓ = 105 m
Outside diameter of the pile	D_0 = 2·134 m
Inside diameter of the pile	D_I = 2·014 m
Density of steel	ρ_s = 7850 kgm^{-3}
Density of sea water	ρ_f = 1025 kgm^{-3}
Centre of mass	≃ 64 m from sea-bed
Modulus of elasticity of steel	E_s = 2·1x10^{11} Nm^{-2}
Wave amplitude	a_0 = 2·83 m
Period of the wave	T = 12·3 secs.
Wavelength of the wave	λ = 234·5 m
Velocity of the current: At mudline	0·35 ms^{-1}
12·0 m elevation	0·35 ms^{-1}
33·5 m elevation	0·50 ms^{-1}
54·0 m elevation	0·50 ms^{-1}
75·9 m elevation	0·70 ms^{-1}
105·0 m elevation	1·00 ms^{-1}
Time history of analysis	200 secs.

Table 2.3.1: The particulars of the pile stick-up problem.

From the discussion on the C_D and C_M values in section 2.1, the following values were decided on:

C_D : 0·53
C_M : 1·47
C_{M1} : 1·00 (from eqn 2.2c)

An Airy wave theory was used throughout the analysis for the calculation of the free stream velocities and accelerations.

Figures 2.3.1 and 2.3.2 show the node numbering and element numbering, respectively, used for the ABAQUS models. Although it is reported[43] that the numbering of nodes should be towards the fixity to ensure that the operations in an equation solver proceed from the more flexible part of a structure toward the stiffer part and thus avoid the possibility of ill-conditioning, different solution algorithms may have different sensitivity to equation sequencing[38]. The example problems[8] supplied by the developers of the ABAQUS program don't adhere to this suggestion.

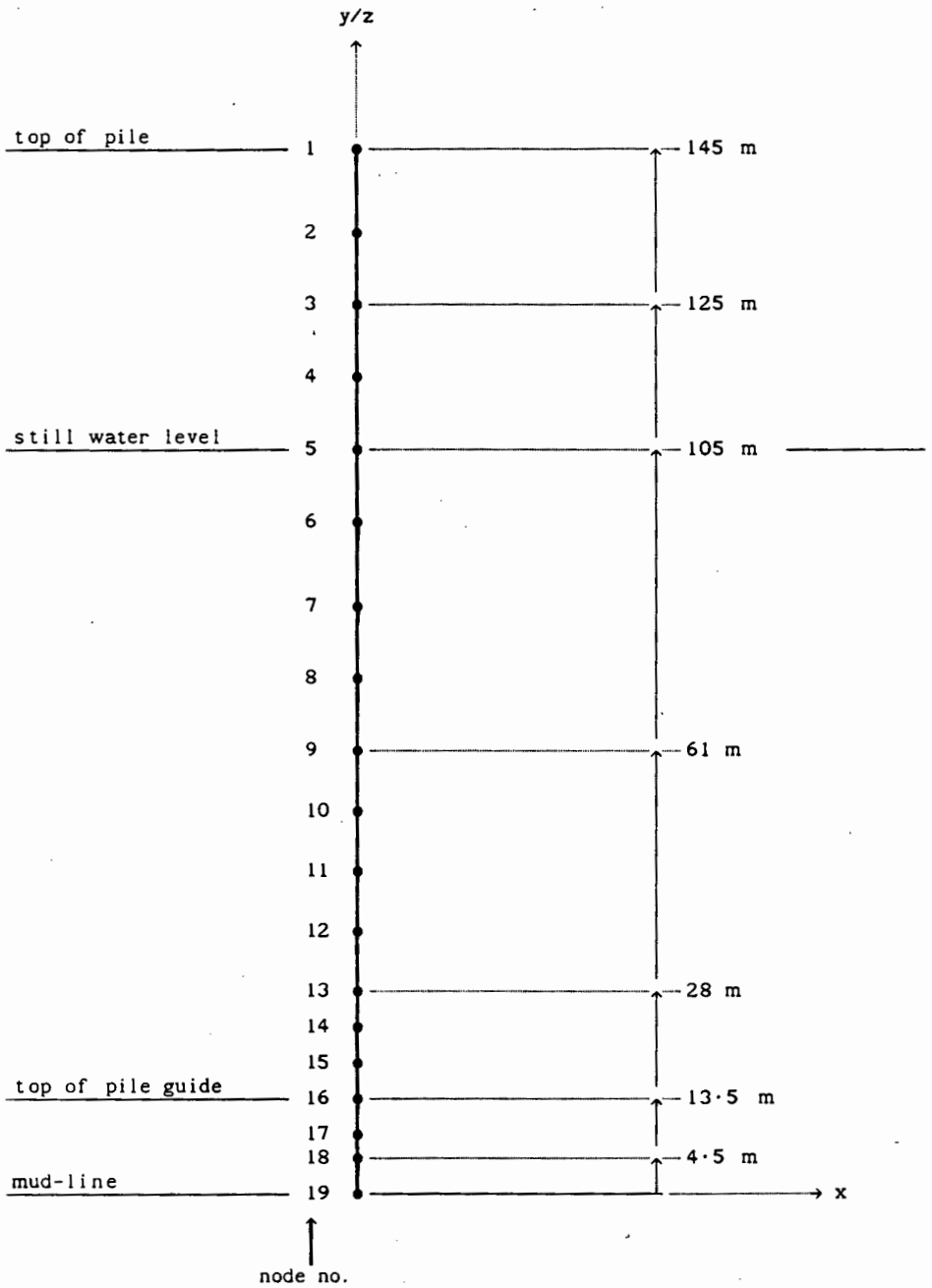

Figure 2.3.1: ABAQUS model of pile showing node numbering.

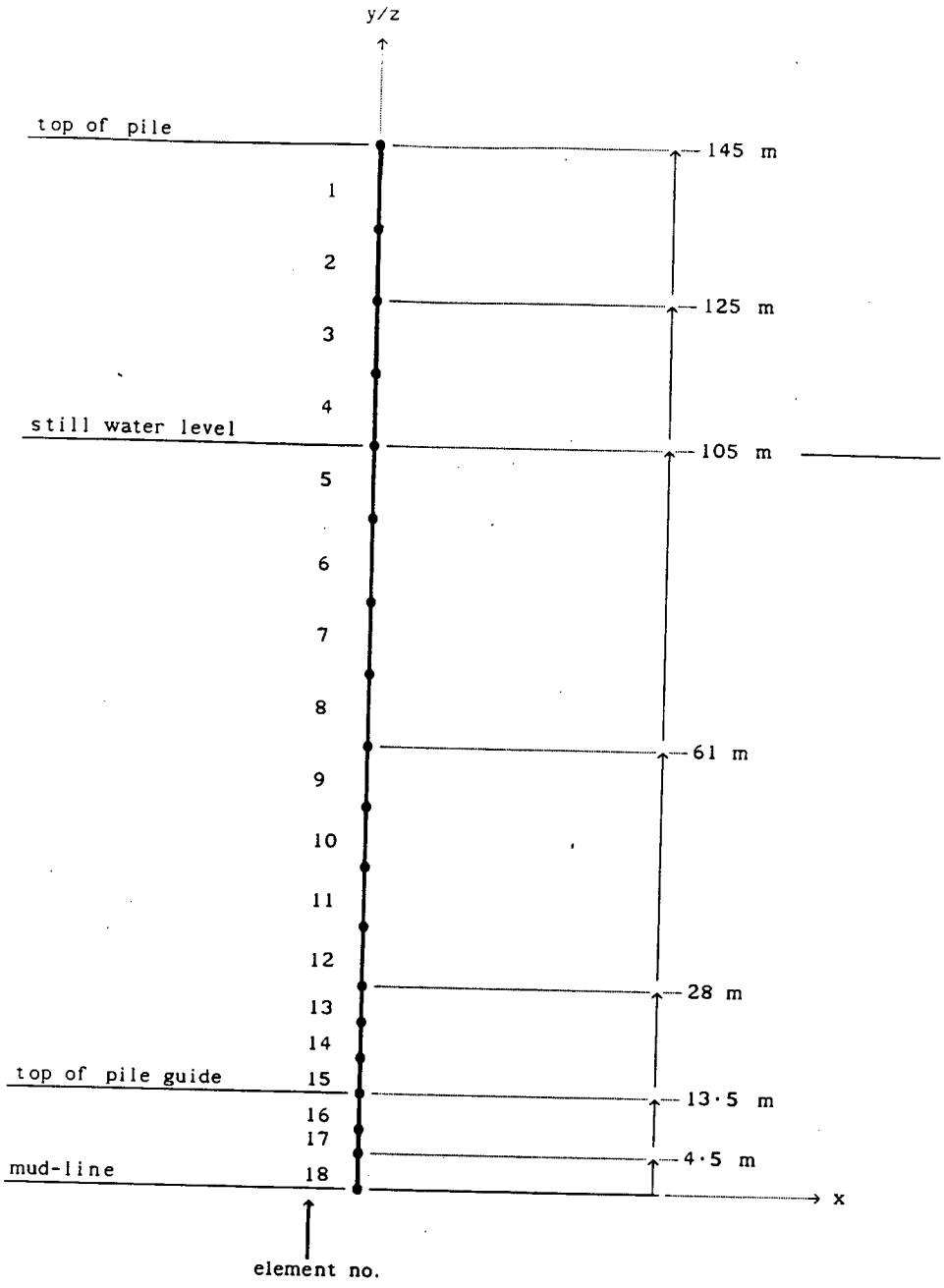

Figure 2.3.2: ABAQUS model of pile showing element numbering.

Cubic interpolation elements, B23 (two dimensional) and B33 (three dimensional), were selected for Models A and B respectively. Although there is little difference in accuracy between these and the lower order elements, the cubic elements were reported to be up to 48% cheaper[14] than the linear elements since version 4-6 of the program. (Ref.[19], using version 4-5, preferred linear elements to higher order elements because of their lower cost

in terms of computational time). Large displacement analyses were used throughout. Using the hybrid versions of these elements resulted in singularities and a successful solution could not be obtained. It is thought that the axial stiffness to bending stiffness ratio is not big enough in this problem to justify the use of the hybrid elements. (Ref.[37] illustrates a problem where the area to second moment of area ratio is 160. For the pile, this ratio is in the region of 1·9). The water inside the pile (it is assumed that during the installation process, water will fill up the pile up to sea level since the pile is open at both ends) was accounted for by adding its mass to the density of the beam elements. The vertical reaction at the bottom of the pile was then corrected by specifying a correcting PY/PZ distributed load to the submerged elements. Included in this is the buoyancy force, which is constant. The PB label on the *DLOAD option activates a buoyancy force on the vertical component of the exposed surface area only, i.e an element in a horizontal attitude (parallel to the surface of the sea) would be buoyed up correctly with the PB label, whilst the same element standing upright would not be buoyed at all. In these models where large displacements were anticipated, it was reasoned that the error in neglecting the additional buoyancy due to the submersion of more of the pile, is smaller than that due to overspecifying the buoyancy for the deflected pile, when there will be an appreciable surface area in the vertical direction. For this reason the PB label was omitted.

Another way of modelling the mass of the water is to add elements with zero stiffness over the submerged nodes. However, computation time was estimated to be over 51% longer.

The gaps at nodes 16 to 18 of Model B were set to 0·165 m corresponding to a lack of verticality of the pile of 0·7 degrees. The choice of a three dimensional model for Model B was made after difficulty arose with the uni-directional gap elements.

The need for spring elements at the bottom of the pile is two-fold. Firstly, the pile represents a mechanism in Model B without them and, secondly, the fixation here is somewhere between fully built-in and pinned. The exact degree of fixation will of course depend on the nature of the soil and the extent to which the pile was stabbed into the sea-bed. The value of 2×10^{8} $Nm.rad^{-1}$ was found to allow the gap at the top of the pile guide to close with the current alone acting and the value was left at that.

The values for the drag coefficient and the inertia coefficient are specified on the PD label on the *DLOAD card. It is noted that with cubic elements, the drag loading will act over the original length of the elements only. The error in this is thought to be minimal.

Probably the most difficult to assign was the value of the HAFTOL parameter on the *DYNAMIC card. Because of the non-linearities (and particularly the gap elements in Model B), a fixed time step increment will be impractical, if found at all. By specifying a value for the HAFTOL parameter, the program adjusts the time increment according to the residual forces at the half-step mark. The smallest value of HAFTOL that was possible for Model A was $5x10^6$, the value for Model B being $1x10^7$. This value for Model A compares favourably with the maximum reaction forces computed: the horizontal reaction at node 16 has a maximum value of $7{\cdot}5x10^6$ and the vertical reaction at the bottom of the pile is approximately $4x10^6$. Thus, it can be concluded that the response given by Model A would be a high accuracy one. As for Model B, the half-step residual value is approximately 2·5 times the largest reaction force. The guide lines in ref.[10] suggest that a value of up to 10 times the expected reaction forces constitutes a high accuracy solution.

2.4: RESULTS.

In this section, the results achieved with Models A and B are given simultaneously. The analyses are performed over a 200 second time history. A table of comparison (Table 2.4.1) appears overleaf.

Figure 2.4.1. gives the horizontal displacements of the top of the pile. The displacement history of Model A clearly reflects the frequency of the wave. In Figure 2.4.2 the vertical displacement of node 5 (at the still water level) is given. It shows that the error in neglecting the buoyancy due to the additional submersion of the pile by these amounts is very small indeed.

The displacement in the gap element at the top of the pile guide (node 16 of Model B) is given in Figure 2.4.3. The maximum is clearly maintained at 0·165 m (approx.). The other two gaps representing the pile guide never closed.

Figure 2.4.4 compares the horizontal forces at the top of the pile guide. The order of magnitude of these forces are not too dissimilar (see Table 2.4.1) in comparison to, for example, the axial stresses calculated by the two models.

Due to the greater freedom in the horizontal movement that node 16 (top of the pile guide) of Model B has, it would be expected that the rotation at the bottom of the pile would therefore be substantially more. This fact is reflected in Figure 2.4.5.

It can be predicted that the maximum axial stresses would occur in that region of the pile immediately above the point of contact with the pile guide. In both Models A and B, this maximum axial stress did occur in element 15, and indeed at the 3^{rd} integration point, the integration point closest to the contact point. The axial stresses at the trailing edge of the pile is shown in Figure 2.4.6.

	Model A	Model B
Halfstep residual (-)	$0{\cdot}5x10^{7}$	$1x10^{7}$
CPU time required (minutes)	245	906
Time history (seconds)	200	200
Axial stresses: (Nmm^{-2})		
element 15, int.pt. 1	-433	-166
element 15, int.pt. 2	-440	-173
element 15, int.pt. 3	-448	-180
element 16, int.pt. 1	-434	-176
element 16, int.pt. 2	-376	-155
Max. hor. reaction: node 16 (N)	$-7{\cdot}46x10^{6}$	$-4{\cdot}54x10^{6}$
Max. rotation at bottom (rad)	$0{\cdot}446x10^{-2}$	$1{\cdot}210x10^{-2}$
Max. hor. displ. of top (m)	10·9	5.2
Max. hor. displ. of node 5 (m)	6·56	3.33
Max. vert. displ. of node 5 (m)	-0·277	-0.063

Table 2.4.1: Comparison of the maximum response variables found by Model A and Model B.

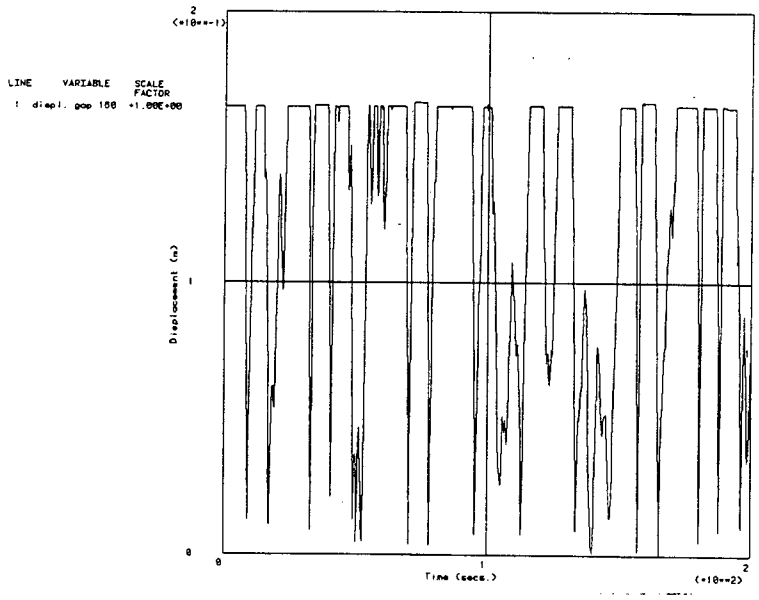

Figure 2.4.3: The gap at the top of the pile guide (Model B)

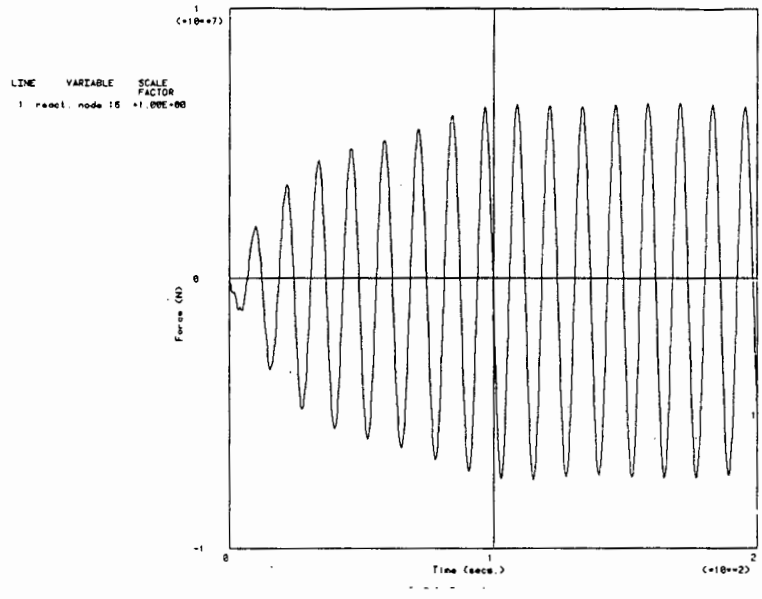

(a)

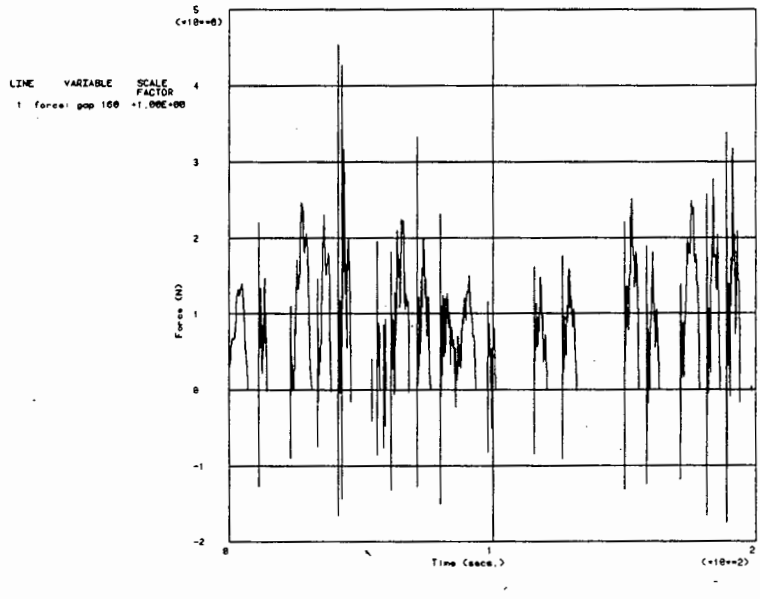

(b)

Figure 2.4.4: Reaction forces at the top of the pile guide.
(a) Results of Model A; (b) Results of Model B.

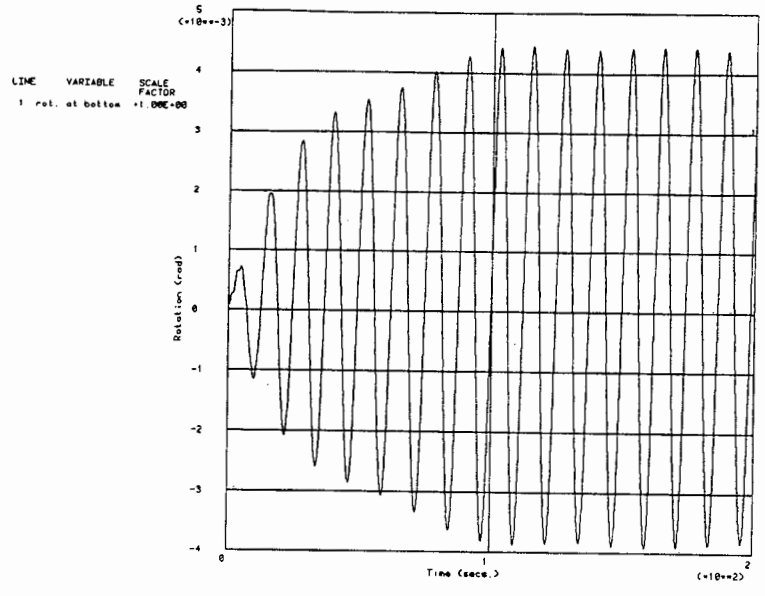

(a)

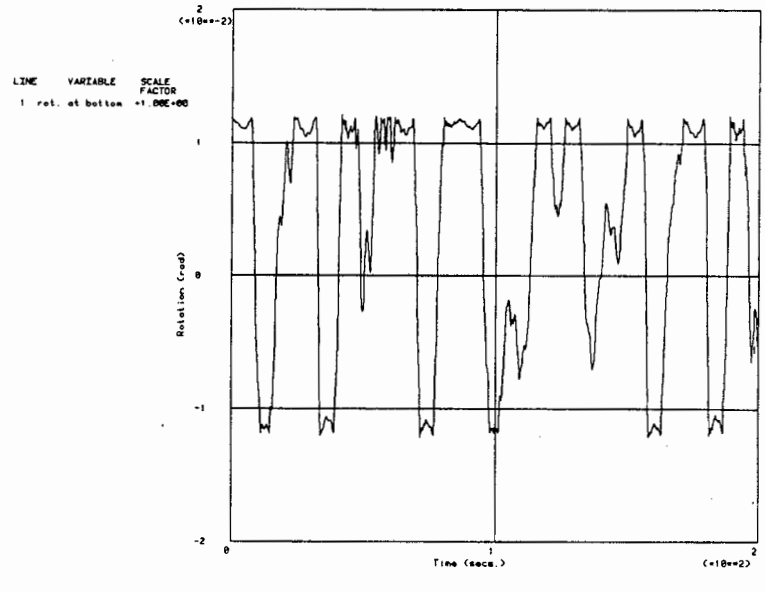

(b)

Figure 2.4.5: Rotations at the bottom of the pile.
(a) Results of Model A; (b) Results of Model B.

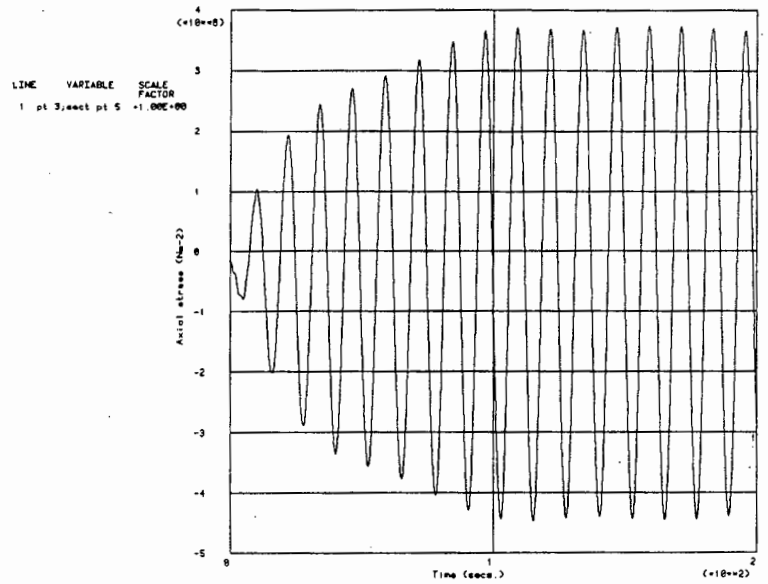

(a)

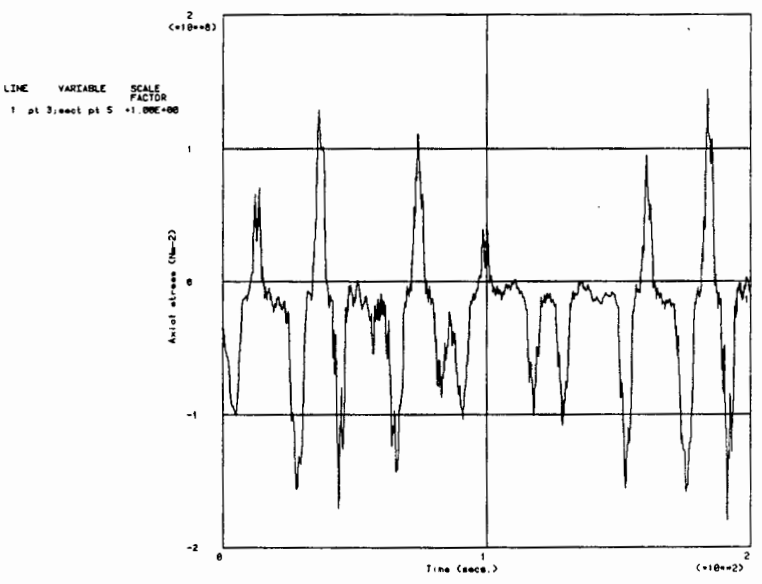

(b)

Figure 2.4.6: Maximum axial stresses in element 15.
(a) Results of Model A; (b) Results of Model B.

2.5: DISCUSSION OF RESULTS.

Probably the most important fact that transpires from the aforementioned analyses is that the time and trouble it takes to develop a more representative model of the pile stick-up problem is well spent. It is difficult to predict the response that will be achieved with Model B beforehand, but that it will not suffer from resonance to the same extent as Model A would, is almost sure. The dominant natural frequency of Model A was estimated from a plot of displacement versus time after the pile was released to vibrate freely from an initial displacement at the top. This mode had a period of 11·56 secs., which is close to that of the wave. (Because an eigenvalue extraction cannot be performed with ABAQUS when the pile is submerged — the system matrix is unsymmetric then — the mass of the entrained water should be added to that of the structure. The result achieved in this way using the *FREQ option of ABAQUS differed by 0·63% from the graphical result mentioned above. The first four natural frequencies of the pile in Model A are tabulated in Table 2.5.1) This mode is clearly the dominant one in the response of Model A. It would appear, from inspection of Figure 2.4.1(b) and Figure 2.4.6(b), that a second mode of vibration is present in the response of Model B: The times at which high axial stresses occur (and a corresponding peak in the force in the gap element appear — see Figure 2.4.4(b)) do not have a particularly large displacement in conjunction.

The large running time of Model B should be placed in perspective here: when Model A was run as a three dimensional problem as well, the required CPU time increased to 396 minutes. It can therefore be stated that the inclusion of gap elements to the problem resulted in a 129% increase in computational effort.

Mode	ω (rads^{-1})	f (s^{-1})	T (secs.)
1	0·5470	0·08705	11·488
2	3·2413	0·51587	1·939
3	8·8950	1·4157	0·7064
4	17·982	2·8620	0·3494

Table 2.5.1: The first four natural frequencies of the pile in Model A.

3. THE GEOMETRICALLY LINEARISED MODEL

3.1: INTRODUCTION.

To explore the impact of the uncertainty of the drag coefficient and the inertia coefficient on the response of the undriven pile, it was necessary to develop a customised finite element program which will serve as a basis for the implementation of the probabilistic finite element method (PFEM) in the next chapter. Such an implementation can not be effected using the ABAQUS program since the velocity of the structure is not available to the user subroutines (see section 2.2). It was decided to keep such a vehicle simple while the applicability of the PFEM to this problem is still unknown. Hence, the program explained in this chapter treats the structure geometry and its material properties as linear. Only the drag force in the loading term in eqn (2.3) remains non-linear. The forces and the corresponding displacements, velocities and accelerations in the x-direction and the y-direction are completely uncoupled.

3.2: DESCRIPTION OF THE PROGRAM PILE.

The program has its roots in the code found in Hinton and Owen[24] which was used by Phaal[19] to model marine riser problems. It is this program (called RISER) that was customised for the application to the pile stick-up problem and is referred to in this work by the name PILE. The routines ASSEMB (to assemble the global system matrices), GREDUC (the Gauss reduction routine) and BAKSUB (to solve the reduced equations by back-substitution) were extracted from ref.[24] virtually unchanged, while NEWMARK (the time integration routine) and the Secant iterative scheme (to solve the non-linear velocity term) were taken verbatim from ref.[19].

The equilibrium equations in the horizontal direction are given by:

$$\mathbf{M}_s\mathbf{a} + \mathbf{C}\mathbf{v} + \mathbf{K}\mathbf{d} = \mathbf{F} \tag{3.1}$$

where $\mathbf{F}$ was derived in Chapter 2:

$$\mathbf{F} = \tfrac{1}{2}\rho_f C_D D_0 \left| u - \mathbf{v}_x \right| (u - \mathbf{v}_x) + C_M \rho_f A_0 \dot{u} \mathbf{I}_x - (C_M - C_{M1}) \rho_f A_0 \mathbf{a}_x \tag{2.3}$$

where $\mathbf{I}_x$ is a matrix containing entries of unity in positions corresponding to a degree of freedom in the x-direction. The last term of eqn (2.3) is included in the appropriate position in the system mass matrix and eqn (3.1) becomes:

$$\mathbf{Ma} + \mathbf{Cv} + \mathbf{Kd} = \mathbf{f} \tag{3.2}$$

$$\text{where } \mathbf{M} = \mathbf{M}_s + (C_M - C_{M1})\rho_f A_0 \mathbf{I}_x \tag{3.3}$$

$$\text{and } \mathbf{f} = \tfrac{1}{2}\rho_f C_D D_0 \left| u - \mathbf{v}_x \right| (u - \mathbf{v}_x) + C_M \rho_f A_0 \dot{u} \mathbf{I}_x \tag{3.4}$$

The mass associated with the structure, $\mathbf{M}_s$, comprises the structural mass and the mass of the water inside the pile. The total mass, **M**, includes the mass of the entrained water. This total mass is evenly distributed along an element and includes rotary inertia at the nodes:

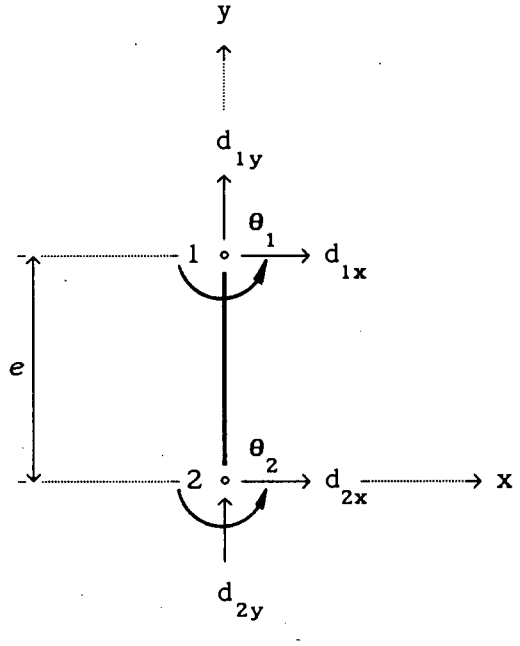

The consistent mass matrix for the element of mass m, using cubic (Hermitian) interpolation, is given in ref.[38] and is recommended when the trapezoidal method is used as direct integration scheme, as lumping the masses underestimates frequencies. With reference to the element shown above, it is given as:

$$
\mathbf{m} = \frac{m}{420}
\begin{array}{c}
\begin{matrix} d_{1x} & d_{1y} & \theta_1 & d_{2x} & d_{2y} & \theta_2 \end{matrix} \\
\begin{bmatrix}
156 & 0 & 22e & 54 & 0 & -13e \\
 & 0 & 0 & 0 & 0 & 0 \\
 & & 4e^2 & 13e & 0 & -3e^2 \\
 & & & 156 & 0 & -22e \\
 & & & & 0 & 0 \\
\text{symmetrical} & & & & & 4e^2
\end{bmatrix}
\begin{matrix} d_{1x} \\ d_{1y} \\ \theta_1 \\ d_{2x} \\ d_{2y} \\ \theta_2 \end{matrix}
\end{array}
$$

The damping matrix, **C**, is popularly constructed as the sum of certain ratios of the mass matrix and stiffness matrix:

$$\mathbf{C} = \xi\mathbf{M} + \chi\mathbf{K} \tag{3.5}$$

The factors ξ and χ are determined from:

$$\xi + \chi\omega_k^2 = 2\omega_k\zeta_k \tag{3.6}$$

where ζ_k is the damping ratio of the k^{th} mode of vibration and ω_k corresponds to the circular frequency of this mode. The first two modes of the vibration (with the lowest frequencies) can be used to find ξ and χ. In the validation of PILE (see section 3.3), no damping was used, and only stiffness proportional damping ($\xi = 0$) was used in Chapter 4, for reasons explained there.

Euler-Bernoulli beam elements with cubic interpolation of the displacements were installed in the program. Because of the assumption of linear geometry, the displacement in the x and y directions of the element shown below is independent of each other:

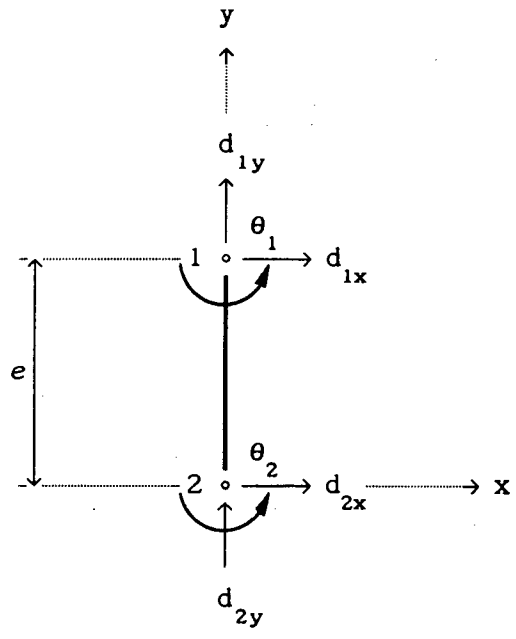

The corresponding element stiffness matrix of the element above is given by:

$$\mathbf{k} = \frac{1}{e}\begin{bmatrix} d_{1x} & d_{1y} & \theta_1 & d_{2x} & d_{2y} & \theta_2 & \\ \frac{12EI}{e^2} & 0 & \frac{6EI}{e} & \frac{-12EI}{e^2} & 0 & \frac{6EI}{e} & d_{1x} \\ & AE & 0 & 0 & -AE & 0 & d_{1y} \\ & & 4EI & \frac{-6EI}{e} & 0 & 2EI & \theta_1 \\ & & & \frac{12EI}{e^2} & 0 & \frac{-6EI}{e} & d_{2x} \\ & & & & AE & 0 & d_{2y} \\ \text{symmetrical} & & & & & 4EI & \theta_2 \end{bmatrix}$$

The force vector, as given by eqn (3.4), constitutes the only non-linearity in the problem. Since this vector involves the drag coefficient and this coefficient is treated as a random variable in Chapter 4, it was decided not to linearise this as well. In order to solve eqn (3.2), the Secant method was used to converge to the appropriate value of $\mathbf{v}_x$. With reference to Figure 3.2.1, this involves making an initial guess at the velocity of the structure, $v_x^{p(1)}$. (For a full explanation of the notation used here, the reader is

referred to Appendix C. Suffice it here to say that the superscripts 'p' refers to a predicted value, 'c' is the corrected value (or the value obtained by solving eqn (3.2) with the predicted value), i refers to the value pertaining to the initial guess, while i+1, i+2,... implicates subsequent values of the iteration; m refers to the slope of a line and k is the v_x^c-intercept of that line.)

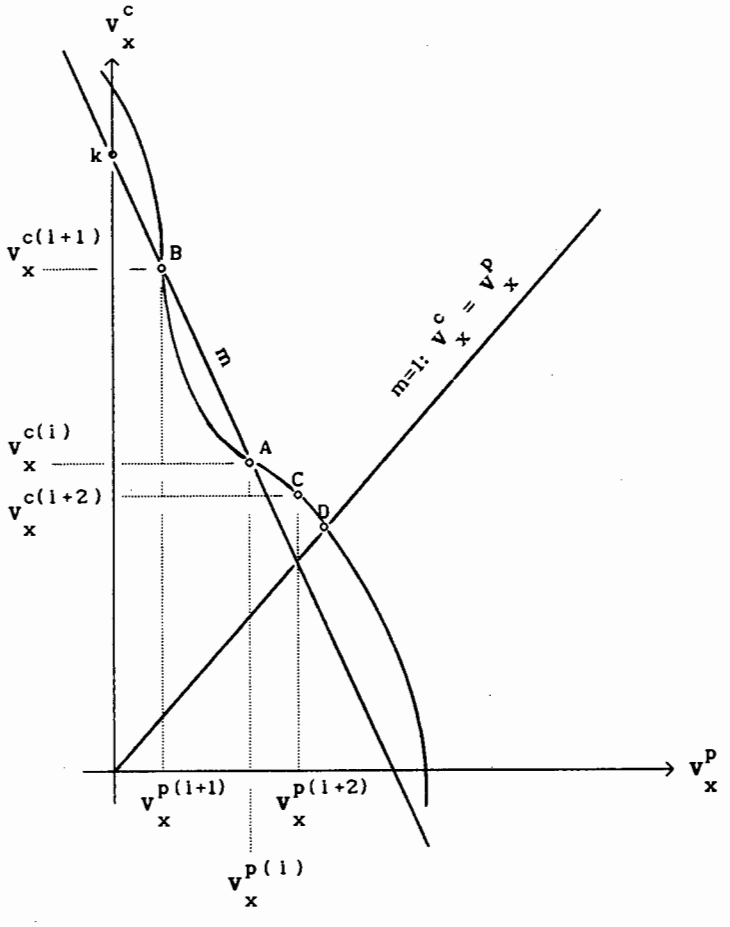

Figure 3.2.1: Schematic representation of the velocity iterative procedure.

The point A on the graph is thus arrived at. A second guess of the structure velocity is now made (typically a fraction of the initial guess) and point B is obtained. The equation of the line through A and B will be $v_x^c = mv_x^p + k$, and this is equated to the unit slope line, $v_x^c = v_x^p$:

$$v_x^p = mv_x^p + k$$

$$(1 - m)\, v_x^p = k$$

$$\therefore\ v_x^p = \frac{k}{(1 - m)}$$

This value ($v_x^{p(1+2)}$ in Figure 3.2.1) will give point C, from where the above procedure is repeated by forming a line through B and C. This form of the Newton method is perhaps the most elegant of all iterative schemes to find the roots of a non-linear equation for which a mathematical expression is not known, the equation in the above description being the difference between v_x^c and v_x^p. The convergence of this method is rather insensitive to the initial guesses, provided they are valid.

The distributed forces, f, in the lateral direction of an element of length e, are applied by the consistent element load vector:

$$\begin{matrix} & d_{1x} & \theta_1 & d_{2x} & \theta_2 \\ \mathbf{f}_e = fe \Big[& \frac{1}{2} & \frac{e}{12} & \frac{1}{2} & \frac{-e}{12} \Big]^T \end{matrix}$$

while those in the axial direction are effectively lumped at the two nodes of the element. Because the program assumes small displacements, the drag loading is applied perpendicularly to the full length of an element. Similarly, the weight and buoyancy forces are assumed to act parallel to the axis of the element (i.e. these forces don't have a component in the lateral direction of the element.) In short, the forces in the x and the y directions are independent of each other.

The Newmark direct integration scheme[39] was used to integrate equation (3.2) with respect to time. A good choice of the Newmark parameters for an implicit method that is unconditionally stable (for linear problems) is γ=0·5 and β=0·25[38]. (This method is then referred to as the trapezoidal method.) In this form the scheme gives no amplitude errors in any sine-wave motion, regardless of its frequency, but the periods of these types of wave are overestimated. A fixed time step of 0·1 seconds (approximately one hundredth of the period of the lowest mode of vibration) was used.

For the calculation of the free stream properties, the Airy wave theory was used while the velocity of the current is specified in the input as an average at the midpoint of an element.

To summarise the simplifying assumptions made in the developement of PILE, the following:

1. Small displacement formulation;
2. No coupling exists between the axial and transverse strain components;
3. The material is assumed homogeneous, isotropic and linearly elastic;
4. Viscosity and density are constant with depth (temperature). Therefore C_M and C_D are constant;
5. The effects of partial submersion of elements on the drag and buoyancy forces are neglected.

3.3: VALIDATION OF PROGRAM PILE.

To establish a degee of confidence in the program formulated in the previous section, the static and dynamic behaviour of the model given in section 2.3 was analysed using the ABAQUS finite element program to supply the benchmark solution. This solution was obtained by using Model A of Chapter 2, with two differences:

1. The torsional spring at the bottom of the pile was discarded. This end of the pile was considered pinned only;
2. The NLGEOM flag was removed, giving a small displacement solution.

3.3.1: Static tests.

Two tests were carried out. In the first, the pile was deflected by the current alone and in the second test the top of the pile was displaced horizontally by 10m. The displacements and reaction forces were compared in both tests and the results are given in Tables 3.3.1 and 3.3.2. A schematic representation of the ABAQUS model appears in Figure 2.3.1 and Figure 2.3.2, while the model with PILE is given overleaf in Figure 3.3.1.

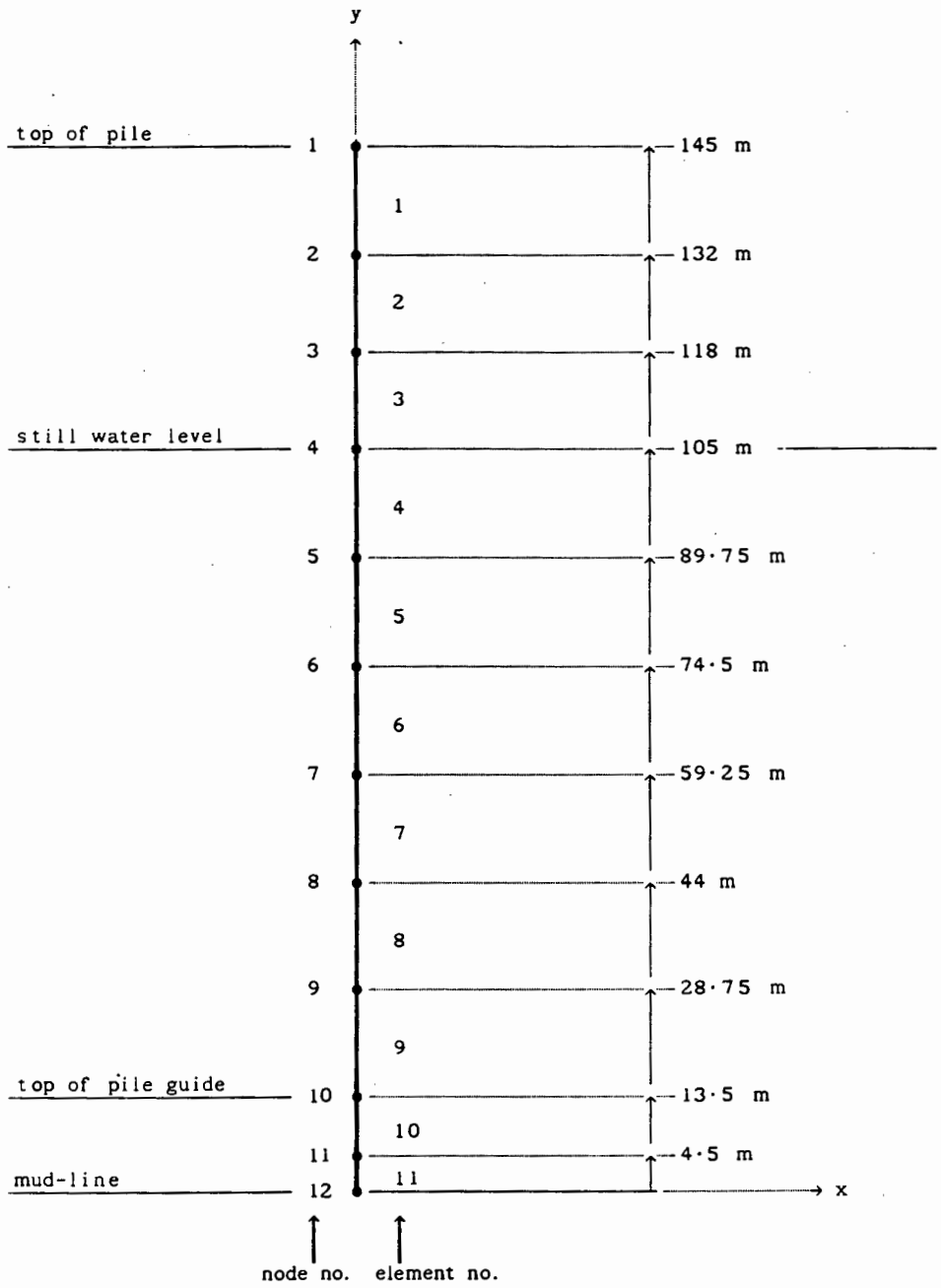

Figure 3.3.1: Model of the pile stick-up problem used with PILE.

	Node	ABAQUS	Node	PILE
		Displacements:		
d_x (m)	1	0·1301	1	0·1300
	5	$8·250x10^{-2}$	4	$8·251x10^{-2}$
	13*	$4·864x10^{-3}$	9*	$5·276x10^{-3}$
	18*	$-2·702x10^{-4}$	11*	$-2·710x10^{-4}$
d_y (m)	1	$-3·591x10^{-3}$	1	$-3·591x10^{-3}$
	5	$-3·298x10^{-3}$	4	$-3·298x10^{-3}$
	13*	$-1·223x10^{-3}$	9*	$-1·252x10^{-3}$
	18*	$-2·134x10^{-4}$	11*	$-2·134x10^{-4}$
θ (rad)	1	$-1·190x10^{-3}$	1	$-1·190x10^{-3}$
	5	$-1·189x10^{-3}$	4	$-1.187x10^{-3}$
	13*	$-5·188x10^{-4}$	9*	$-5·375x10^{-4}$
	18*	$4·503x10^{-5}$	11*	$4·520x10^{-5}$
	19	$6·754x10^{-5}$	12	$6·776x10^{-5}$
		Reaction forces:		
RF_x (N)	16	$-1·203x10^{5}$	10	$-1·208x10^{5}$
	19	$9·815x10^{4}$	12	$9·855x10^{4}$
RF_y (N)	19	$3·953x10^{6}$	12	$3·953x10^{6}$

Table 3.3.1: Comparison of displacements and reaction forces of the pile in a steady current found by ABAQUS and PILE. (The nodes marked with an '*' don't exactly correspond in location in the two models.)

	Node	ABAQUS	Node	PILE
		Displacements:		
d_x (m)	1	10·000	1	10·000
	5	5·7060	4	5·7065
	13*	0·2620	9*	0·2839
	18*	$-1·416\times10^{-2}$	11*	$-1·416\times10^{-2}$
d_y (m)	1	$-3·591\times10^{-3}$	1	$-3·591\times10^{-3}$
	5	$-3·298\times10^{-3}$	4	$-3·298\times10^{-3}$
	13*	$-1·223\times10^{-3}$	9*	$-1·252\times10^{-3}$
	16	$-6·209\times10^{-4}$	10	$-6·209\times10^{-4}$
θ (rad)	1	-0·1105	1	-0·1105
	5	-0·1010	4	-0.1010
	13*	$-2·864\times10^{-2}$	9*	$-2·968\times10^{-2}$
	16	$-7·080\times10^{-3}$	10	$-7·080\times10^{-3}$
	19	$3·540\times10^{-3}$	12	$3·540\times10^{-3}$
		Reaction forces:		
RF_x (N)	1	$5·2815\times10^{5}$	1	$5·2860\times10^{5}$
	16	$-5·6727\times10^{6}$	10	$-5·6776\times10^{6}$
	19	$5·1446\times10^{6}$	12	$5·1490\times10^{6}$

Table 3.3.2: Comparison of displacements and reaction forces of the pile with a 10 m horizontal displacement at the top found by ABAQUS and PILE. (The nodes marked with an '*' don't exactly correspond in location in the two models.)

In the test where the current alone was responsible for deflections and reaction forces, the maximum error in displacement never exceeded 0·33%, while that of the reaction forces was 0·42%. With the second static test, the errors in displacements are negligible and the maximum error in the reaction forces is less than 0·09%. The slight discrepancy in the static values found by the two methods is therefore mainly due to differing fluid forces calculated by the two methods and this difference can be tracked down to the specification of the velocity of the current: ABAQUS uses a linear variation of velocity of the current over an element whereas these values are specified at the mid point of the element (and is constant) for PILE.

3.3.2: Dynamic tests.

An Airy wave with an amplitude of 2·83 m and a period of 12·3 seconds was applied to the models for comparison of the dynamic responses. Figure 3.3.2 shows a time history of 100 seconds for the response calculated by the ABAQUS/AQUA program. The response found by PILE is given in Figure 3.3.3.

A slight difference in phase angle (due to the way the wave was specified) is noticeable. The amplitudes of the deflections at the top of the pile in the horizontal direction calculated by ABAQUS are slightly lower than that calculated by PILE. This difference is probably partly due to the slight numerical damping used in ABAQUS's Hilber-Hughes-Taylor integration scheme necessary to find a converged solution.

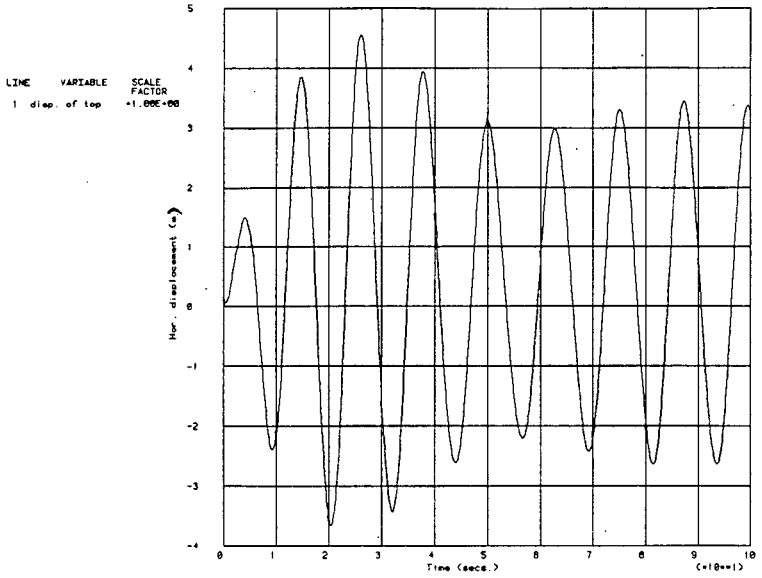

Figure 3.3.2: The dynamic response of the linearised version of Model A. Horizontal displacement at the top of the pile.

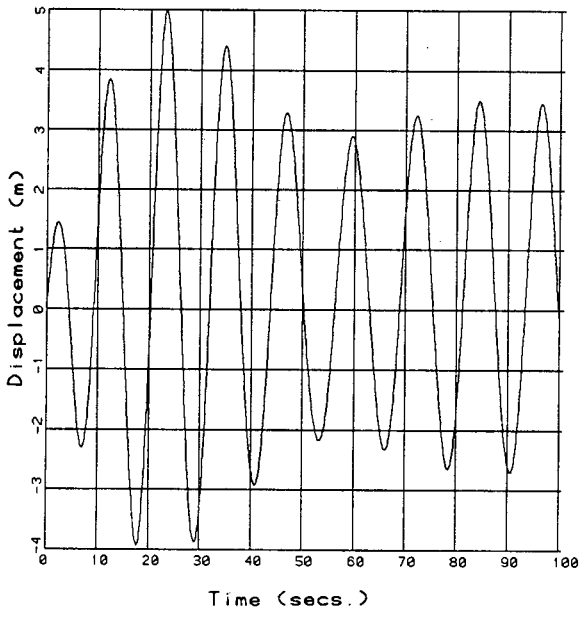

Figure 3.3.3: The dynamic response calculated with PILE. Horizontal displacement at the top of the pile.

A free vibration test was done where the pile was released from an initial 10 m horizontal displacement at the top, in still water. Here, the numerical damping parameter, α, was specified zero for the ABAQUS solution. The free vibration response of the ABAQUS model is shown in Figure 3.3.4, while that calculated by PILE is given as Figure 3.3.5. The frequency of the dominant mode of vibration was estimated from these graphs and is compared in Table 3.3.3 with the first natural frequency as calculated by the eigenvalue routine of ABAQUS. The difference between the frequency found graphically by ABAQUS and that attained by PILE is very small indeed. There are practically no phase differences, but despite no numerical damping in the ABAQUS integration scheme (and both methods integrated using the trapezoidal scheme therefore), it calculates amplitudes that are approximately 5% less than that found by PILE at the end of a 100 second history. The amplitude differences are not consistent either: ABAQUS found the amplitude of the first peak after release 1% greater than did PILE.

	ABAQUS		PILE
	Values from graph in Figure 3.3.4	Values from *FREQ routine	Values from graph in Figure 3.3.5
T_1 (secs.)	10·303	10·227	10·306
ω_1 (rad.s^{-1})	0·6099	0·6144	0·6097

Table 3.3.3: Comparison of the natural frequencies found graphically and by the eigenvalue extractor of ABAQUS.

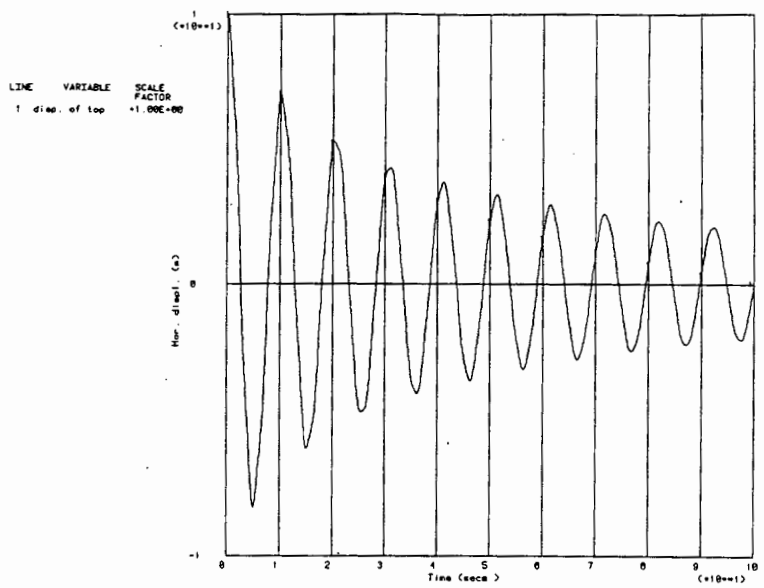

Figure 3.3.4: Free vibration of the linearised version of Model A. Horizontal displacement at the top of the pile.

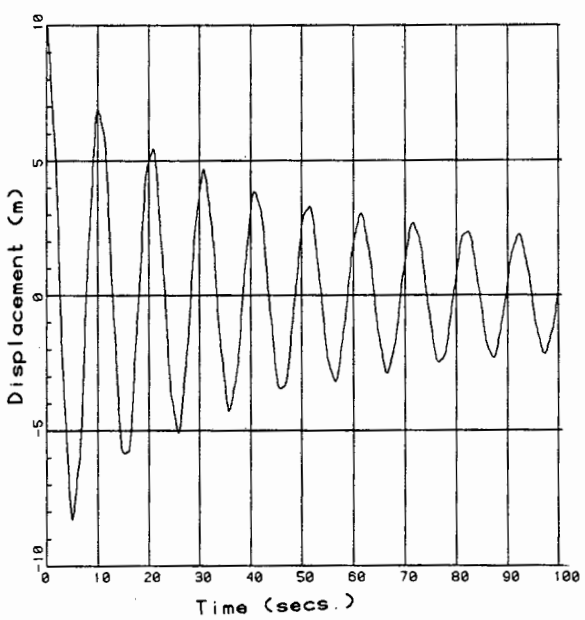

Figure 3.3.5: Free vibration of the PILE model. Horizontal displacement at the top of the pile.

3.3.3: Conclusion.

Provided a problem can be acceptably simplified according to the assumptions outlined at the end of section 3.2, PILE has demonstrated its ability to solve it very accurately (and economically: The above 100 second history was performed with PILE in less than 6% of the CPU time that ABAQUS required). Having shown that the problem at hand can be successfully analysed with PILE, it can be used as a basis for the probabilistic finite element (PFEM) in the next chapter with confidence.

4. THE PROBABILISTIC FINITE ELEMENT METHOD (PFEM).

4.1: INTRODUCTION.

After an algorithm for the solution of a deterministic response of a structure in the ocean has been established (as in the previous chapters), the problem of estimating the dynamic behaviour of the structure has only just begun: the physical uncertainty in the problem, the sparse statistical data and the uncertainty with regards to the model itself may render such a deterministic solution unreliable and of limited practical use.

A lot of work has gone into addressing the problem of uncertain loading of a structure in the ocean. For linear systems, modal techniques in both the time and frequency domain are well documented and an 'equivalent linearisation' approach has been applied to the drag term. Mostly, uncertainty analyses in structural mechanics have concentrated on problems of an almost totally stochastic nature[18], requiring Monte Carlo simulation techniques which is computationally repetitive and expensive. But they apply to both linear and non-linear systems.

In most structural analyses with uncertainties, concern lies more with deviations in the load from a deterministic path and with uncertainties in model properties to which a variance can be assigned[18]. The well established finite element method moved into the realms of probability theory (perhaps naturally) and a fine review of probabilistic structural analyses with the finite element method is given in ref.[25].

In this emerging field, the 'stochastic finite element method (which embraces both statistical methods and non-statistical methods such as the PFEM) is frequently used to denote the study of systems with parametric uncertainties, whether or not the loads are random[25]. The pioneering work done with perturbation methods[18,21,23,26] has the advantage that it follows all the steps of a conventional deterministic analysis, and can thus make use of the existing routines. Moreover, the PFEM requires only the first and second statistical moments of the random parameters while other methods (such as Monte Carlo simulation) usually require knowledge of the probability density functions as well. Many of the limitations inherent in the PFEM have been

successfully eliminated (see section 4.3) and several researchers[19,25] have applied the method with some degree of success.

In what follows, the methods of Liu, Belytscho *et al* (ref.[18]) will be applied to the geometrically linearised model developed in Chapter 3 for the pile stick-up problem, with a system non-linearity arising in the drag loading, where the uncertain parameters will be the drag coefficient (C_D) and the inertia coefficient (C_M). These coefficients are notoriously difficult to obtain[27].

4.2: THE FORMULATION OF THE PFEM.

(The derivation of the following equations is given in appendix B. The prefix $\mathcal{B}$ to the equation numbers below refer to the corresponding equations in that appendix. The notation is consistent with that used by the majority of authors of probability theory such as ref.[13,20,29].)

Consider the structural system to be governed by the following system of non-linear algebraic equations in the x-direction which arise from the finite element discretisation from a previous section:

$$\mathbf{Ma} + \mathbf{Cv} + \mathbf{Kd} = \mathbf{f} \tag{3.2}$$

$$\text{where } \mathbf{f} = \tfrac{1}{2}\rho_f C_D D_0 s\mathbf{V}^2 + \rho_f C_M A_0 \dot{u}\mathbf{I}_x \tag{4.1}$$

Eqn (4.1) is a compacted version of eqn (3.4) where the relative velocity vector is now given by $\mathbf{V} = (u - \mathbf{v}_x)$, and s represents the sign of $\mathbf{V}$ to preserve the direction of the drag force.

The q-dimensional vector of random parameters, **b**, contains the chosen uncertain quantities of C_D and C_M:

$$\mathbf{b} = \begin{bmatrix} C_D \\ C_M \end{bmatrix}$$

where q = 2. The assumption will be made that C_D and C_M are uncorrelated. It is known[3] that these parameters are not simple constants, and both are functions of at least R_e , K_c and the cylinder roughness. In this way they are not independent, but need not necessarily be correlated[20]. This assumption does not limit the applicability of the PFEM, since Eigen techniques can be used to decouple the correlated random variables (see section 4.3)

If $\varphi(\mathbf{b})$ is a random function of the random vector $\mathbf{b}$, the expected value of $\varphi(\mathbf{b})$ can be approximated by the second order equation:

$$E[\varphi(\mathbf{b})] \simeq \varphi(\mu_{\mathbf{b}}) + \left.\frac{\partial^2\varphi}{2!\partial \mathbf{b}^2}\right|_{\mu_{\mathbf{b}}} \mathrm{Var}(\mathbf{b}) = \varphi(\mu_{\mathbf{b}}) + \frac{1}{2}\sum_{j=1}^{q}\left.\frac{\partial^2\varphi}{\partial b_j^2}\right|_{\mu_{\mathbf{b}}} \mathrm{Var}(b_j) \qquad (\mathcal{B}5)$$

Applying the expectancy operator to eqn (3.2), separating and equating the terms of like order gives the following equations:

$$\overline{\mathbf{M}}\,\overline{\mathbf{a}} + \overline{\mathbf{C}}\,\overline{\mathbf{v}} + \overline{\mathbf{K}}\,\overline{\mathbf{d}} = \overline{\mathbf{f}} \qquad (\mathcal{B}11)$$

$$\overline{\mathbf{M}}\,\overline{\Delta\mathbf{a}} + \overline{\mathbf{C}}\,\overline{\Delta\mathbf{v}} + \overline{\mathbf{K}}\,\overline{\Delta\mathbf{d}} = \overline{\Delta\mathbf{f}} \qquad (\mathcal{B}12)$$

where

$$\overline{\Delta\mathbf{d}} = \frac{1}{2}\sum_{j=1}^{q}\left(\overline{\frac{\partial^2\mathbf{d}}{\partial b_j^2}}\right)\mathrm{Var}(b_j) \qquad (\mathcal{B}14a)$$

$$\overline{\Delta\mathbf{v}} = \frac{1}{2}\sum_{j=1}^{q}\left(\overline{\frac{\partial^2\mathbf{v}}{\partial b_j^2}}\right)\mathrm{Var}(b_j) \qquad (\mathcal{B}14b)$$

$$\overline{\Delta\mathbf{a}} = \frac{1}{2}\sum_{j=1}^{q}\left(\overline{\frac{\partial^2\mathbf{a}}{\partial b_j^2}}\right)\mathrm{Var}(b_j) \qquad (\mathcal{B}14c)$$

$$\overline{\Delta f} = \frac{1}{2}\sum_{j=1}^{q}\left\{\rho_f D_0 s\left[2\overline{V}\left(-\frac{\overline{\partial v}_x}{\partial b_j}\right)\frac{\overline{\partial C}_D}{\partial b_j} + \left(-\frac{\overline{\partial v}_x}{\partial b_j}\right)^2\overline{C}_D + \overline{V}\left(-\overline{\frac{\partial^2 v}{\partial b_j^2}}_x\right)\overline{C}_D\right] - 2\,\frac{\overline{\partial M}}{\partial b_j}\frac{\overline{\partial a}}{\partial b_j}\right\}\mathrm{Var}(b_j) \qquad (\mathcal{B}13)$$

The bar denotes variables evaluated at the mean value of the independent (random) parameter, and therefore the zero order response (given by eqn ($\mathcal{B}11$)) is equivalent to the deterministic response. The second order response is added to this, so that the second order approximation of the mean response is given by:

$$E[\mathbf{d}] \simeq \overline{\mathbf{d}} + \overline{\Delta\mathbf{d}} \qquad (\mathcal{B}10a)$$

$$E[\mathbf{v}] \simeq \overline{\mathbf{v}} + \overline{\Delta\mathbf{v}} \qquad (\mathcal{B}10b)$$

$$E[\mathbf{a}] \simeq \overline{\mathbf{a}} + \overline{\Delta\mathbf{a}} \qquad (\mathcal{B}10c)$$

The first order approximation of the response variances are given by:

$$\mathrm{Var}(\mathbf{d}) \simeq \sum_{j=1}^{q} \left(\frac{\overline{\partial \mathbf{d}}}{\partial b_j} \right)^2 \mathrm{Var}(b_j) \qquad (\mathcal{B}15a)$$

$$\mathrm{Var}(\mathbf{v}) \simeq \sum_{j=1}^{q} \left(\frac{\overline{\partial \mathbf{v}}}{\partial b_j} \right)^2 \mathrm{Var}(b_j) \qquad (\mathcal{B}15b)$$

$$\mathrm{Var}(\mathbf{a}) \simeq \sum_{j=1}^{q} \left(\frac{\overline{\partial \mathbf{a}}}{\partial b_j} \right)^2 \mathrm{Var}(b_j) \qquad (\mathcal{B}15c)$$

To obtain the first order sensitivity vectors, $\frac{\overline{\partial \mathbf{d}}}{\partial \mathbf{b}}$, $\frac{\overline{\partial \mathbf{v}}}{\partial \mathbf{b}}$ and $\frac{\overline{\partial \mathbf{a}}}{\partial \mathbf{b}}$, needed in eqn ($\mathcal{B}$15) and that also appear in the $\overline{\Delta \mathbf{f}}$-term (eqn $\mathcal{B}$13), the system equation (eqn (3.2)) is differentiated with respect to **b**. The global mass matrix, **M**, is a function of $C_M(b_2)$, while the damping and the stiffness matrices are independent of **b**. The first order sensitivity vectors are then obtained from:

$$\overline{\mathbf{M}} \frac{\overline{\partial \mathbf{a}}}{\partial \mathbf{b}} + \overline{\mathbf{C}} \frac{\overline{\partial \mathbf{v}}}{\partial \mathbf{b}} + \overline{\mathbf{K}} \frac{\overline{\partial \mathbf{d}}}{\partial \mathbf{b}} = \tfrac{1}{2} \rho_f D_0 s \left[\frac{\overline{\partial C_D}}{\partial \mathbf{b}} \overline{\mathbf{V}}^2 + 2\overline{\mathbf{V}} \left(- \frac{\overline{\partial \mathbf{v}_x}}{\partial \mathbf{b}} \right) \overline{C}_D \right] +$$

$$\rho_f A_0 \dot{u} \mathbf{I}_x \frac{\overline{\partial C_M}}{\partial \mathbf{b}} - \frac{\overline{\partial \mathbf{M}}}{\partial \mathbf{b}} \bar{\mathbf{a}} \qquad (\mathcal{B}16)$$

The same system matrices ($\overline{\mathbf{M}}$, $\overline{\mathbf{C}}$, and $\overline{\mathbf{K}}$) derived in Chapter 3 and the same Secant iteration scheme used in the deterministic dynamic response are used to converge to the solution of $\frac{\overline{\partial \mathbf{v}}}{\partial \mathbf{b}}$, which appears on both sides of eqn ($\mathcal{B}$16).

From here two solution procedures exist to find the second order component of the mean response:

1. Eqn ($\mathcal{B}$16) is differentiated with respect to **b** again to yield:

$$\overline{\mathbf{M}} \frac{\overline{\partial^2 \mathbf{a}}}{\partial \mathbf{b}^2} + \overline{\mathbf{C}} \frac{\overline{\partial^2 \mathbf{v}}}{\partial \mathbf{b}^2} + \overline{\mathbf{K}} \frac{\overline{\partial^2 \mathbf{d}}}{\partial \mathbf{b}^2} = \tfrac{1}{2} \rho_f D_0 s \left[4\overline{\mathbf{V}} \left(- \frac{\overline{\partial \mathbf{v}_x}}{\partial \mathbf{b}} \right) \frac{\overline{\partial C_D}}{\partial \mathbf{b}} + 2 \left(- \frac{\overline{\partial \mathbf{v}_x}}{\partial \mathbf{b}} \right)^2 \overline{C}_D + \right.$$

$$\left. 2\overline{\mathbf{V}} \left(- \frac{\overline{\partial^2 \mathbf{v}_x}}{\partial \mathbf{b}^2} \right) \overline{C}_D \right] - 2 \frac{\overline{\partial \mathbf{M}}}{\partial \mathbf{b}} \frac{\overline{\partial \mathbf{a}}}{\partial \mathbf{b}} \qquad (\mathcal{B}17)$$

Excepting the force vector, i.e. the right hand side of eqn ($\mathcal{B}$17), the same procedure as that to find the first order sensitivity vectors is simply repeated in the same b_j-loop. The second order components of the mean response are then calculated from eqn ($\mathcal{B}$14) before being added in eqn ($\mathcal{B}$10)

to the zero order components.

2. $\overline{\Delta \mathbf{f}}$ is computed from eqn ($\mathcal{B}$13) (or rather eqn ($\mathcal{B}$18)) and the second order components of the mean response are calculated directly from eqn ($\mathcal{B}$12) using a similar method to that used to find the deterministic response in Chapter 3.

The second method will result in a minimum of q+2 integration per time increment, in total, to obtain the approximation to E[**d**]. The former method will result in 2q+1 time integrations. ('Minimum' here implies the situation where no iterations are necessary, for instance when the force vector is linear). With the investigation of the pile stick-up problem, approximately 16% CPU time was saved with the second method over the first method. Only when there is only one random parameter will the two methods be equivalent as far as computational effort is concerned, while the second method will require just over half the integrations required by the first method when q becomes large.

The two procedures described above derive from the same equations and, apart from differences in truncation error due to more (or fewer) computations, should give the same results. This fact was borne out with the particular pile stick-up analysis.

Similar procedures can also be developed for the probabilistic distribution of stresses, although this was not entertained in the current work. For physical parameters that are not discrete but continuous functions in space, the aforesaid analysis can be extended to random fields[21].

4.3: LIMITATIONS AND FUTURE DEVELOPMENTS OF THE PFEM.

A major drawback of the PFEM, as formulated in the previous section, is that it is only accurate for short duration analyses (See the results in section 4.6). In the application of the PFEM for dynamic analyses, both linear and non-linear, it has been observed that secular terms arise in the statistical distributions causing erroneous results. The secularities appear in the higher order equations due to resonance: examining equations ($\mathcal{B}$11) and ($\mathcal{B}$16), it is evident that because the same mass, damping and stiffness matrices are used in both equations, their damped natural frequencies will be the same. From eqn ($\mathcal{B}$16) it can be seen that the excitation involves the result $\bar{\mathbf{a}}$ obtained from eqn ($\mathcal{B}$11) and is, therefore, a resonant excitation. This resonance is

then further transmitted in the excitation of eqn (B12) where $\overline{\Delta f}$ is constructed of these resonating first order sensitivity vectors. The errors in the variance and the second order component of the mean response then grow unbounded unless damped. A numerical method[26] for eliminating secularities requires the separation of the resonant and non-resonant parts of the first and second order forcing functions and the Fast Fourier Transform is applied. To do this, the forcing functions must be decoupled.

In ref.[26] it is illustrated how the eigen problem is solved for the zero order equations in order to decouple also the first and second order equations. This effort, together with that mentioned in the next paragraph, are prerequisites for the improved computational procedures via a Lanczos vector basis which results in a considerable reduction in the number of equations to be solved. This matter will not be further pursued here.

In the derivations of section 4.2, it was assumed that the random variables of interest in this investigation were uncorrelated. If this is not the case, the number of computations will increase dramatically due to the double summations that were eliminated, for instance, by reducing

$$\mathrm{Var}(\mathbf{d}) \simeq \sum_{i,j=1}^{q} \left(\frac{\overline{\partial \mathbf{d}}}{\partial b_i} \right) \left(\frac{\overline{\partial \mathbf{d}}}{\partial b_j} \right) \mathrm{Cov}(b_i, b_j)$$

to

$$\mathrm{Var}(\mathbf{d}) \simeq \sum_{j=1}^{q} \left(\frac{\overline{\partial \mathbf{d}}}{\partial b_j} \right)^2 \mathrm{Var}(b_j) \ .$$

By transforming the correlated full covariance matrix,

$$\mathrm{Cov}(b_i, b_j) = \mathbb{B}_{ij}$$

to an uncorrelated diagonal variance matrix,

$$\mathrm{Var}(c_i, c_j) = \mathrm{Var}(c_i)\ \delta_{ij} = \mathbb{T}_{ij} \text{ (with no sum on i)},$$

where $\mathbb{T}$ is a diagonal matrix and δ_{ij} is the Krönecker delta, the double summations are reduced to single summations. This is achieved by solving the eigen problem as was discussed in the previous paragraph.

A remaining limitation, inherent to all perturbation methods is that the coefficient of variation of the random (uncertain) parameter must be 'small'. This is due to the fact that higher order terms of the Taylor series are

order to preserve the statistical properties. In analysing the performance of the basic generator by the Spectral Test[32], the following results were achieved:

n	ν_n
2	$3{\cdot}44 \times 10^8$
3	$4{\cdot}29 \times 10^5$
4	$1{\cdot}72 \times 10^4$
5	$1{\cdot}92 \times 10^3$
6	593
7	198
8	108
9	67

An informal interpretation of the quantities ν_n is that consecutive n-tuples are statiscally uncorrelated to an accuracy of $\frac{1}{\nu_n}$. It is stressed that in practice the degree of randomness is usually much greater than these theoretical results may suggest, but the fact remains that the accuracy does drop rapidly as the number of dimensions become large, a property of all multiplicative congruential generators. Even for samples of only a few random numbers, long cycle periods are necessary.

So, although the sample size must be large enough to represent the statistical properties accurately, there is also an upper bound to the size of the sample. In deciding on the magnitude of N, the computational effort that will be required for N deterministic solutions (*à la* Chapter 3) of the response must be weighed up against the accuracy of the statiscal properties of the N random input values generated. In separate tests performed with the random number generator described above, the accuracy of the mean and standard deviations of the random values from a normal distribution did not improve markedly with increased N, although the coefficients of skewness and kurtosis did show a clear improvement. There appears to be no definite trend common to all of the first four statistical moments with increasing N: the moments achieved with N=200 are comparable to those when N=4000, and in between the moments improve and deteriorate (independently of each other) literally at random. When the numbers were generated with a uniform distribution, much the same behaviour was found: The accuracy improves initially with increasing N, and then stagnates. For N>6000, a marked drop in the accuracy of the mean was observed.

The value of N=200 was decided on. From the above mentioned tests, the accuracy of the statistical moments appeared to remain constant from this value of N onwards. Although computationally demanding, this number of simulations was thought to be justified by the importance of the comparison that would be made between PFEM and Monte Carlo simulations (MCS).

The random numbers, x, generated with a normal distribution have the probability density function:

$$p(x) = \frac{1}{\sigma \sqrt{2\pi}} \exp\left[\frac{-(x - \mu_x)^2}{2\sigma^2}\right]$$

where μ_x is the mean of the distribution, and σ is the standard deviation. The following values for the uncertain parameters were used:

For $x = C_D$: $\mu_x = 0{\cdot}53$
$\sigma = 0{\cdot}053,\ 0{\cdot}106,\ 0{\cdot}159,\ 0{\cdot}1767$

For $x = C_M$: $\mu_x = 1{\cdot}47$
$\sigma = 0{\cdot}147,\ 0{\cdot}294,\ 0{\cdot}441,\ 0{\cdot}490$

The four values of σ correspond to a c.o.v. of 0·1, 0·2, 0·3 and $0{\cdot}\dot{3}$ (i.e 0·333...) respectively. The upper bound for the c.o.v. was chosen such that 99·74% of the values generated will lie in the range $0 \leq C_D \leq 1{\cdot}06$ and $0 \leq C_M \leq 2{\cdot}94$. Although these ranges do not faithfully represent all the possible values reported in the literature, they do include a sizable proportion thereof (see section 2.1). The NAG® library's exploratory data analyser (EDA) was used to calculate the statistical properties of the 200 randomly generated values for C_D and C_M according to a normal distribution. Table 4.4.1 (overleaf) shows these results where the values were obtained from a specified c.o.v. of $0{\cdot}\dot{3}$ (approx).

The sample of random values for C_D:	
Size	200
Mean value	0·52916
Standard deviation	0·18137
Coefficient of skewness	0·035142
Coefficient of kurtosis	0·39179
Minimum value	-0·023283
Maximum value	1·1597

The sample of random values for C_M:	
Size	200
Mean value	1·4677
Standard deviation	0·50305
Coefficient of skewness	0·035142
Coefficient of kurtosis	0·39179
Minimum value	-0·06458
Maximum value	3·2164

Table 4.4.1: The statistical properties of the random input values of C_D and C_M. (Normal distribution; c.o.v.≃ $0\dot{3}$)

It is noted from this table that the distribution has an appreciable skewness coefficient and kurtosis coefficient. For a normal distribution, these coefficients should be zero.

For a sample with an arbitrary distribution, the expected values of the order statistics, known as normal scores, and the variance-covariance matrix of the order statistics can be computed. When the ordered data is plotted against the normal scores (the normal probability plot), a straight line of unit slope indicates that this sample is normally distributed. Again employing NAG® routines, a typical normal probability plot of the random input values generated above were obtained and is given in Figure 4.4.1 . The histogram of these values is shown in Figure 4.4.2, and it shows the characteristic 'bell' shape. A scatterplot of C_M *vs.* C_D values is included as Figure 4.4.3 .

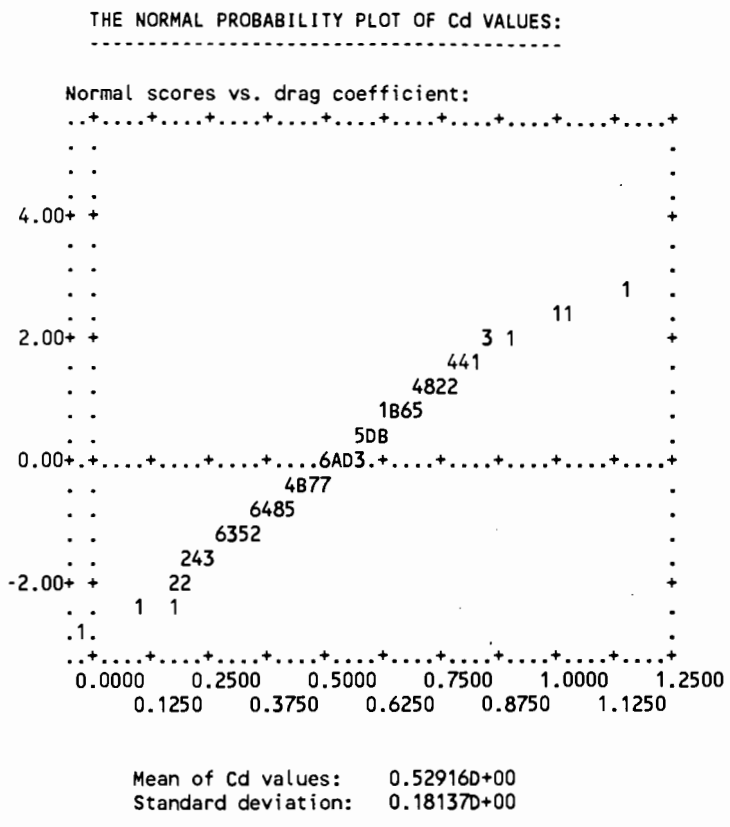

Figure 4.4.1: The Normal probability plot of normally distributed C_D input values. 1 - 9 indicates 1 - 9 observations; A - Z indicates 10 - 35 observations.

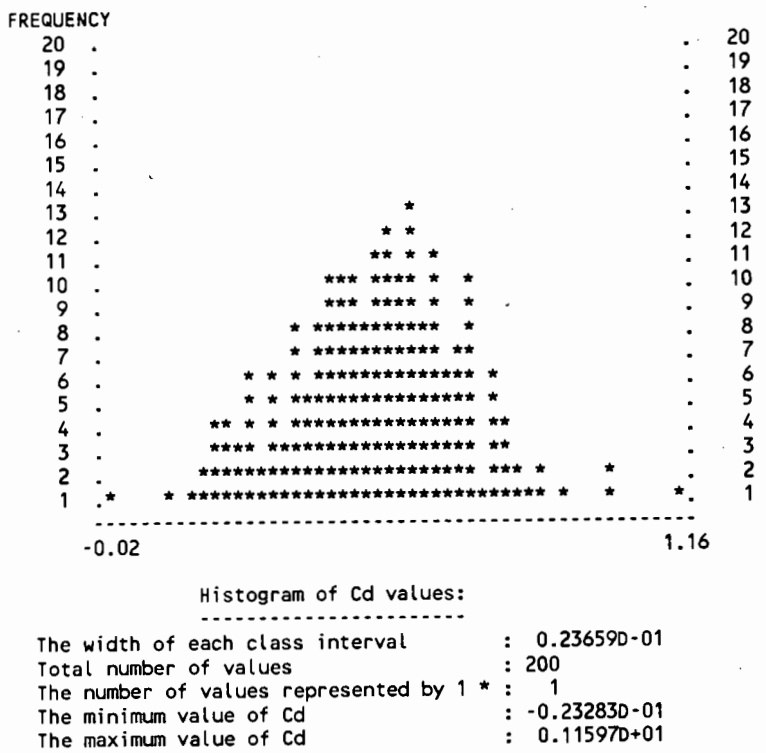

Figure 4.4.2: Histogram of normally distributed C_D input values.

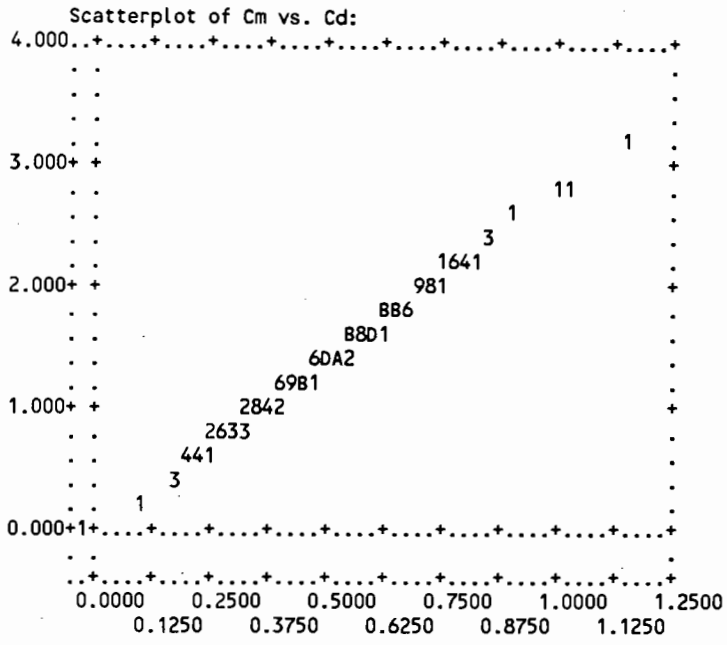

Figure 4.4.3: Scatterplot of normally distributed C_M *vs.* C_D input values. 1 - 9 indicates 1 - 9 observations; A - Z indicates 10 - 35 observations.

The random values of C_D and C_M according to a uniform distribution were manipulated such as to fall in similar ranges to that of the normal distribution described earlier, i.e.

$$(\mu_x - 3\sigma) < x < (\mu_x + 3\sigma)$$

where σ is the standard deviation of the above normal distribution. In this way, the statistical properties of the responses from the two distributions of the random parameters may be more easily compared to establish the sensitivity of the structure response to the distribution of the uncertain input parameters. Table 4.4.2 reflects the statistical properties of the C_D and C_M values generated over the maximum approximate ranges ($0 < C_D < 1{\cdot}06$ and $0 < C_M < 2{\cdot}94$) according to a uniform distribution. It is apparent that the skewness coefficients are not zero, but the error was tolerated.

The sample of random values for C_D:	
Size	200
Mean value	0·50582
Standard deviation	0·31500
Coefficient of skewness	-0·0060011
Coefficient of kurtosis	-1·22910
Minimum value	-0·0004296
Maximum value	1·0571

The sample of random values for C_M:	
Size	200
Mean value	1·4901
Standard deviation	0·86684
Coefficient of skewness	-0·057426
Coefficient of kurtosis	-1·2727
Minimum value	-0·00061901
Maximum value	2·9341

Table 4.4.2: The statistical properties of the random input values of C_D and C_M.
(Uniform distribution; Maximum range)

Figure 4.4.4 and Figure 4.4.5 show the histograms of C_D and C_M values, respectively, with a uniform distribution and over the maximum ranges. The rectangular shapes of the distributions are evident. A scatter plot of C_M *vs.* C_D is included as Figure 4.4.6 .

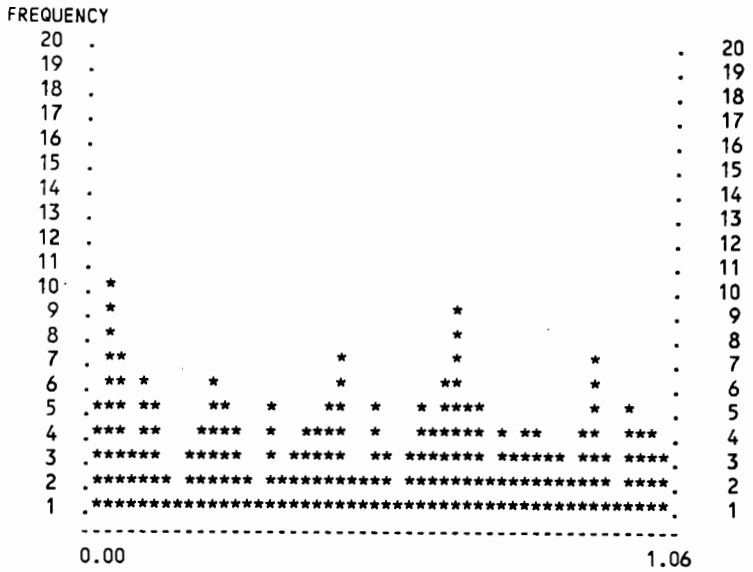

Histogram of Cd values:

The width of each class interval	: 0.21133D-01
Total number of values	: 200
The number of values represented by 1 *	: 1
The minimum value of Cd	: 0.42960D-03
The maximum value of Cd	: 0.10571D+01

Figure 4.4.4: Histogram of uniformly distributed C_D input values.

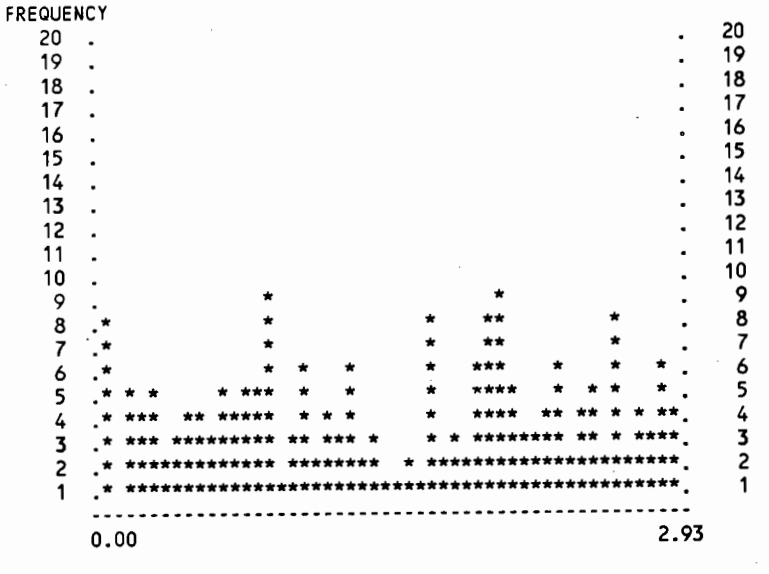

Histogram of Cm values

The width of each class interval	: 0.58670D-01
Total number of values	: 200
The number of values represented by 1 *	: 1
The minimum value of Cm	: 0.61901D-03
The maximum value of Cm	: 0.29341D+01

Figure 4.4.5: Histogram of uniformly distributed C_M input values.

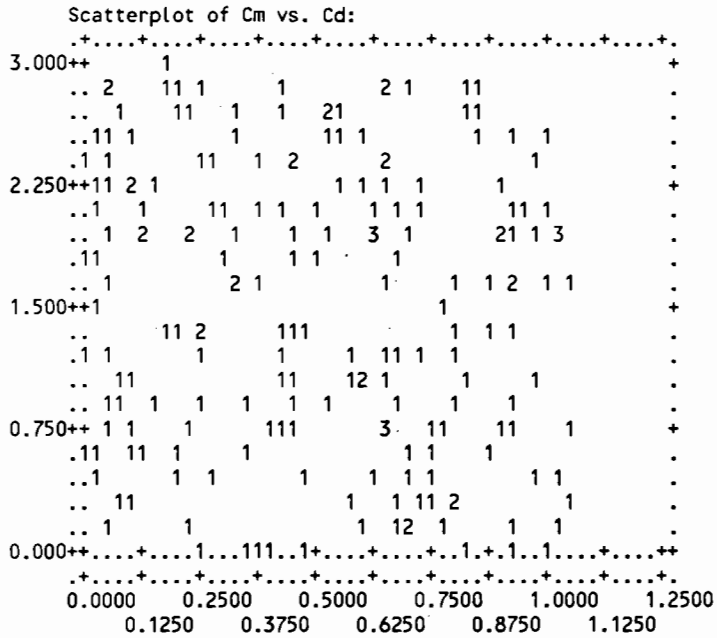

Figure 4.4.6: Scatterplot of uniformly distributed C_M *vs.* C_D input values.
1 - 9 indicates 1 - 9 observations;

Having obtained the N values of C_D and C_M according to the normal and the uniform distribution, the deterministic solution of the response (as was developed in Chapter 3) is performed N times for each distribution of input values. Because the inertia coefficient is random, it is necessary to recalculate the mass matrix for every simulation. The drag force is calculated employing the drag coefficient and this required a new static solution for every simulation. The mean value and standard deviation of the N sets of horizontal displacements at the top of the pile were calculated at each interval in time, and it is these values that were compared in section 4.6 to those found by the PFEM.

4.5: APPLICATION OF THE PFEM.

The PFEM, as formulated in section 4.2, is applied to the pile stick-up model developed in Chapter 3. An additional routine (PROBAB) is included in the program PILE to perform the probabilistic finite element equations of section 4.2. The particulars of the model remain unchanged in this section.

The sensitivity of the undamped reponse to the secular terms in the variance and the second order component of the mean was investigated first. Predictably, these terms suffered unacceptably of resonance and it was decided to include 1% structural damping to the model. The effect of this damping on the variance (or rather, standard deviation) is shown in Figure 4.5.1. The c.o.v. of both C_D and C_M is 0·2 here. Figure 4.5.2 illustrates this same effect on the second order component of the mean response. The 1% structural damping was maintained to obtain all the results presented in this section.

For the maximum c.o.v. of $0\cdot\dot{3}$ used in this study, the size of the two components of the mean response in relation to the mean is illustrated in Figure 4.5.3 .

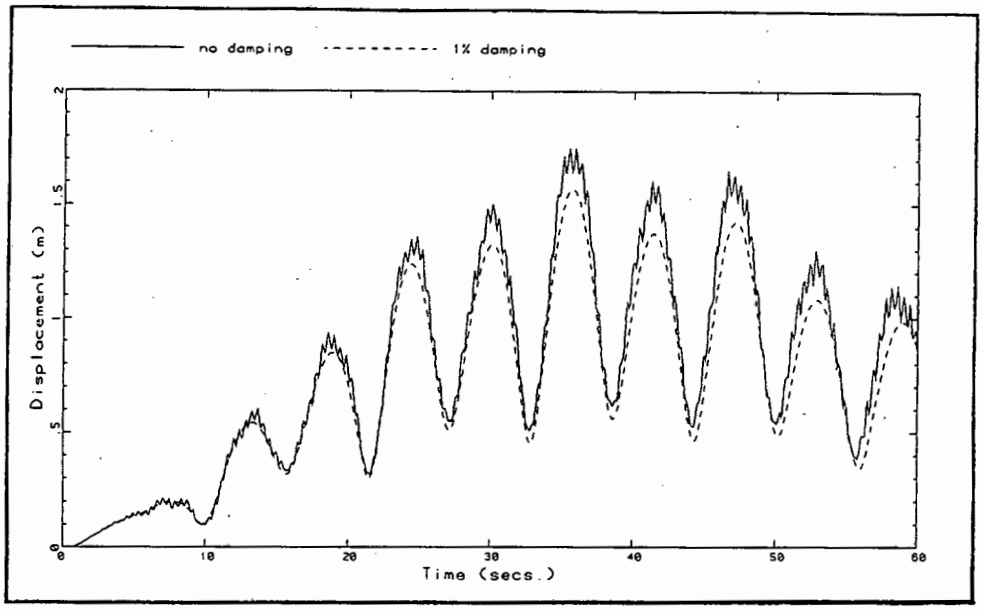

Figure 4.5.1: The effect of stiffness proportional damping on the standard deviation of displacement.

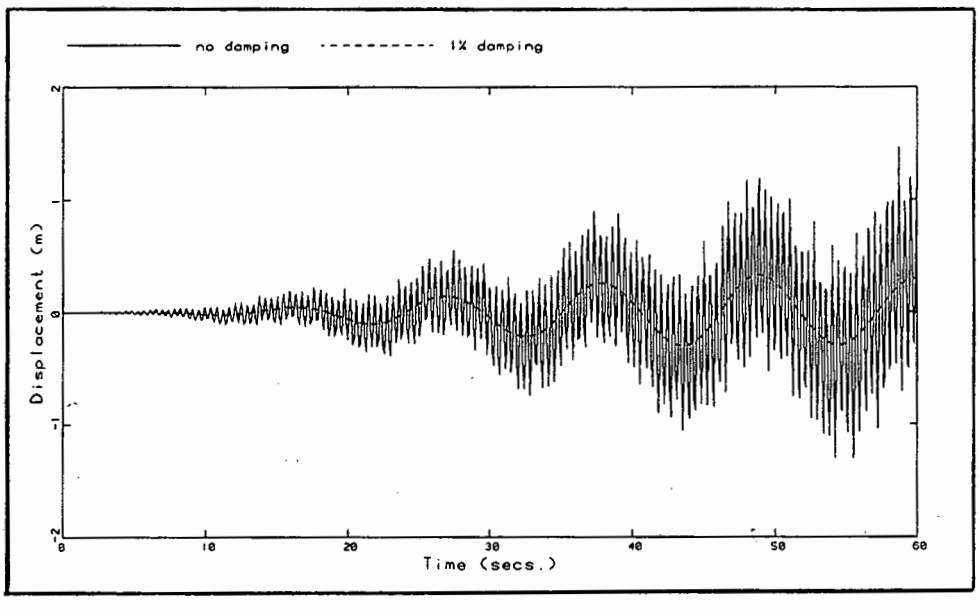

Figure 4.5.2: The effect of stiffness proportional damping on the second order component of the mean response.

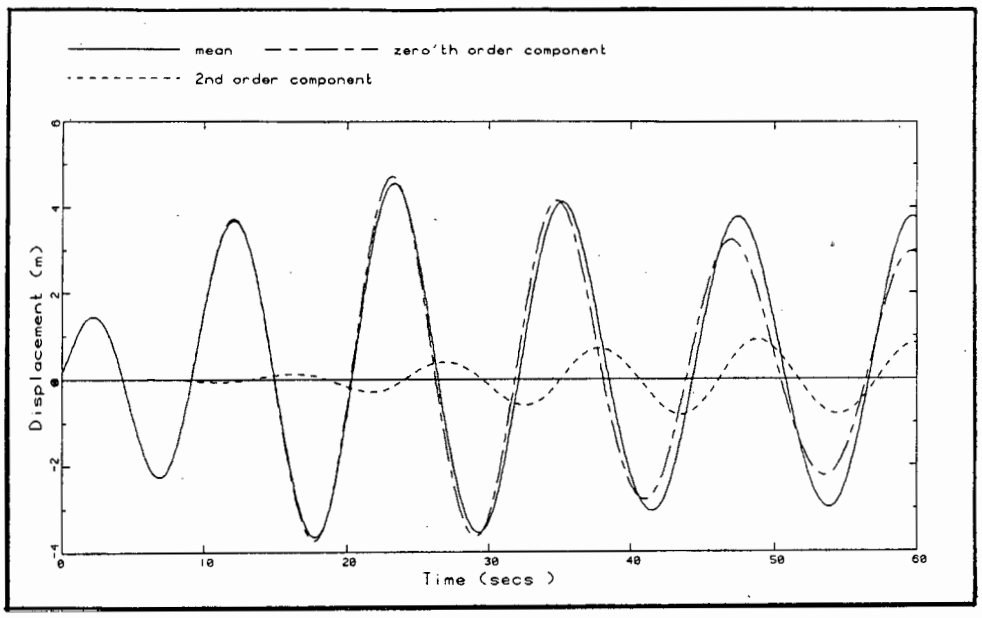

Figure 4.5.3: The mean response of displacements showing the relative sizes of its components.

The second order component makes up approximately 22% of the total mean response at large times. The Monte Carlo simulations (MCS) in the next section will be used to validate this 2^{nd} order approximation of the Taylor expansion.

4.6: COMPARISON OF RESULTS BY PFEM AND MCS.

The results of the mean response and the standard deviations of the horizontal displacements at the top of the pile are calculated using the Monte Carlo simulation (MCS) technique described in section 4.4. To this is compared the corresponding results using the PFEM. The mean and standard deviation of two distributions of C_D and C_M values, as calculated from the input values for the simulations, were used with the latter method.

4.6.1: Input values from a normal distribution.

In the first test, the variance of C_M was specified zero (i.e. C_M is known) while the c.o.v. of C_D values were increased from 10% to 33·3% (approx.). The sensitivity of the mean response to an increased uncertainty in the drag coefficient can thus be established. The results are shown in Figure 4.6.1, while Figure 4.6.2 shows the sensitivity of the standard deviations of the response to the uncertainty in this coefficient. The accuracy achieved with the PFEM of the mean response is remarkable while that for the standard deviations of the response remains very good (the maximum approximate error is 6%) even at large times and large values of the c.o.v. in the drag coefficient. Since the mean response is second order accurate (from inspection of eqn B14) and the variance is only 1^{st} order accurate (see eqn B15), the former would represent a better approximation to the results calculated by MCS. The approximation of the variance is also non-conservative. It can be concluded that the PFEM is satisfactory to find the mean response and standard deviations within 6% for a large uncertainty in the drag coefficient, the real attraction of the PFEM being the fact it achieved this in approximately 2% of the CPU time required to perform 200 simulations.

Figures 4.6.3 and 4.6.4. show a summary of the sensitivity of the response to the uncertainty in the drag coefficient as calculated by PFEM. While the mean response is rather insensitive, the variance of the response increases by the same proportion as the variance of the drag coefficient.

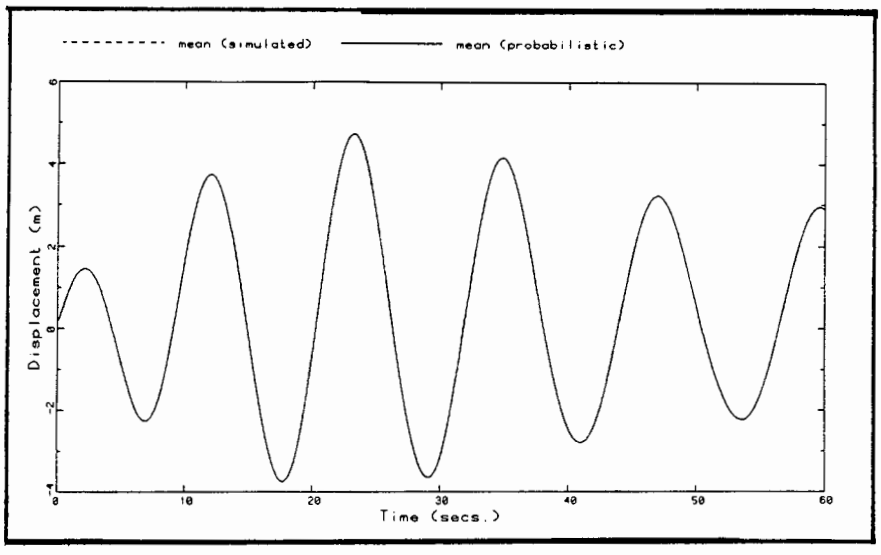

(a)

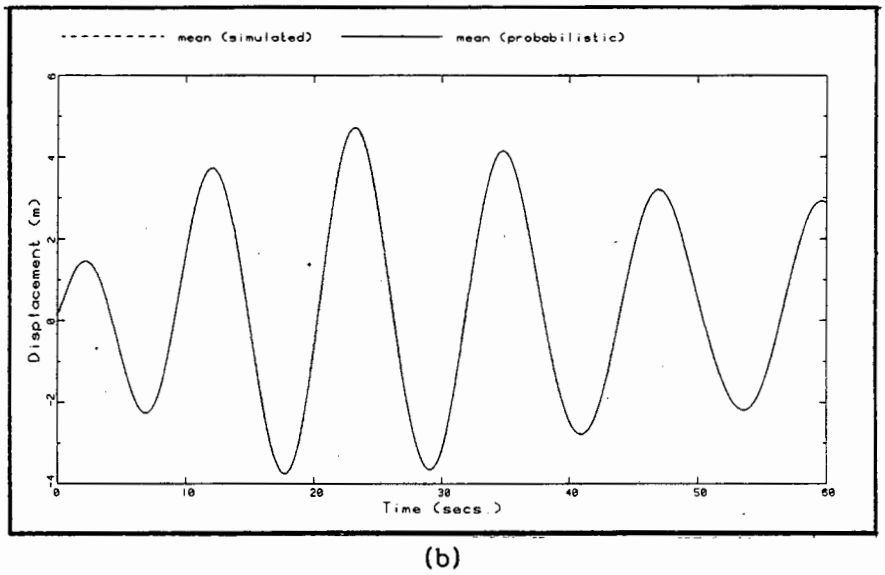

(b)

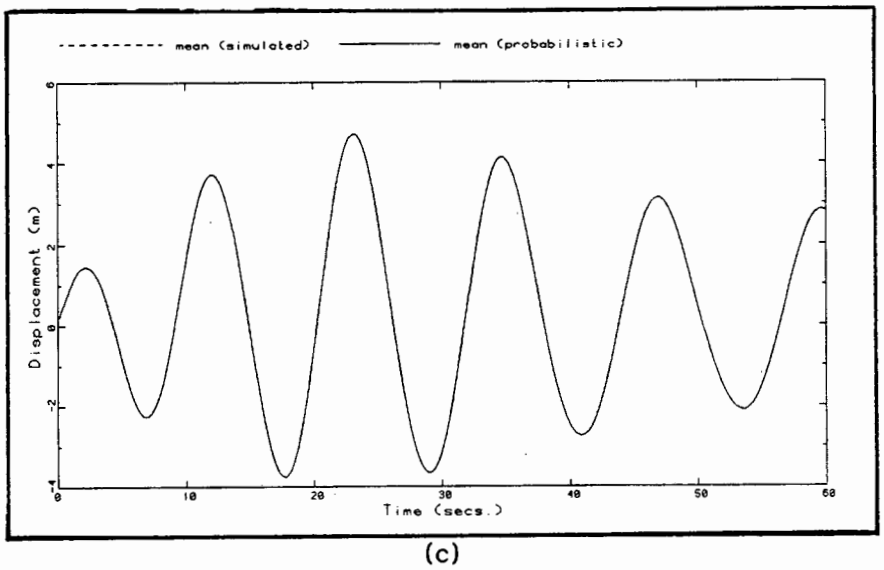

(c)

Figure 4.6.1: The sensitivity of the mean response with respect to the uncertainty in the drag coefficient (Var C_M = 0). Horizontal displacement at the top of the pile.
(a) c.o.v.≃ 0·1, (b) c.o.v.≃ 0·2, (c) c.o.v.≃ 0·3̇

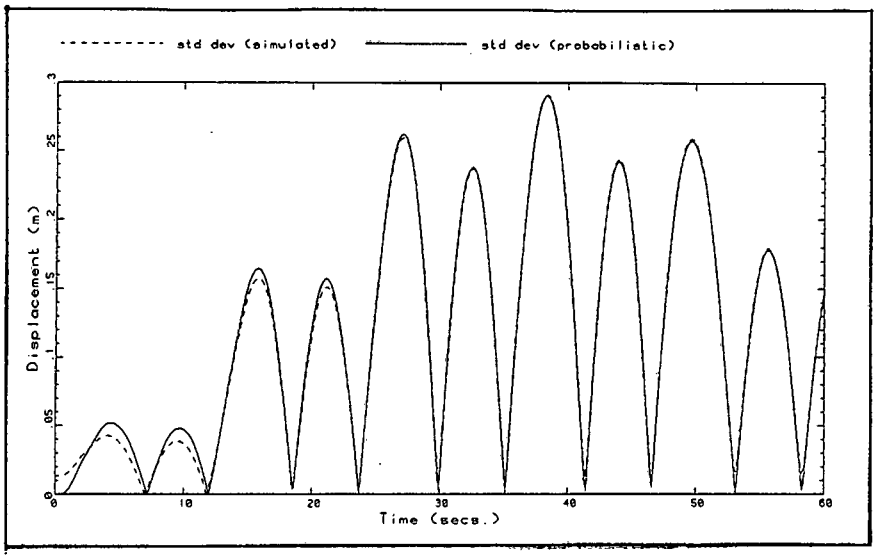

(a)

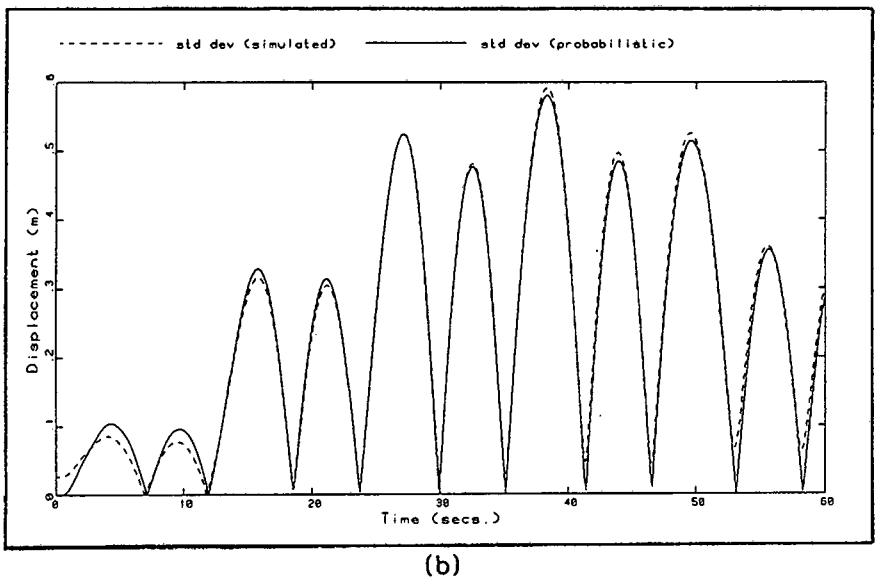

(b)

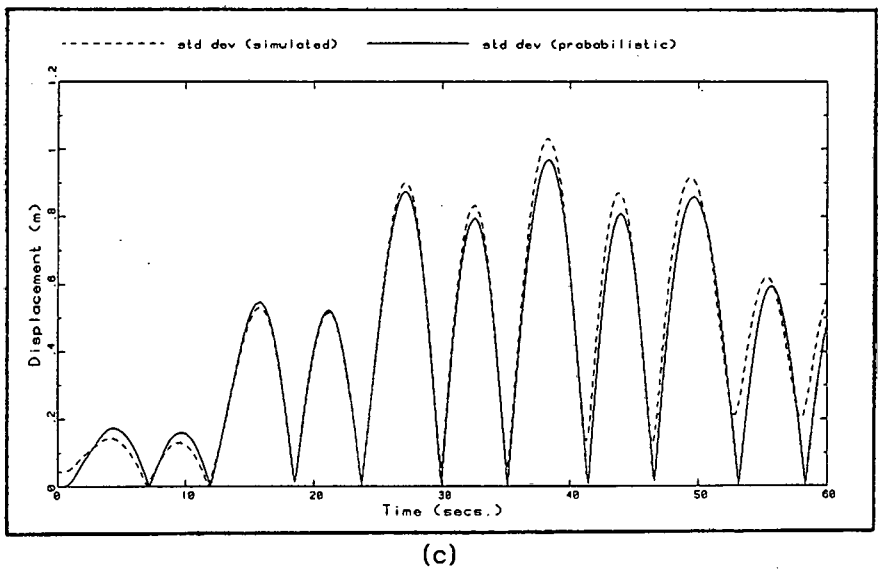

(c)

Figure 4.6.2: The sensitivity of the standard deviations of the response with respect to the uncertainty in the drag coefficient (Var C_M = 0). (a) c.o.v.≃ 0·1, (b) c.o.v.≃ 0·2, (c) c.o.v.≃ 0·$\dot{3}$.

The next test was conducted with the drag coefficient known (Var C_D= 0) and the c.o.v. of C_M increasing from 0·1 to 0·$\dot{3}$ (approx.). The results of the mean response is shown in Figure 4.6.5 and the standard deviations of the response is illustrated in Figure 4.6.6. For lower c.o.v. of C_M , the similarity between the results calculated by the two methods is excellent, but for higher c.o.v. values, the standard deviations found by the PFEM tend to overshoot at large times[18]. The approximation of the standard deviation here is also more conservative than the results found with corresponding c.o.v. of C_D values were non-conservative. It is predictable that the uncertainty in C_M values will have a larger impact on the response than the corresponding uncertainty in C_D, since this parameter appears in both the system mass matrix and the load vector, and thus lends a higher degree of uncertainty to the model.

Figure 4.6.7 reflects this impact of increased c.o.v. in C_M on the mean response (compare with Figure 4.6.3). The standard deviations of the response (see Figure 4.6.8) increase by the same proportion as the standard deviations of the input C_M values, although the error when the c.o.v.≃ 0·$\dot{3}$ is very high (18% approx.). The PFEM could still provide a good approximation of the response for the standard deviation of 0·36 (c.o.v.≃ 0·25), the value quoted by Reid (see section 2.1).

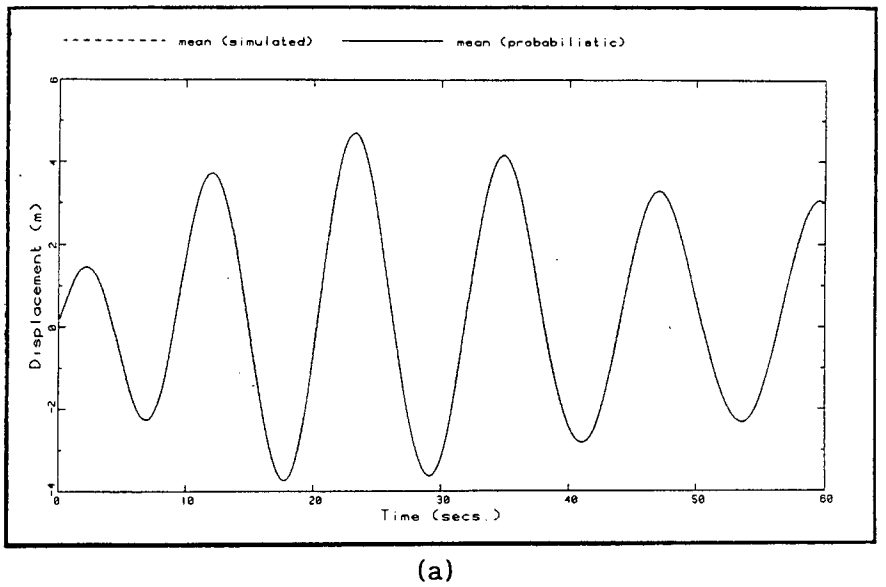

(a)

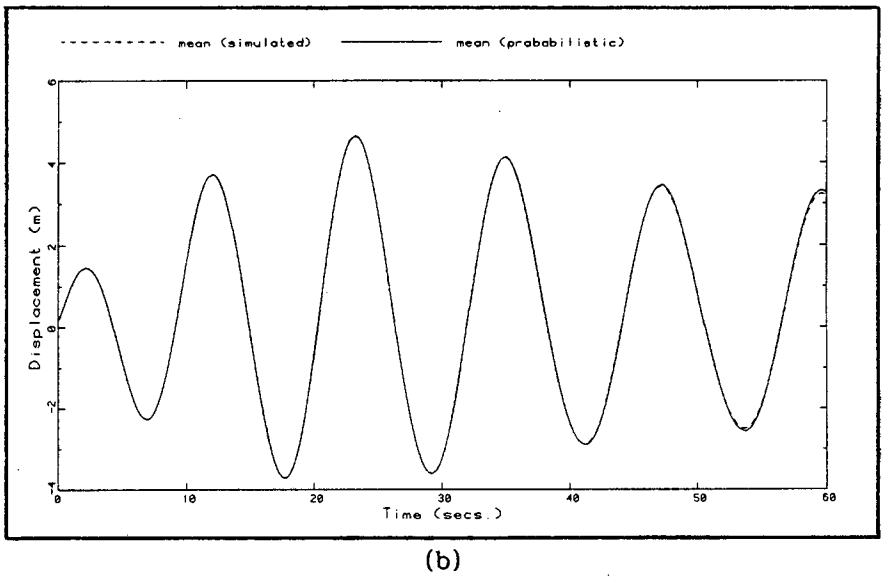

(b)

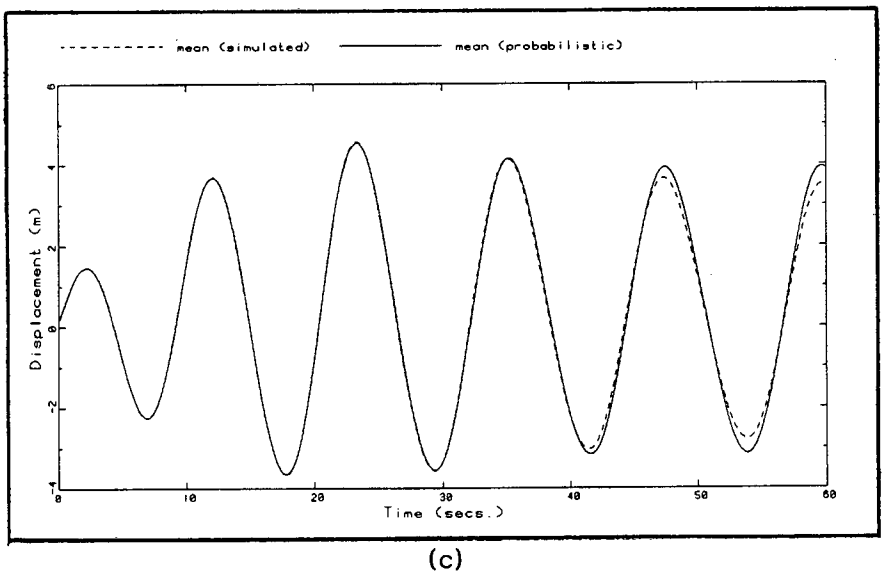

(c)

Figure 4.6.5: The sensitivity of the mean response with respect to the uncertainty in the inertia coefficient (Var C_D = 0). Horizontal displacement at the top of the pile.
(a) c.o.v.≃ 0·1, (b) c.o.v.≃ 0·2, (c) c.o.v.≃ 0·3

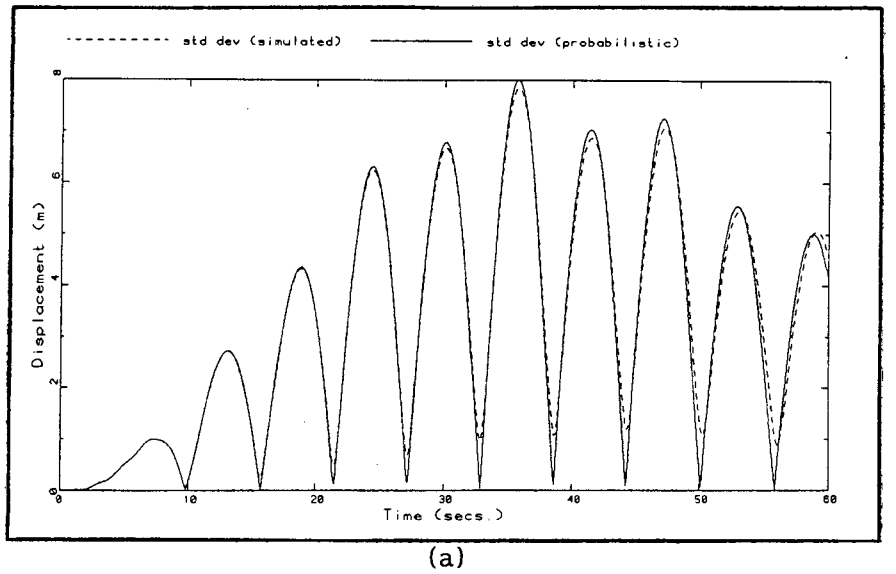

(a)

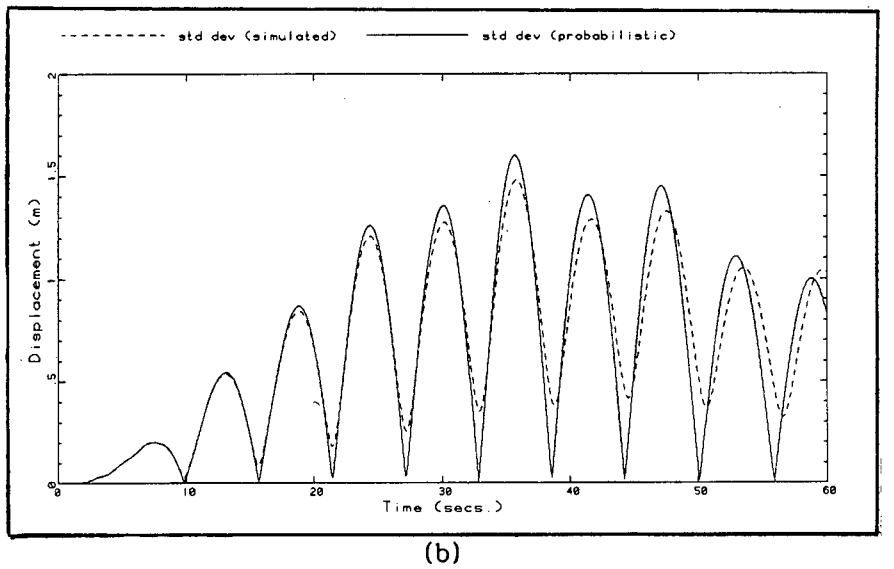

(b)

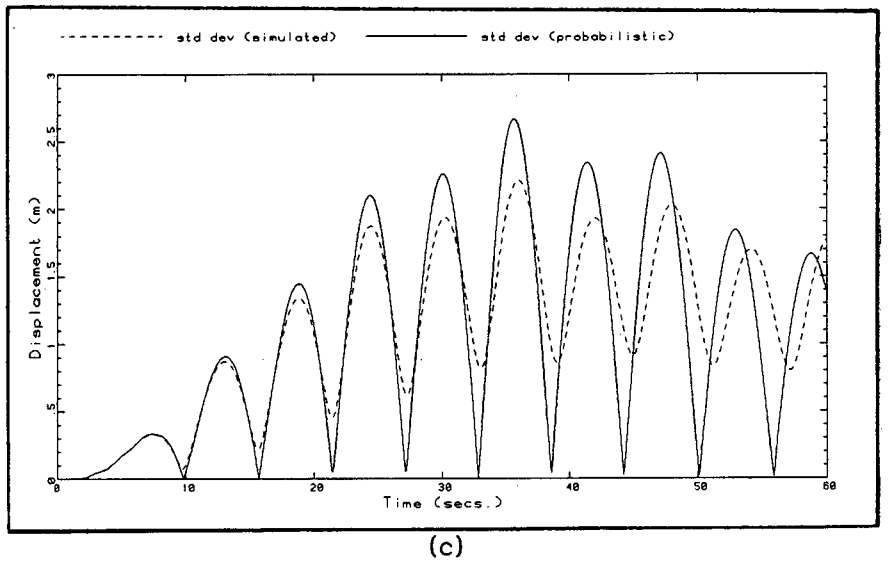

(c)

Figure 4.6.6: The sensitivity of the standard deviations of the response with respect to the uncertainty in the inertia coefficient (Var C_D = 0). Horizontal displacement at the top of the pile. (a) c.o.v.≃ 0·1, (b) c.o.v.≃ 0·2, (c) c.o.v.≃ 0·$\dot{3}$.

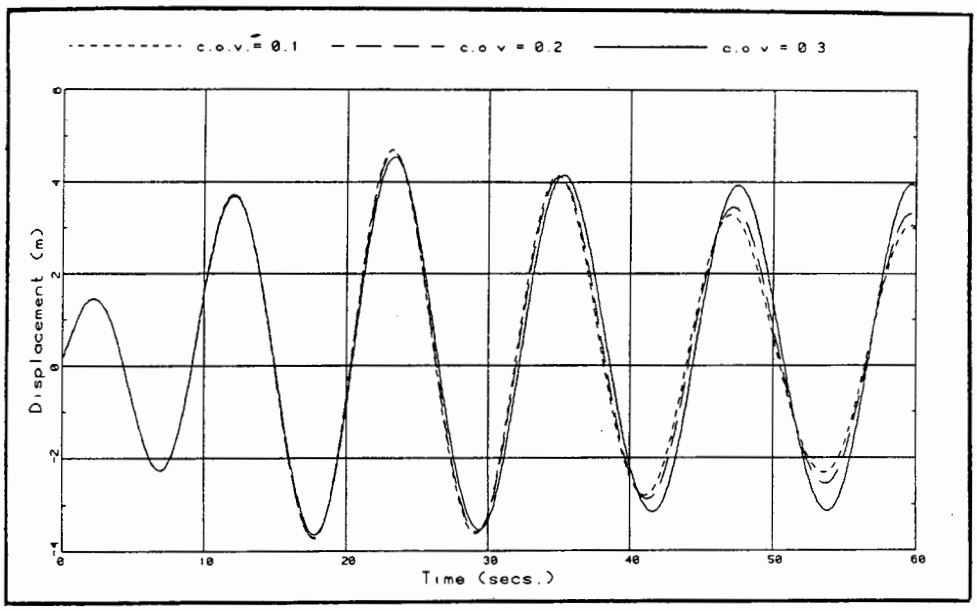

Figure 4.6.7: The sensitivity of the mean response with respect to uncertainty in the inertia coefficient (Var C_D = 0). Results obtained by PFEM.

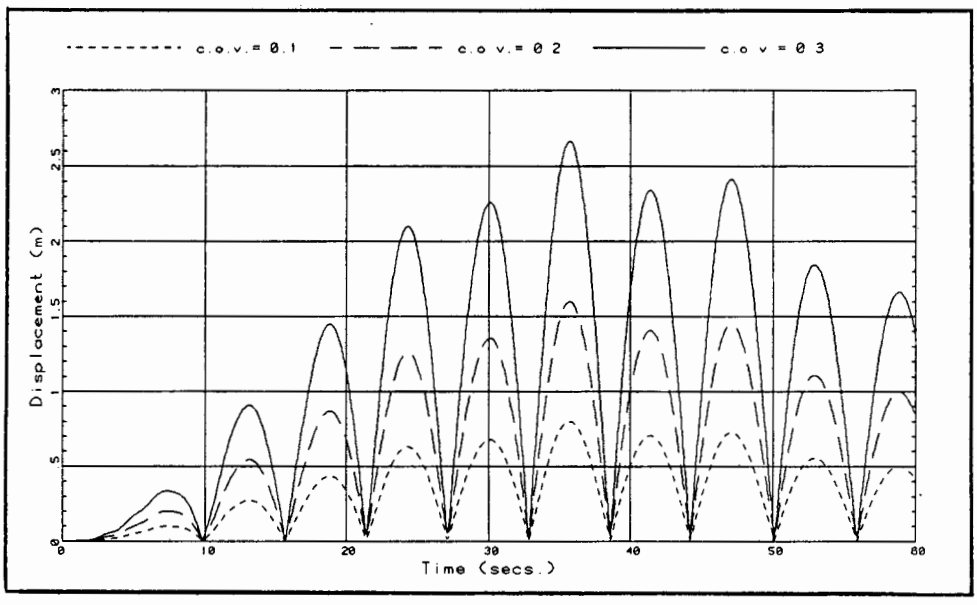

Figure 4.6.8: The sensitivity of the standard deviations with respect to the uncertainty in the inertia coefficient (Var C_D = 0). Results obtained by PFEM.

The c.o.v. of both C_D and C_M values were increased from 0·1 to 0·$\dot{3}$ (approx.) next. The comparative results of the PFEM and MCS for the mean response is given in Figure 4.6.9 and that for the standard deviation of the reponse appear in Figure 4.6.10. The accuracy of the PFEM remains very good for the mean response, even at larger values of c.o.v., but the 1^{st} order approximation of the standard deviation is evidently insufficient at a c.o.v. of 0·$\dot{3}$ when the errors can be as large as 26% . From the previous results, it is predictable that the approximation of the standard deviations by the PFEM will have a trend from being non-conservative to a conservative estimate with increasing variance of input values. It is also observed that the standard deviations are never zero here. From inspection of eqn ($\mathcal{B}15a$), it is clear that for the previous results where either Var C_D or Var C_M was zero, the variance of displacement will be zero when $\overline{\frac{\partial \mathbf{d}}{\partial C_M}}$ or $\overline{\frac{\partial \mathbf{d}}{\partial C_D}}$ (respectively) becomes zero. This situation occurs at different times for the two cases mentioned above, resulting in the standard deviation never being zero when neither the variances of C_D and C_M are zero.

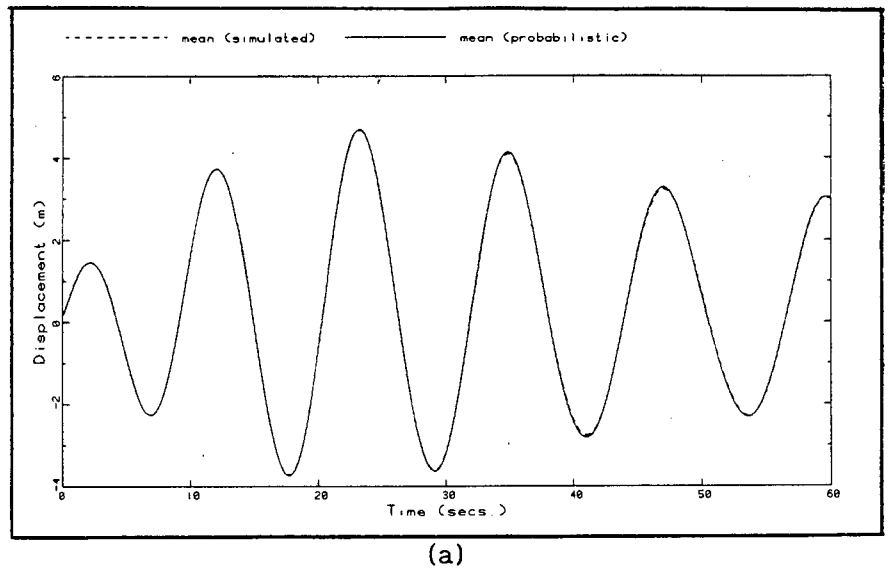

(a)

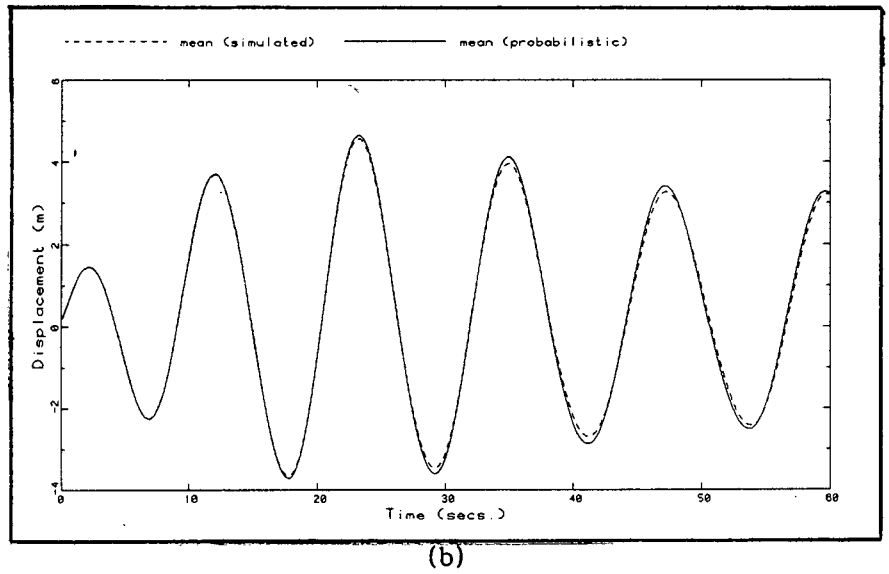

(b)

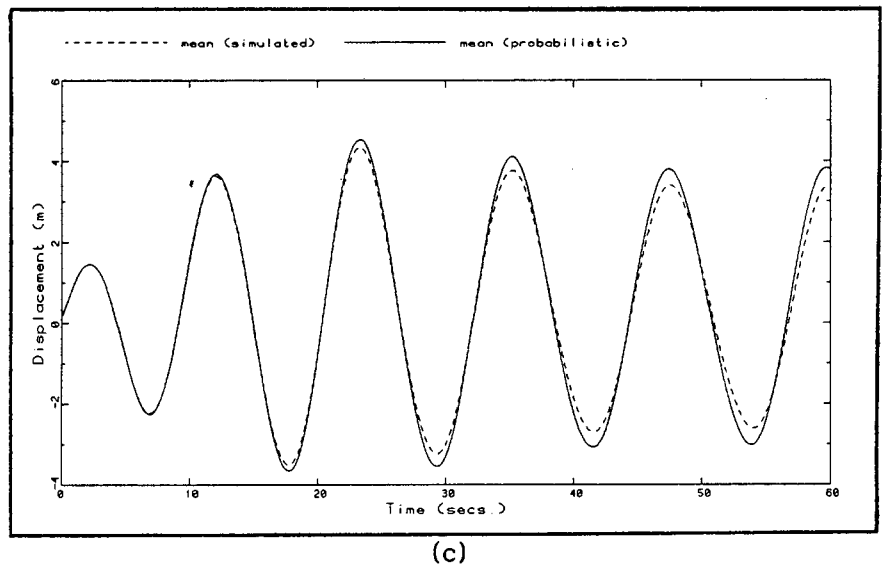

(c)

Figure 4.6.9: The mean response calculated by PFEM and MCS. Horizontal displacement at the top of the pile.
(a) c.o.v.≃ 0·1, (b) c.o.v.≃ 0·2, (c) c.o.v.≃ 0·3̇, for both C_D and C_M .

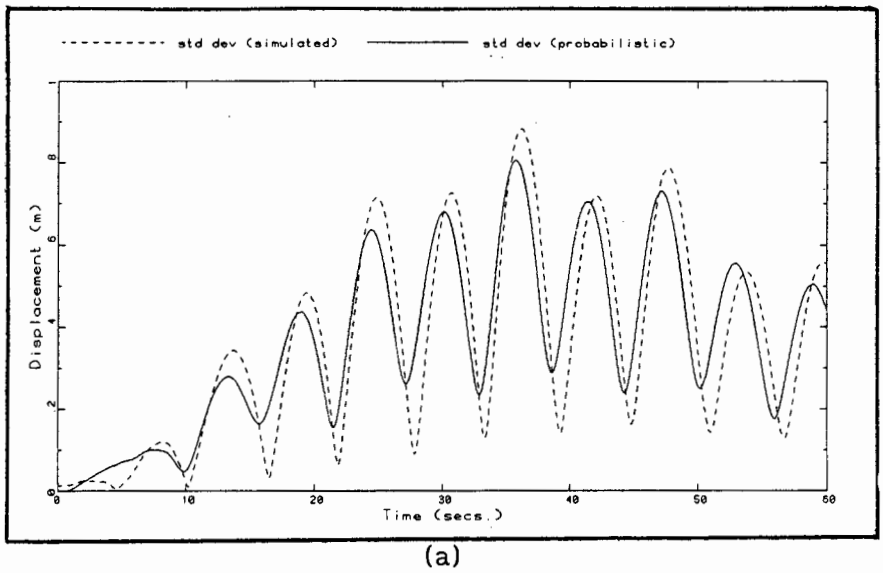

(a)

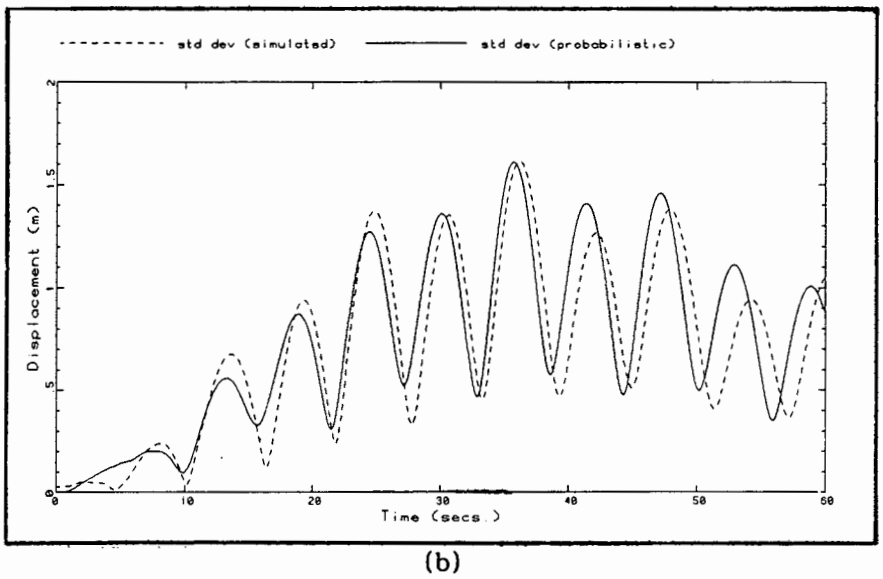

(b)

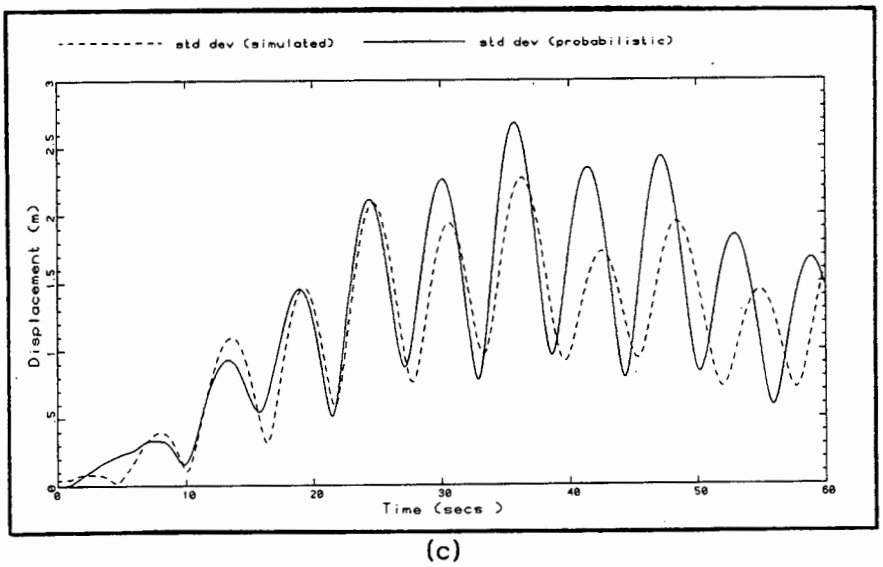

(c)

Figure 4.6.10: The standard deviations of the response calculated by PFEM and MCS. Horizontal displacement at the top of the pile.(a) c.o.v.≃ 0·1, (b) c.o.v.≃ 0·2, (c) c.o.v.≃ 0·3, for both C_D and C_M .

For the maximum c.o.v. of C_D and C_M values, the bounds of the displacement at the top of the pile were estimated. Assuming that the distribution of these displacements (due to the uncertainty in C_D and C_M values) is normal, the bounds with a confidence level of 99·7% (approx.) can be constructed as $\mu \pm 3\sigma$.

From the trends found before, it can be predicted that these bounds calculated by the PFEM will be conservative at larger times and larger values of c.o.v., and this is clear from Figure 4.6.11 and Figure 4.6.12 which show the upper and lower bounds respectively.

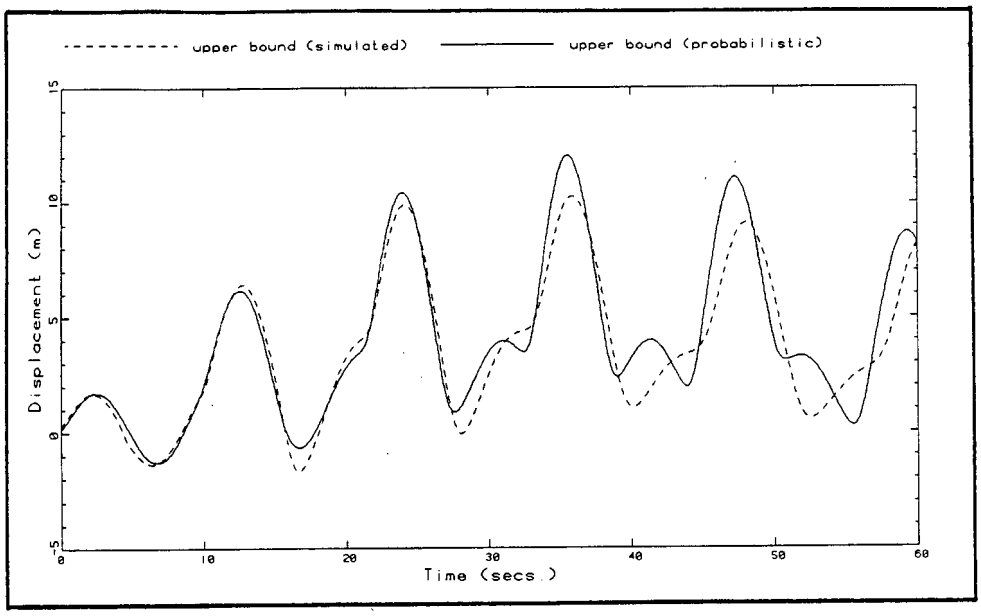

Figure 4.6.11: The upper bound of the horizontal displacement at the top of the pile (c.o.v.≃ $0\cdot\dot{3}$ for both C_D and C_M).

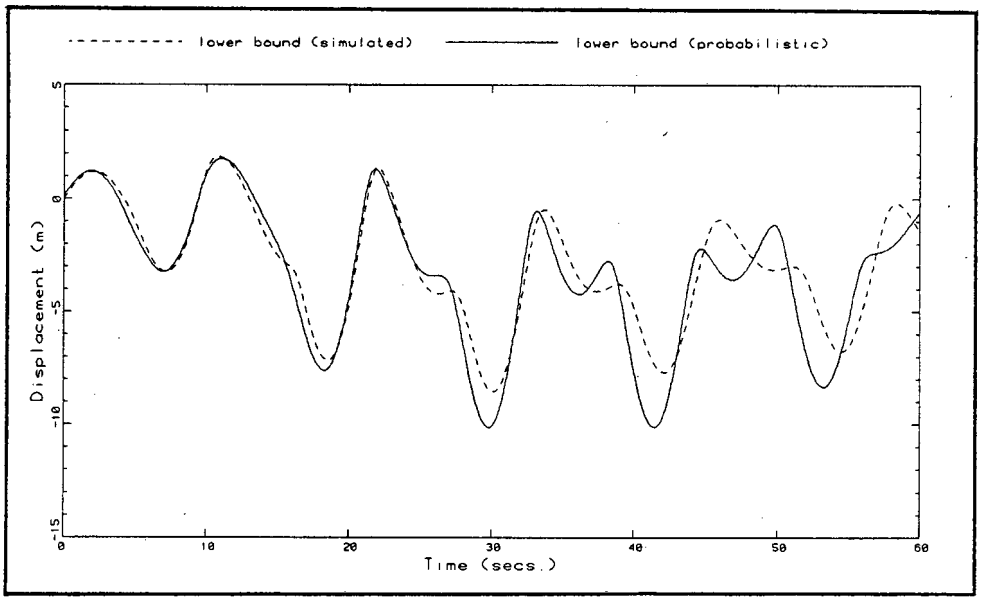

Figure 4.6.12: The lower bound of the horizontal displacement at the top of the pile (c.o.v.≃ $0\cdot\dot{3}$ for both C_D and C_M).

The distribution of the displacements was investigated at six stations in the time history during the MCS run. At the 10 second station (see Figure 4.6.13) the distribution is clearly not normal and the bounds estimated above should be rather tight. This is indeed the case if Figure 4.6.14 and Figure 4.6.15 are scrutinised. At the other stations in time, the distribution of the displacements varied from being very skew to being almost uniform. It can be concluded that the bounds shown in Figure 4.6.14 and Figure 4.6.15 are not representative of any particular confidence level.

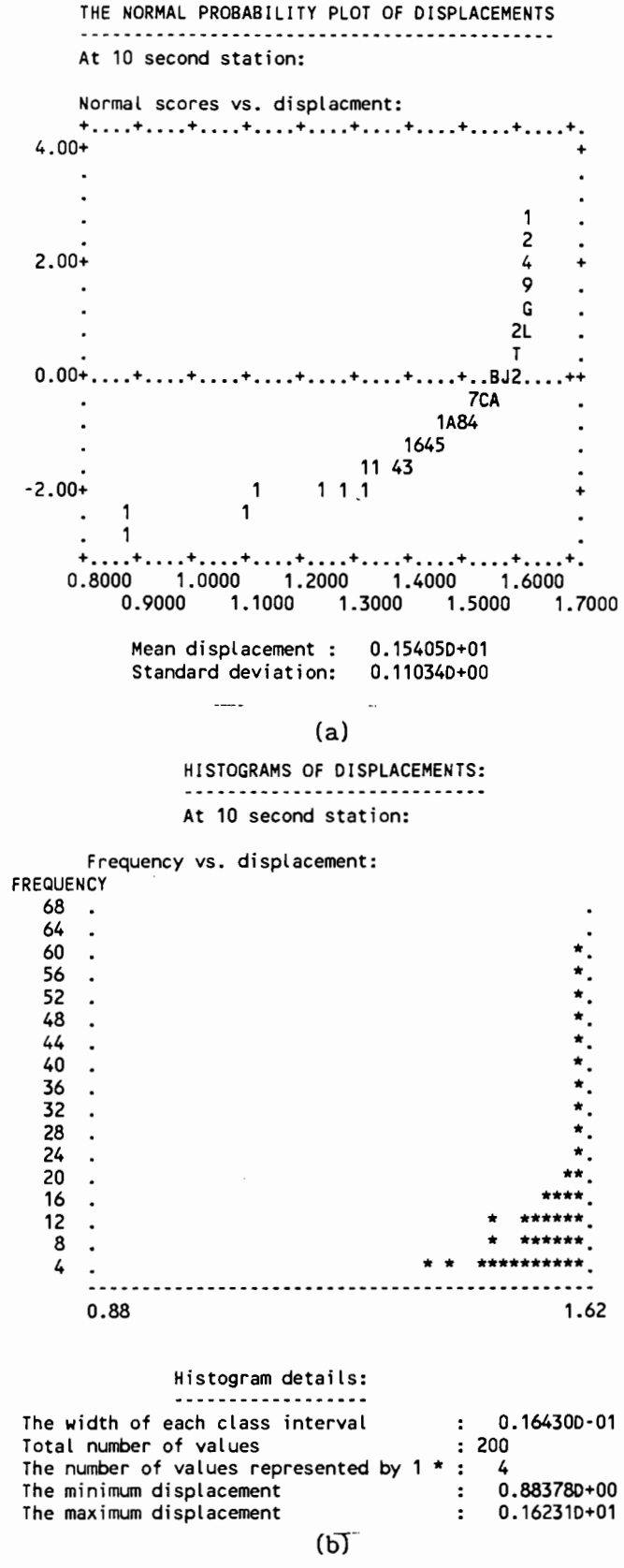

Figure 4.6.13: The distribution of the displacement at the top of the pile at 10 second station. (a) Normal probability plot: 1 - 9 indicates 1 - 9 observations, A - Z indicates 10 - 35 observations; (b) Histogram.

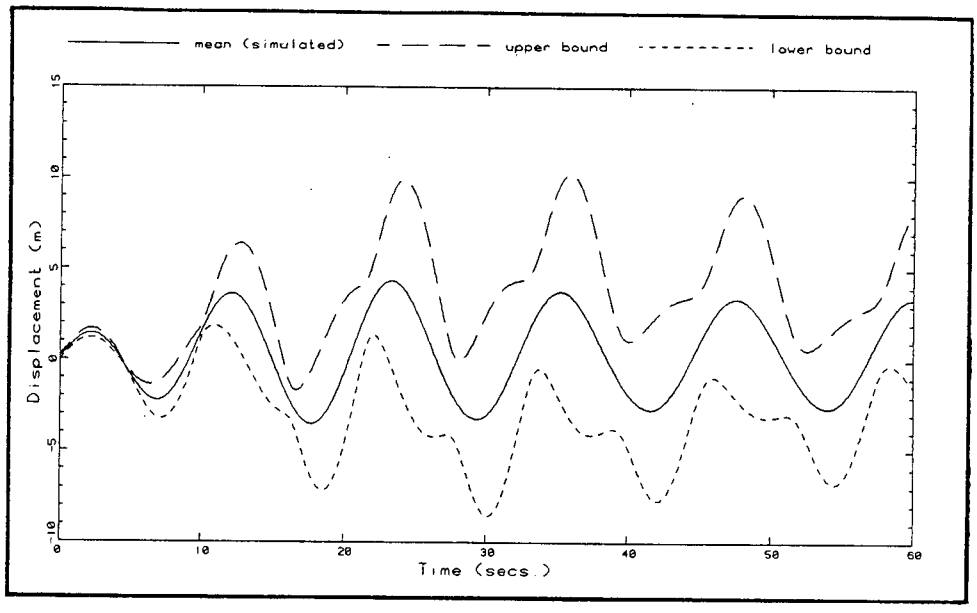

Figure 4.6.14: Bounds for the displacement at the top of the pile as found by MCS (c.o.v.$\simeq 0{\cdot}\dot{3}$ for both C_D and C_M).

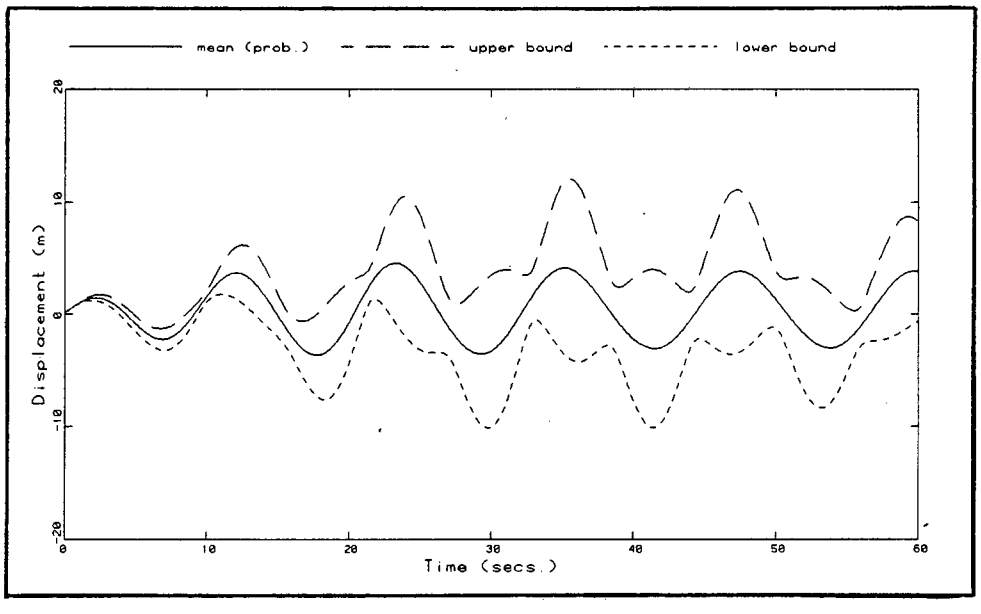

Figure 4.6.15: Bounds for the displacement at the top of the pile as found by the PFEM (c.o.v.$\simeq 0{\cdot}\dot{3}$ for both C_D and C_M).

4.6.2: Input values from a uniform distribution.

The range of the input values of C_D and C_M with a uniform distribution corresponds to 6σ of the values taken from the normal distribution in section 4.6.1. (See section 4.4). Hence, the minimum and maximum values of the input as found in the previous section would be very similar to the corresponding investigation in this section. An immediate consequence of this is that the standard deviations of the input values of C_D and C_M with a uniform distribution will be greater than those found for a normal distribution, and it can be predicted that the results of the PFEM will be less accurate here than that compared in section 4.6.1.

This fact is borne out if Figure 4.6.21 and Figure 4.6.22 (the mean response and standard deviations) are compared to Figure 4.6.1 and Figure 4.6.2. Although the approximation of the PFEM is still very good, it is less accurate than that found before. The same trends, however, are observed. (Compare the Figures 4.6.23 to 4.6.32 to Figures 4.6.3 to 4.6.12, respectively.) The standard deviations of the response is significantly higher when the input values over the same range are taken from a uniform distribution, and the approximation of the mean response is consistently worse.

The distribution of the displacements at the top of the pile at 6 stations in time were again investigated. It is noted that the distributions are more normal than those found with normally distributed input values (see Figure 4.6.33) and it can be concluded that the bounds of the horizontal displacements at the top of the pile, shown in Figure 4.6.34 and Figure 4.6.35 are more representative of the 99·7% confidence level.

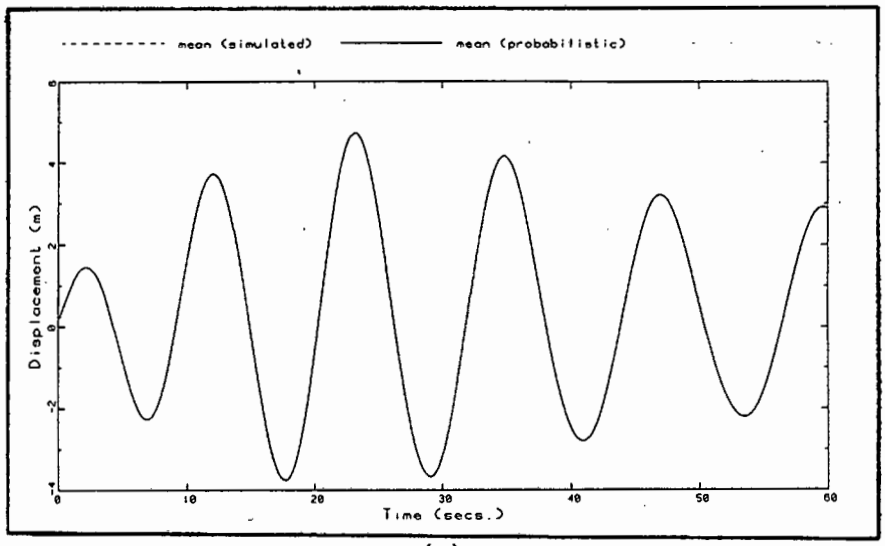

(a)

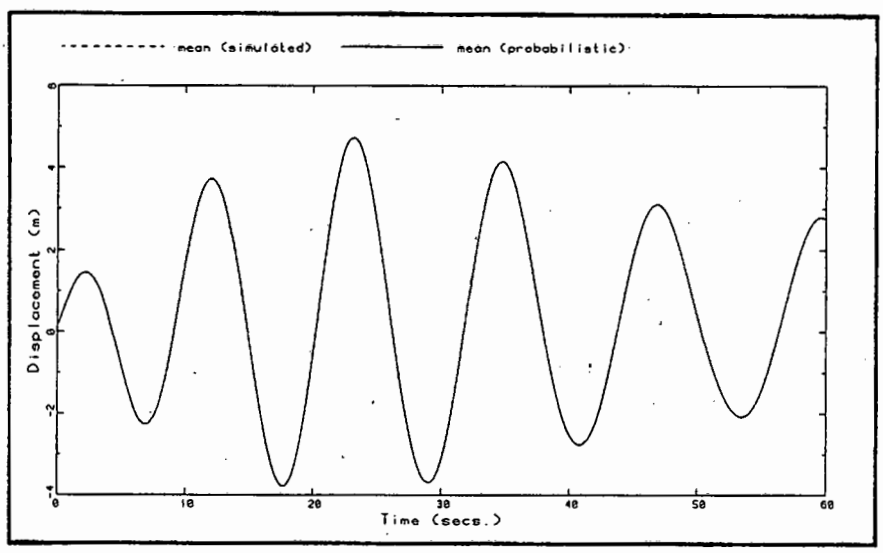

(b)

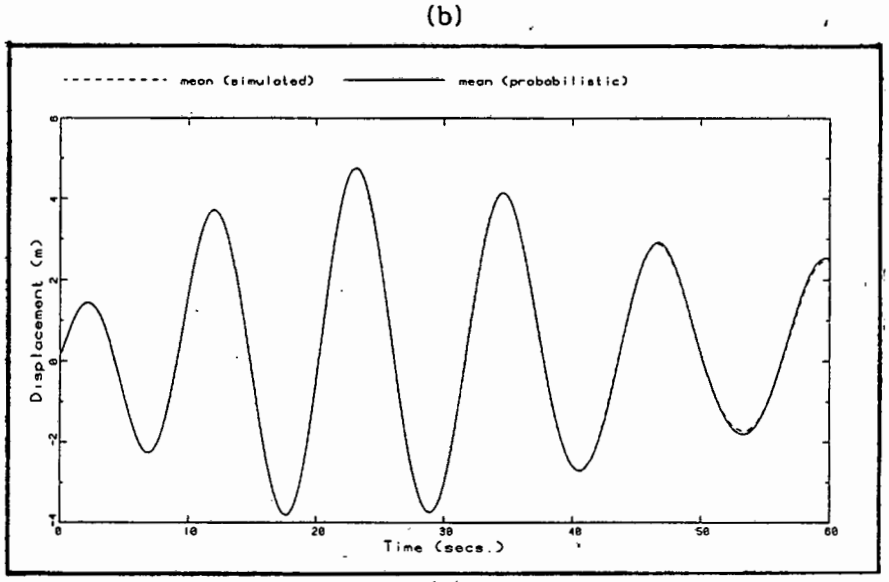

(c)

Figure 4.6.21: The sensitivity of the mean response with respect to the uncertainty in the drag coefficient (Var C_M = 0). Horizontal displacement at the top of the pile.
(a) $0{\cdot}371 < C_D < 0{\cdot}689$, (b) $0{\cdot}212 < C_D < 0{\cdot}848$, (c) $0 < C_D < 1{\cdot}06$

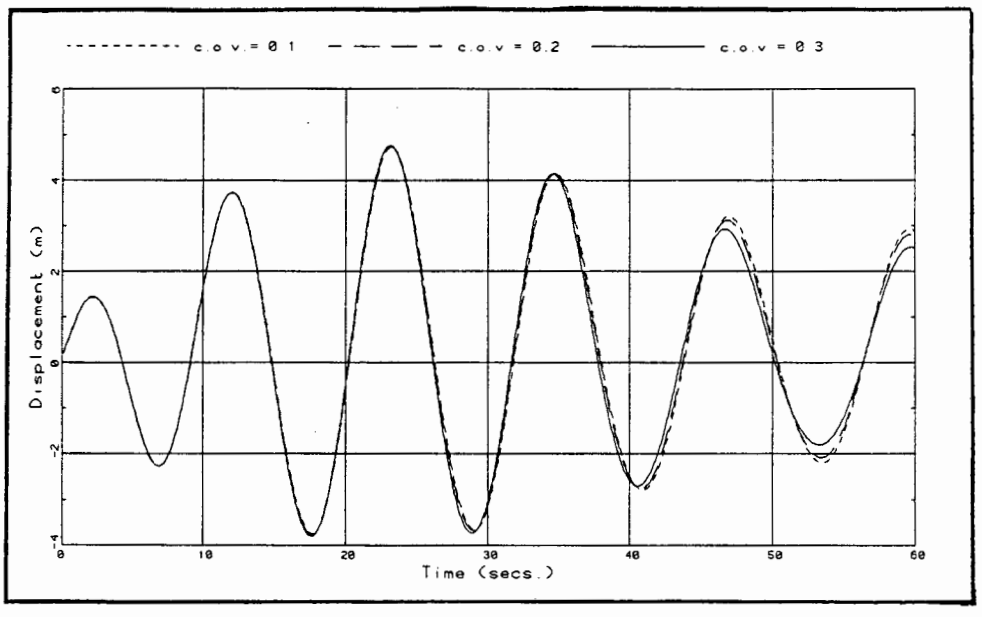

Figure 4.6.23: The sensitivity of the mean response with respect to the uncertainty in the drag coefficient (Var C_M = 0). Results obtained by the PFEM.

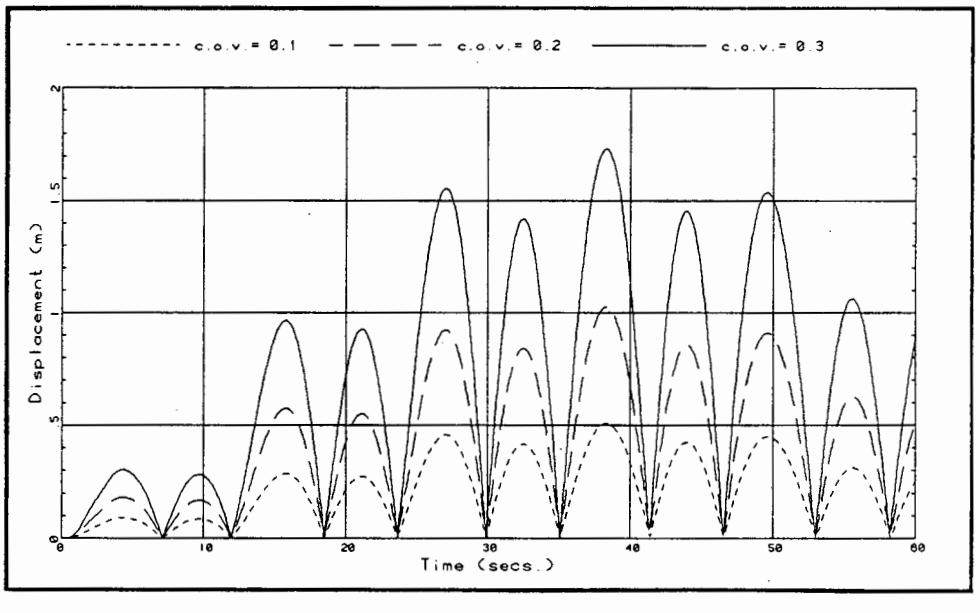

Figure 4.6.24: The sensitivity of the standard deviations of the response with respect to the uncertainty in the drag coefficient (Var C_M = 0). Results obtained by the PFEM.

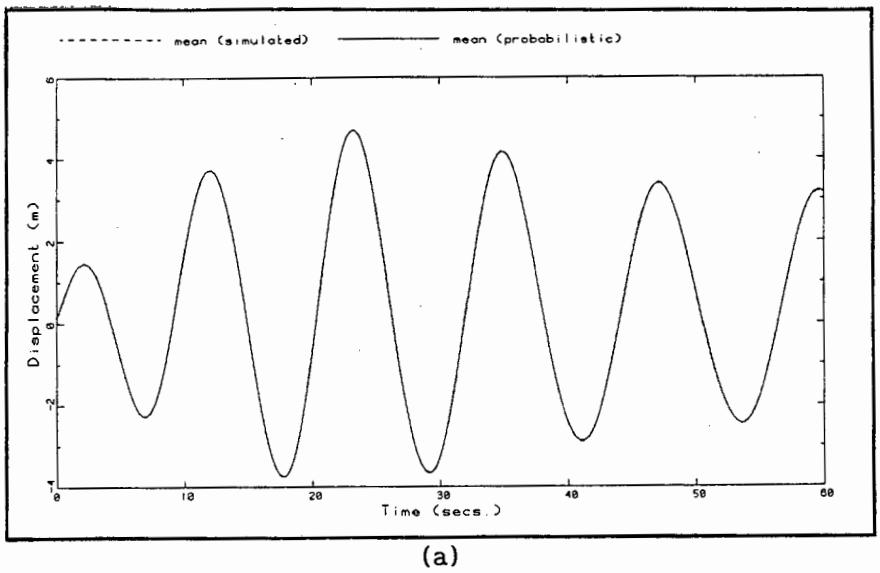

(a)

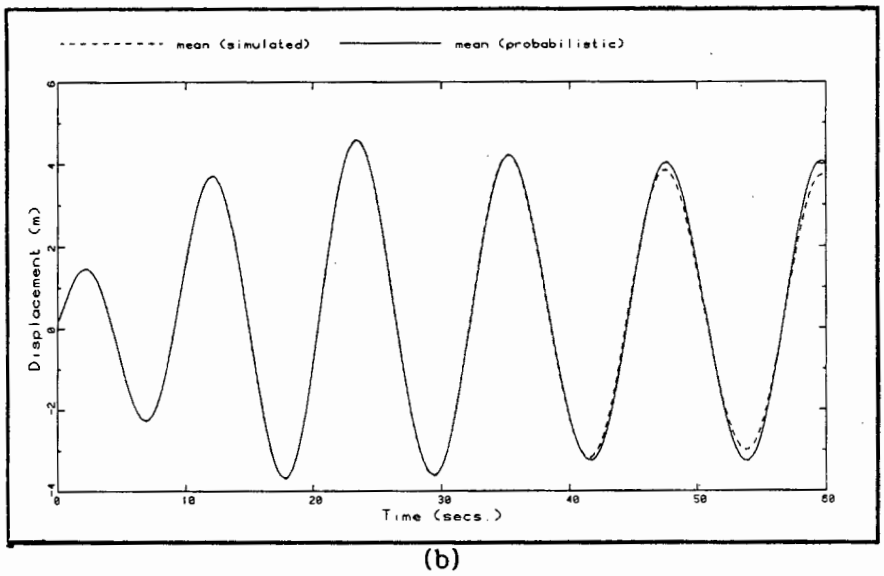

(b)

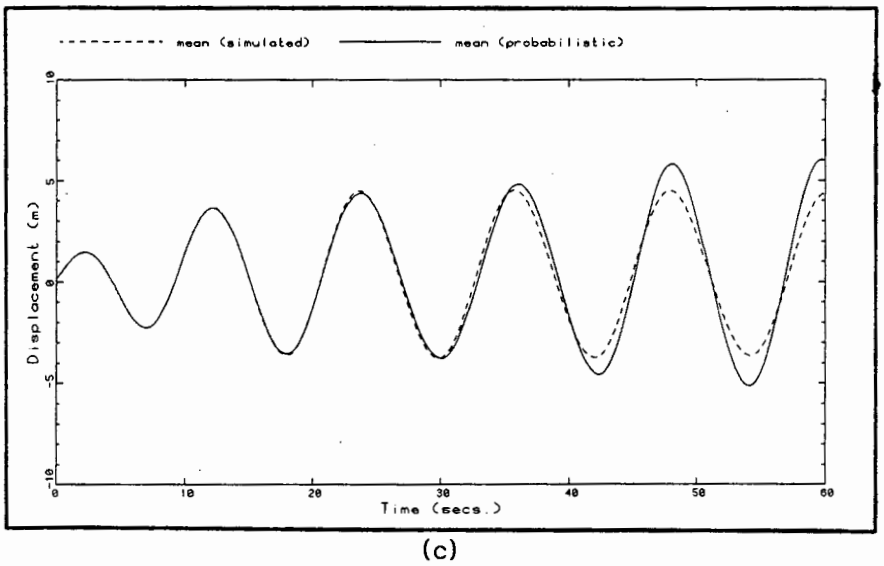

(c)

Figure 4.6.25: The sensitivity of the mean response with respect to the uncertainty in the inertia coefficient (Var C_D = 0). Horizontal displacement at the top of the pile.
(a) $1 \cdot 029 < C_M < 1 \cdot 911$, (b) $0 \cdot 588 < C_M < 2 \cdot 352$, (c) $0 < C_M < 2 \cdot 94$

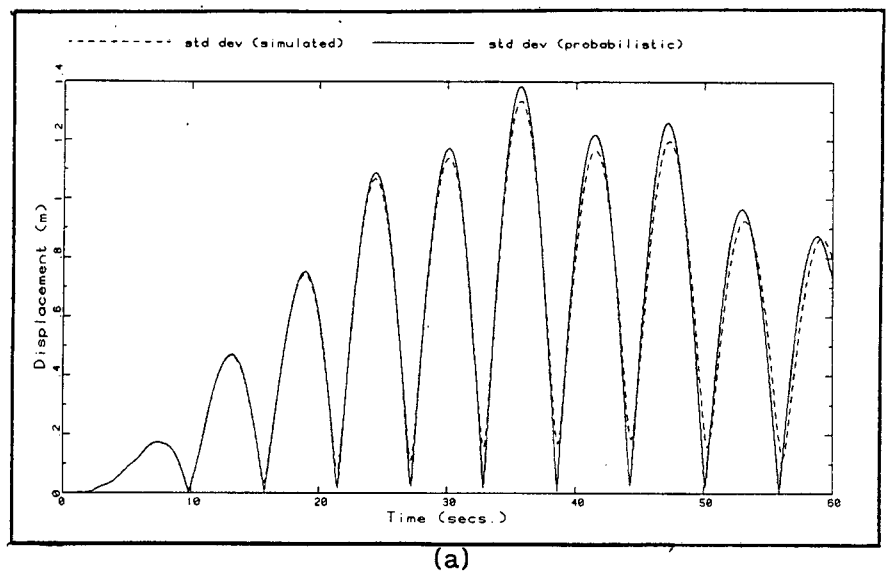

(a)

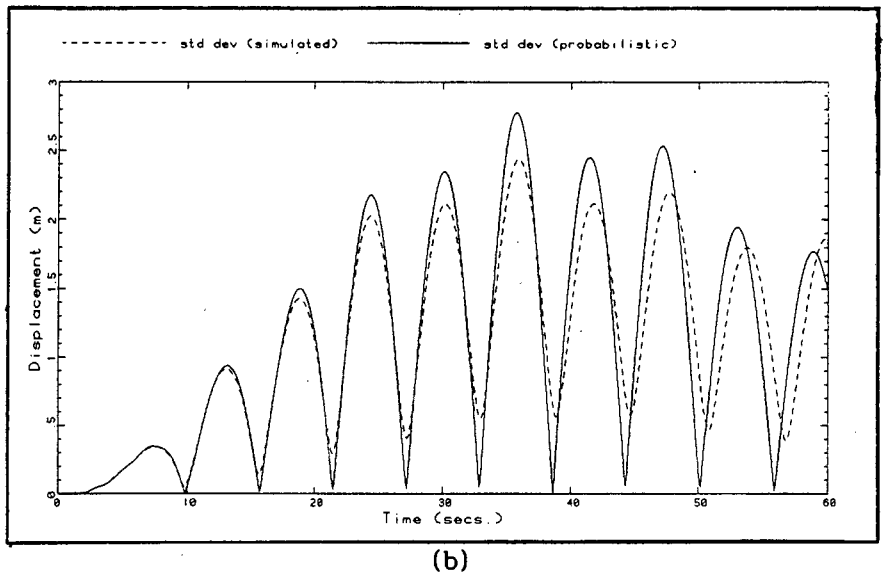

(b)

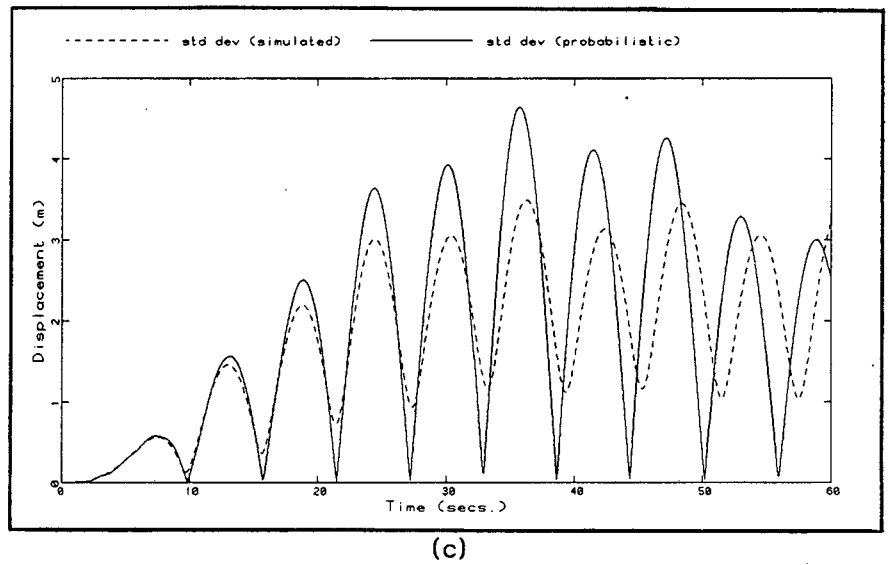

(c)

Figure 4.6.26: The sensitivity of the standard deviations of the response with respect to the uncertainty in the inertia coefficient (Var C_D = 0). Horizontal displacement at the top of the pile. (a) 1·029 < C_M < 1·911, (b) 0·588 < C_M < 2·352, (c) 0 < C_M < 2·94

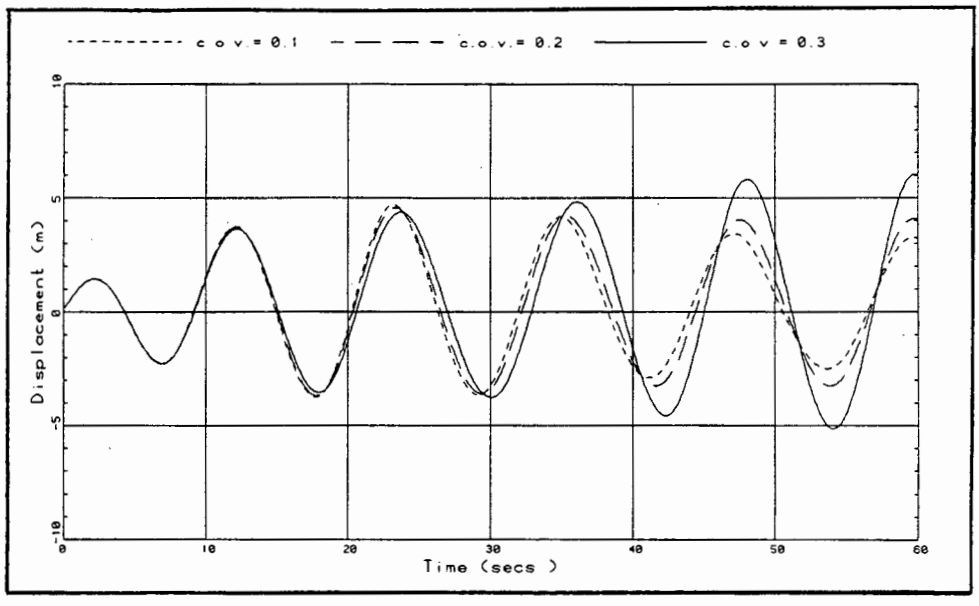

Figure 4.6.27: The sensitivity of the mean response with respect to the uncertainty in the inertia coefficient (Var C_D = 0). Results obtained by PFEM.

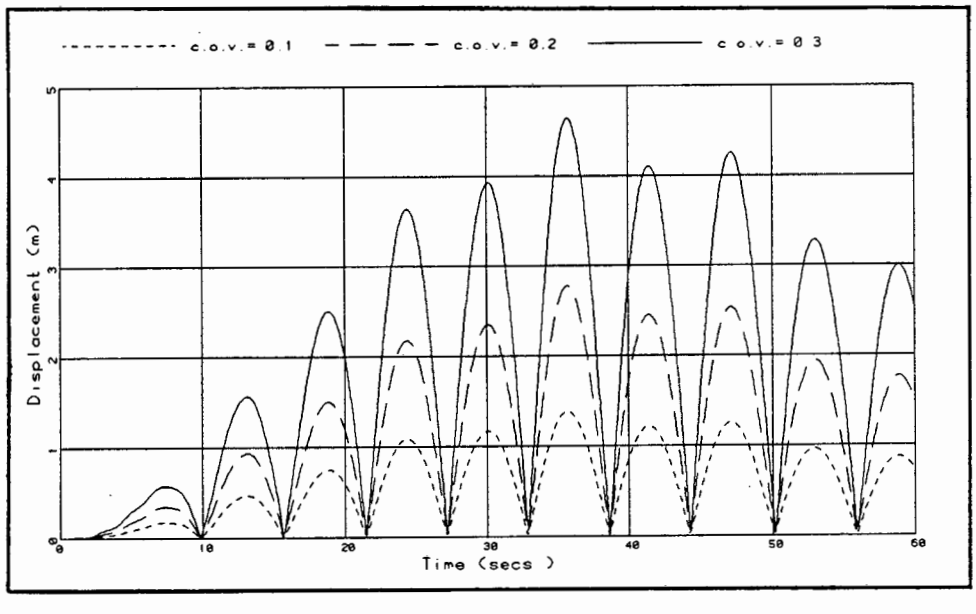

Figure 4.6.28: The sensitivity of the standard deviations of the response with respect to the uncertainty in the inertia coefficient (Var C_D = 0). Results obtained by PFEM.

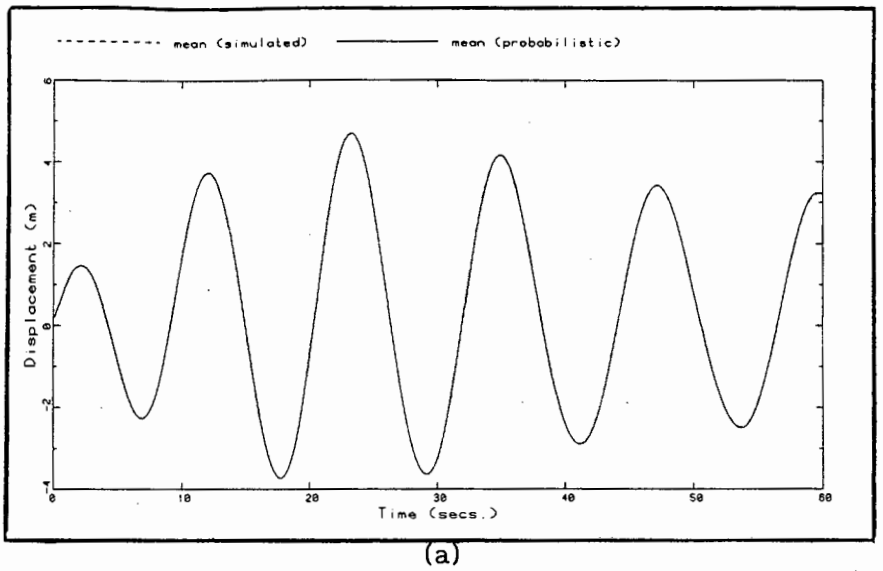

(a)

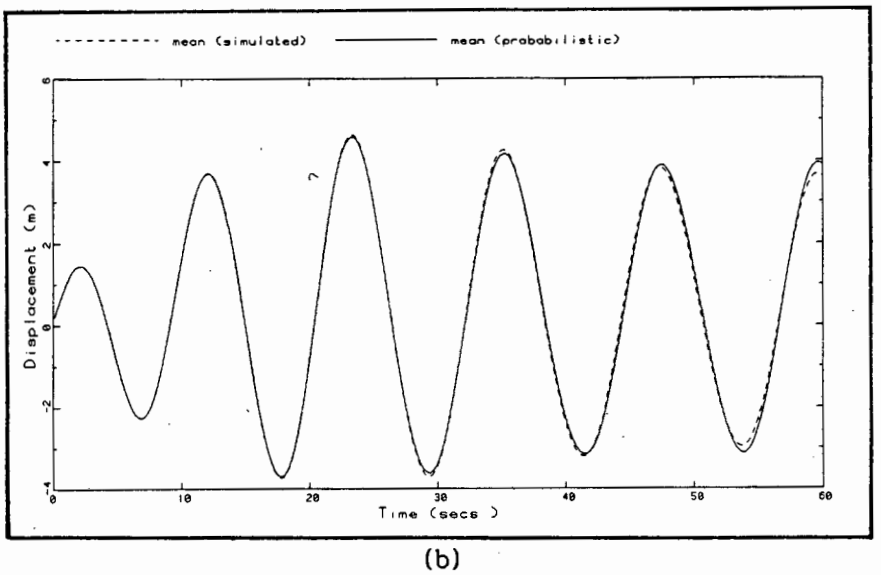

(b)

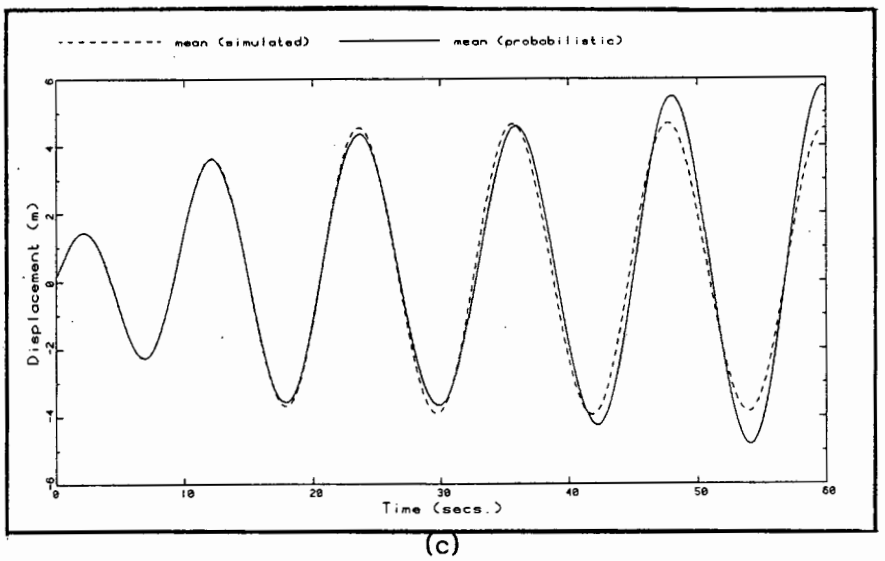

(c)

Figure 4.6.29: The mean response calculated by PFEM and MCS. Horizontal displacement at the top of the pile.

(a) $\begin{cases} 0{\cdot}371 < C_D < 0{\cdot}689 \\ 1{\cdot}029 < C_M < 1{\cdot}911 \end{cases}$ (b) $\begin{cases} 0{\cdot}212 < C_D < 0{\cdot}848 \\ 0{\cdot}588 < C_M < 2{\cdot}352 \end{cases}$ (c) $\begin{cases} 0 < C_D < 1{\cdot}06 \\ 0 < C_M < 2{\cdot}94 \end{cases}$

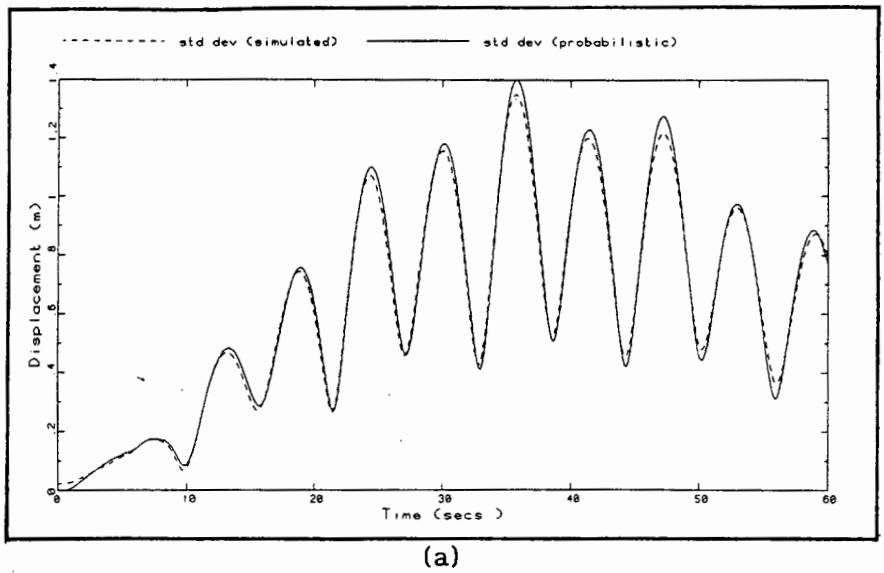

(a)

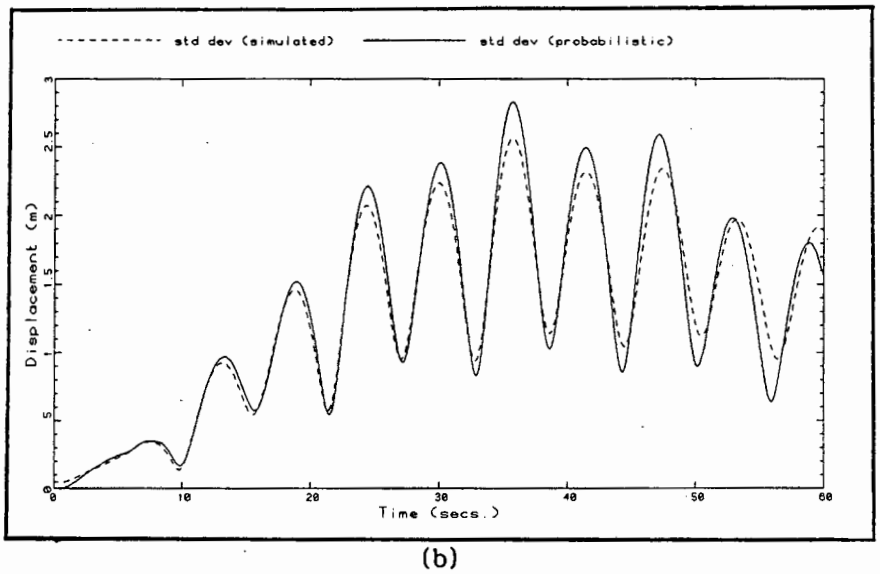

(b)

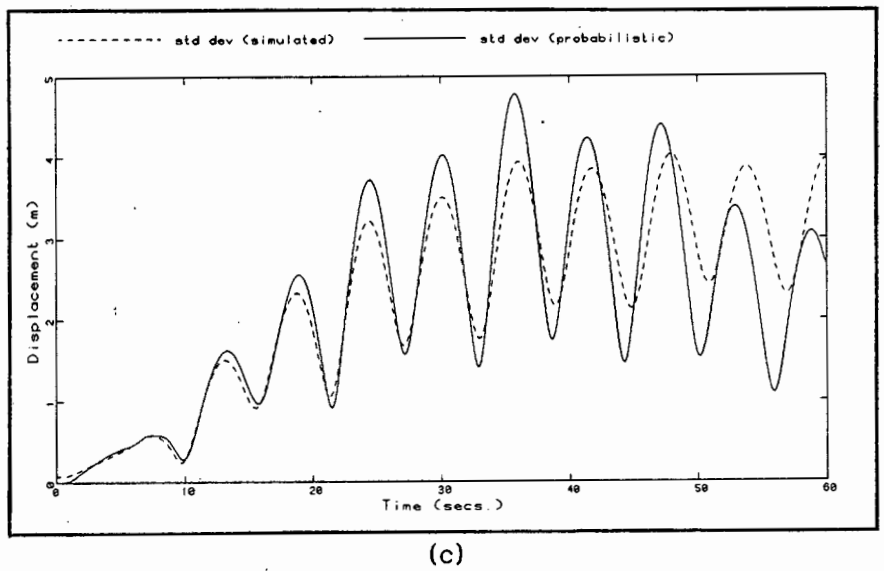

(c)

Figure 4.6.30: The standard deviations of the response calculated by PFEM and MCS. Horizontal displacement at the top of the pile.

(a) $\begin{cases} 0{\cdot}371 < C_D < 0{\cdot}689 \\ 1{\cdot}029 < C_M < 1{\cdot}911 \end{cases}$ (b) $\begin{cases} 0{\cdot}212 < C_D < 0{\cdot}848 \\ 0{\cdot}588 < C_M < 2{\cdot}352 \end{cases}$ (c) $\begin{cases} 0 < C_D < 1{\cdot}06 \\ 0 < C_M < 2{\cdot}94 \end{cases}$

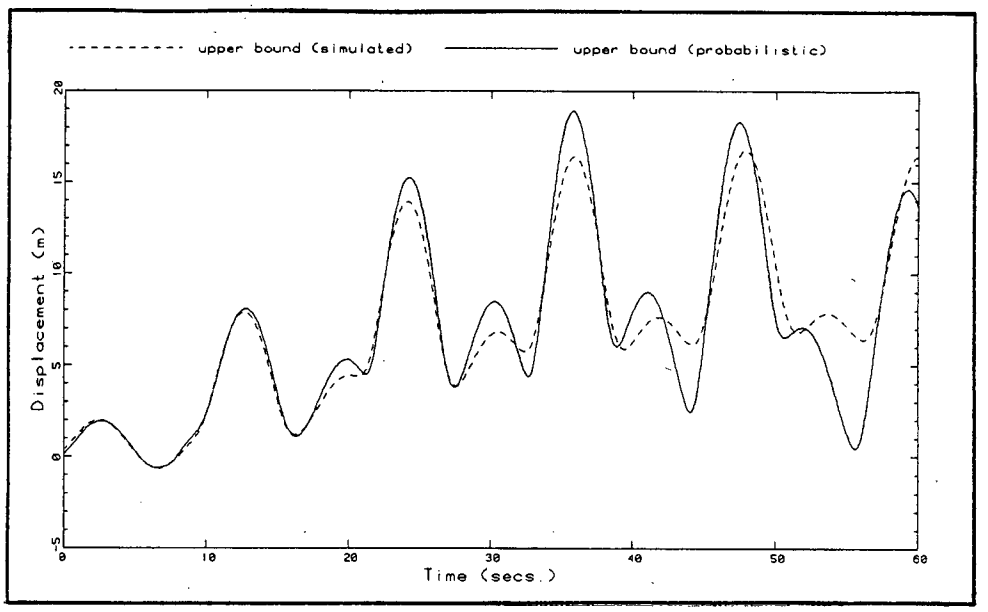

Figure 4.6.31: The upper bound of the horizontal displacement at the top of the pile ($0 < C_D < 1{\cdot}06$; $0 < C_M < 2{\cdot}94$).

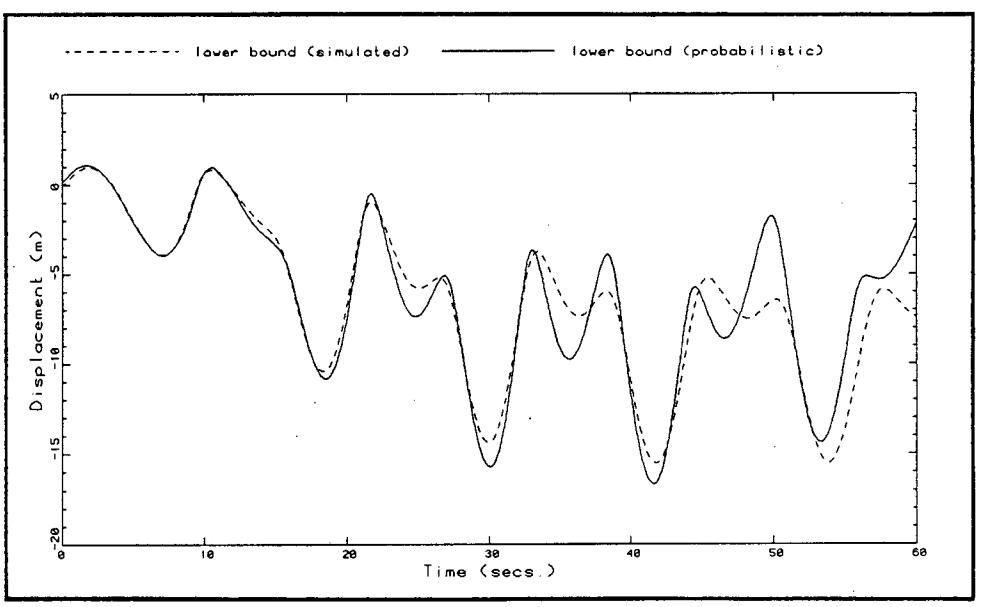

Figure 4.6.32: The lower bound of the horizontal displacement at the top of the pile ($0 < C_D < 1{\cdot}06$; $0 < C_M < 2{\cdot}94$).

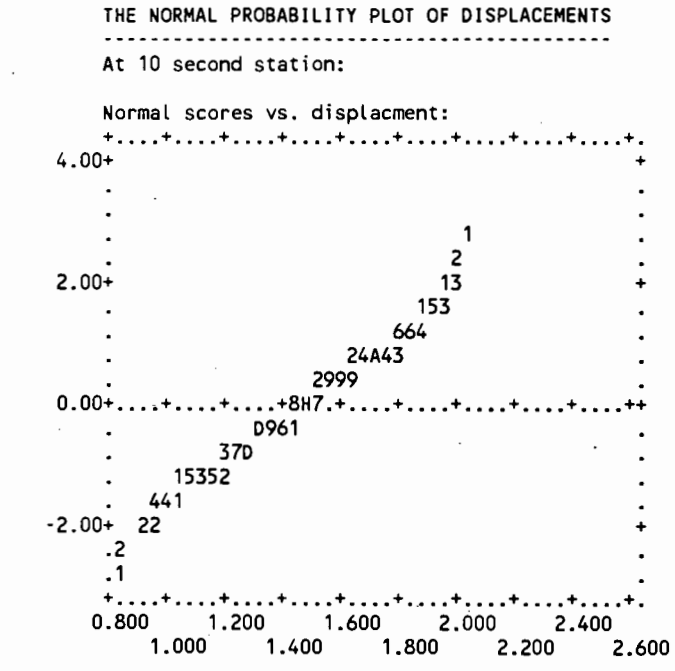

(a)

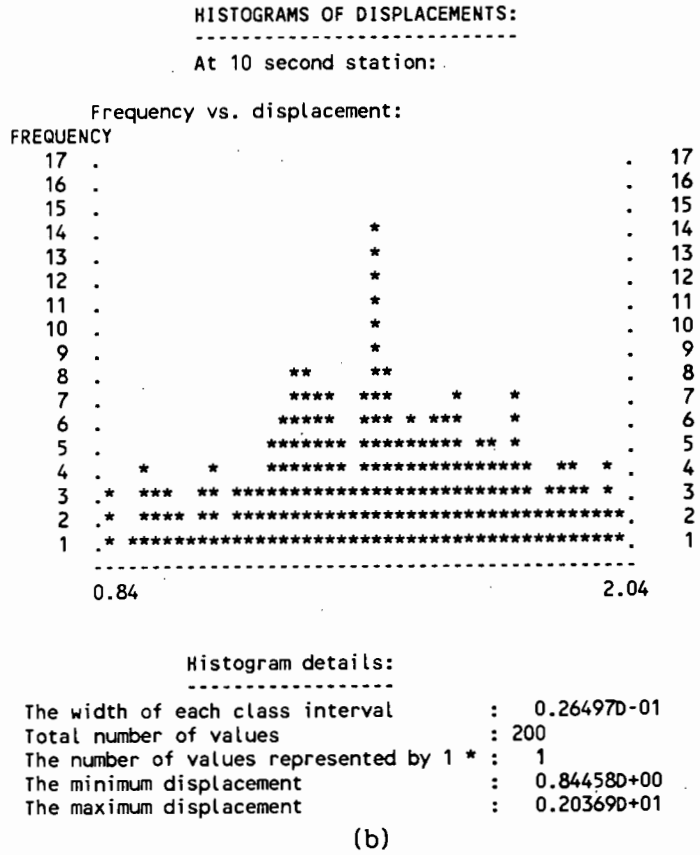

Histogram details:

The width of each class interval	: 0.26497D-01
Total number of values	: 200
The number of values represented by 1 *	: 1
The minimum displacement	: 0.84458D+00
The maximum displacement	: 0.20369D+01

(b)

Figure 4.6.33: The distribution of the displacement at the top of the pile at 10 second station. (a) Normal probability plot: 1 - 9 indicates 1 - 9 observations, A - Z indicates 10 - 35 observations; (b) Histogram.

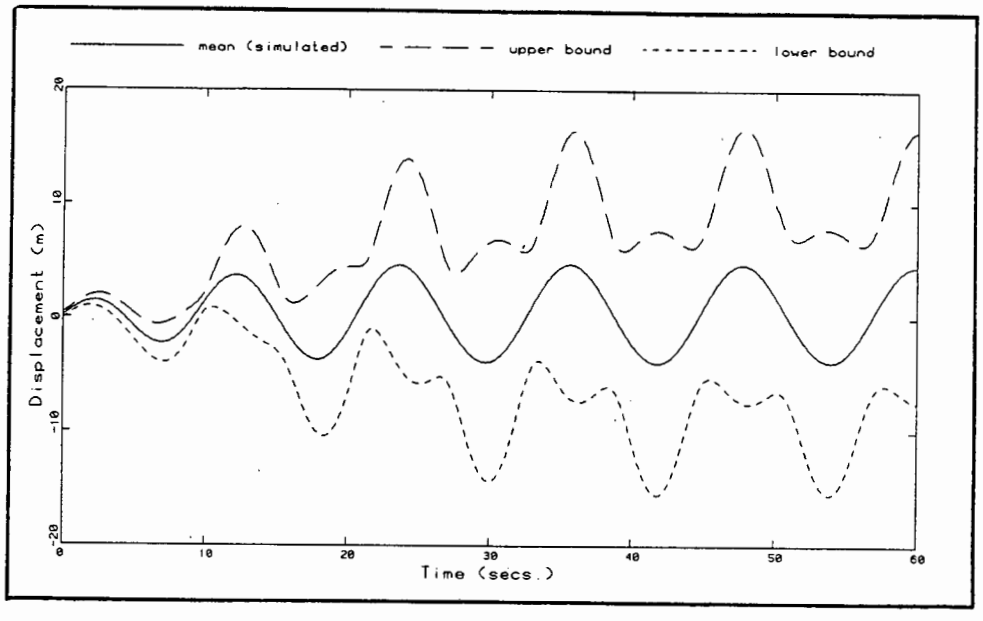

Figure 4.6.34: Bounds for the horizontal displacement at the top of the pile as found by MCS ($0 < C_D < 1{\cdot}06$; $0 < C_M < 2{\cdot}94$).

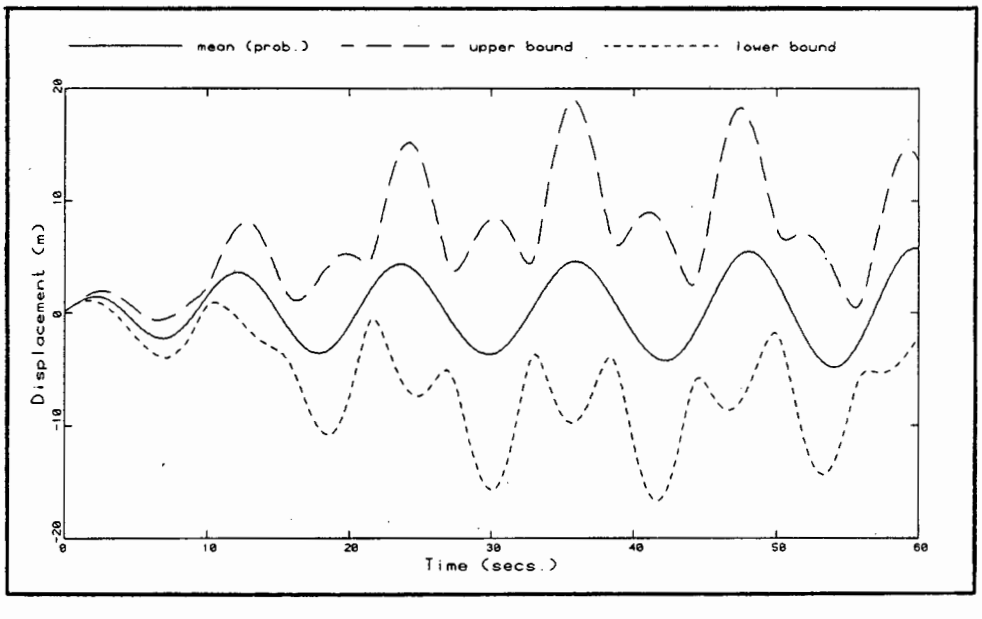

Figure 4.6.35: Bounds for the horizontal displacement at the top of the pile as found by PFEM ($0 < C_D < 1{\cdot}06$; $0 < C_M < 2{\cdot}94$).

5. Conclusion and Recommendation

In Chapter 2, the capability of the ABAQUS finite element package to analyse structural dynamic problems in the ocean in general, and the behaviour of the undriven pile in particular, has been successfully demonstrated. The program has many useful features for these types of problems but the combination of several of them is not always straightforward. Although the input data decks (see Appendix A) appear deceptively simple, the process of achieving acceptable results for the dynamic response of a model with gap elements in the water can be a tedious one. It is the model which simulates the pile guide with gap elements which is not only the superior of the two models developed as far as the accuracy of the model is concerned, but also shows that a very conservative result is arrived at by excluding these gaps. Several users have experienced some kind of problem with dynamic analyses in the sea when the model contains gap elements. The AQUA subprogram is computationally demanding and the teething problems developing a model which invokes this routine could make the finite element analysis very expensive.

While many of the limitations of the ABAQUS program could either be tolerated or modelled in an alternative way, a remaining drawback is the inability of the user to access the structure variables (for example the velocities) via the user subroutines. If this were possible, one could avail oneself of the modal techniques present in version 4-8 of the program by linearising the force vector. Not only would many more features of ABAQUS be available for the dynamic analyses of structures in the ocean (especially with respect to uncertainty analyses), but the time consuming implicit direct integration scheme might be avoided. Furthermore, the need for developing the geometrically linear model of Chapter 3 could be obviated by building the probabilistic finite element method (PFEM) around ABAQUS.

The PFEM has been applied to the problem of the dynamic response of a pile having just been placed in the pile guide of an offshore jacket structure. Large displacements are not considered, but the problem remains non-linear due to the drag loading. Uncertainty in the drag and inertia coefficients of the Morison equation is the only source of statistical variation considered.

The effects of secularities in the perturbed equations were observed but the means of removing these effects were kept as simple as possible: 1% structural damping was included in the system equations.

The PFEM is shown to give adequate results for the probabilistic response quantities of interest, as compared with a Monte Carlo simulation. The uncertainty in the drag and the inertia coefficients should be minimised (preferably to the point where the coefficients of variation of these random values are less than 20%) by obtaining accurate site conditions or by performing extensive laboratory experiments. The success of perturbation methods relies heavily on these 'small' coefficients of variation of the random parameters.

The geometrically linear finite element model of the pile stick-up problem, on which the PFEM was based in this work, is inaccurate and non-conservative. Now that the applicability of the PFEM has been proven for this problem, a more advanced vehicle is necessary (e.g. Model B of Chapter 2). Although such an analysis will demand a long computer run, the results should be well suited for design purposes.

APPENDICES

APPENDIX A1: ABAQUS INPUT DECK FOR MODEL A

```
**********************************************************************
** Refined model: 18 elements; 2-D analysis;
** Bottom restrained with torsional spring elements;
** Submerged in 105m water;
** Airy wave applied.
**********************************************************************
**----------MODEL DATA INPUT----------
**********************************************************************
**                A. INITIAL CARDS
**********************************************************************
**DATA CHECK
**PREPRINT
**********************************************************************
**                B. NODE POINT DATA
**********************************************************************
*NODE,NSET=PILE
19,0.00,0.00
18,0.00,4.50
17,0.00,9.00
16,0.00,13.50
15,0.00,18.00
14,0.00,23.00
13,0.00,28.00
12,0.00,36.25
11,0.00,44.50
10,0.00,52.75
9,0.00,61.00
8,0.00,72.00
7,0.00,83.00
6,0.00,94.00
5,0.00,105.00
4,0.00,115.00
3,0.00,125.00
2,0.00,135.00
1,0.00,145.00
```

```
********** Node sets
*NSET,NSET=TOP
1
*NSET,NSET=BOTTOM
19
*NSET,NSET=RIM
16
*NSET,NSET=SLEEVE
16,17,18,19
*NSET,NSET=PRINT
5,10,15,SLEEVE,TOP
*NSET,NSET=PLOT
5,TOP
**********************************************************************
**              C. ELEMENT DATA
**********************************************************************
********** Elements for pile
*ELEMENT,TYPE=B23
1,1,2
*ELGEN,ELSET=ABOVE
1,4
*ELEMENT,TYPE=B23
5,5,6
*ELGEN,ELSET=BELOW
5,14
********** Element for torsional restraint at bottom
*ELEMENT,TYPE=SPRING1,ELSET=MUDY
419,19
*ELEMENT,TYPE=SPRING1,ELSET=MUDZ
519,19
********** Element sets
*ELSET,ELSET=PILE
ABOVE,BELOW
*ELSET,ELSET=PRINT
14,15,16,MUDY,MUDZ
*ELSET,ELSET=PLOT1
14,15,16
*ELSET,ELSET=PLOT2
MUDZ
```

```
**********************************************************************
**              D. ELEMENT PROPERTY DATA
**********************************************************************
*BEAM SECTION,MATERIAL=STEEL,SECTION=PIPE,ELSET=ABOVE
1.067,0.06
*BEAM SECTION,MATERIAL=S&W,SECTION=PIPE,ELSET=BELOW
1.067,0.06
*SPRING,ELSET=MUDY
5
1.E20
*SPRING,ELSET=MUDZ
6
2.E8
**********************************************************************
**                E. MATERIAL DATA
**********************************************************************
*MATERIAL,NAME=STEEL
*DENSITY
7850.0
*ELASTIC,TYPE=ISO
2.1E11,0.3
*MATERIAL,NAME=S&W
*DENSITY
16202.6
*ELASTIC,TYPE=ISO
2.1E11,0.3
**********************************************************************
**                G. KINEMATIC CONDITIONS
**********************************************************************
*BOUNDARY
BOTTOM,PINNED
RIM,1
*AQUA
0.0,105.0,9.81,1025.0
0.0,0.0,0.0,0.0
0.0,0.0,0.0,11.9
0.35,0.0,0.0,12.0
0.5,0.0,0.0,33.5
0.5,0.0,0.0,54.0
0.7,0.0,0.0,75.9
```

```
1.0,0.0,0.0,105.0
*WAVE,TYPE=AIRY
2.83,234.5,270.0,1.0
**********************************************************************
**--------------HISTORY DATA INPUT-------------------------------------
**********************************************************************
**                A. PROCEDURES
**********************************************************************
*STEP,NLGEOM
Loading of submerged pile
*STATIC,PTOL=100,MTOL=14500
0.25,1.0
*DLOAD
PILE,GRAV,9.81,0.0,-1.0,0.0
BELOW,PY,35964.3
BELOW,PD,1.0,2.134,0.53,0.0,1.47
************************* PRINTING
*NODE PRINT,NSET=PRINT,FREQUENCY=100
U
*NODE PRINT,NSET=BOTTOM,FREQUENCY=100
RF
*ELPRINT,ELSET=PRINT,FREQUENCY=100
S
*ENDSTEP
**********************************************************************
**                A. PROCEDURES
**********************************************************************
*STEP,NLGEOM,CYCLE=15,INC=4000
Single Airy wave on submerged pile
*DYNAMIC,PTOL=500,MTOL=70000,HAFTOL=0.5E7
0.1,200.0,,0.1
************************ PRINTING
*NODE PRINT,NSET=PRINT,FREQUENCY=0
U
*NODE PRINT,NSET=BOTTOM,FREQUENCY=0
RF
*EL PRINT,ELSET=PRINT,FREQUENCY=0
S
*PRINT,RESIDUAL=NO
```

```
********** POST-PROC.
*NODE FILE,NSET=PLOT
U
*EL FILE,ELSET=PLOT1
S
*EL FILE,ELSET=PLOT2
S,E
*ENDSTEP
```

APPENDIX A2: ABAQUS INPUT DECK FOR MODEL B

```
**************************************************************************
** Refined model: 18 elements; 3-D analysis;
** Cylindrical gap elements;
** Bottom restrained with torsional spring elements;
** Submerged in 105m water;
** Airy wave applied.
**************************************************************************
**---------------MODEL DATA INPUT-----------------------------------
**************************************************************************
**                A. INITIAL CARDS
**************************************************************************
**DATA CHECK
**PREPRINT
**************************************************************************
**                B. NODE POINT DATA
**************************************************************************
*NODE,NSET=PILE
19,0.00,0.00,0.00
18,0.00,0.00,4.50
17,0.00,0.00,9.00
16,0.00,0.00,13.50
15,0.00,0.00,18.00
14,0.00,0.00,23.00
13,0.00,0.00,28.00
12,0.00,0.00,36.25
11,0.00,0.00,44.50
10,0.00,0.00,52.75
9,0.00,0.00,61.00
8,0.00,0.00,72.00
7,0.00,0.00,83.00
6,0.00,0.00,94.00
5,0.00,0.00,105.00
4,0.00,0.00,115.00
3,0.00,0.00,125.00
2,0.00,0.00,135.00
1,0.00,0.00,145.00
```

```
*NODE,NSET=GAPS
180,0.00,0.00,4.5
170,0.00,0.00,9.0
160,0.00,0.00,13.5
****************** Node sets
*NSET,NSET=TOP
1
*NSET,NSET=BOTTOM
19
*NSET,NSET=PRINT
5,10,15,16,17,18,19,TOP
*NSET,NSET=PLOT
5,TOP
**********************************************************************
**              C. ELEMENT DATA
**********************************************************************
****************** Elements for pile
*ELEMENT,TYPE=B33
1,1,2
*ELGEN,ELSET=ABOVE
1,4
*ELEMENT,TYPE=B33
5,5,6
*ELGEN,ELSET=BELOW
5,14
****************** Elements for bottom gap
*ELEMENT,TYPE=GAPCYL,ELSET=GAPS
160,16,160
170,17,170
180,18,180
****************** Element for torsional restraint at bottom
*ELEMENT,TYPE=SPRING1,ELSET=MUDX
419,19
*ELEMENT,TYPE=SPRING1,ELSET=MUDY
519,19
*ELEMENT,TYPE=SPRING1,ELSET=MUDZ
619,19
```

```
****************** Element sets
*ELSET,ELSET=PILE
ABOVE,BELOW
*ELSET,ELSET=PRINT
14,15,16,MUDY,GAPS
*ELSET,ELSET=PLOT1
14,15,16
*ELSET,ELSET=PLOT2
MUDY,160
**********************************************************************
**              D. ELEMENT PROPERTY DATA
**********************************************************************
*BEAM SECTION,MATERIAL=STEEL,SECTION=PIPE,ELSET=ABOVE
1.067,0.06
0.0,1.0,0.0
*BEAM SECTION,MATERIAL=S&W,SECTION=PIPE,ELSET=BELOW
1.067,0.06
0.0,1.0,0.0
*GAP,ELSET=GAPS
0.1649,0.0,0.0,1.0
*SPRING,ELSET=MUDX
4
1.E20
*SPRING,ELSET=MUDY
5
2.E8
*SPRING,ELSET=MUDZ
6
1.E20
**********************************************************************
**              E. MATERIAL DATA
**********************************************************************
*MATERIAL,NAME=STEEL
*DENSITY
7850.0
*ELASTIC,TYPE=ISO
2.1E11,0.3
*MATERIAL,NAME=S&W
*DENSITY
16202.6
```

```
*ELASTIC,TYPE=ISO
2.1E11,0.3
**********************************************************************
**                G. KINEMATIC CONDITIONS
**********************************************************************
*BOUNDARY
BOTTOM,PINNED
GAPS,PINNED
*AQUA
0.0,105.0,9.81,1025.0
0.0,0.0,0.0,0.0
0.0,0.0,0.0,11.9
0.35,0.0,0.0,12.0
0.5,0.0,0.0,33.5
0.5,0.0,0.0,54.0
0.7,0.0,0.0,75.9
1.0,0.0,0.0,105.0
*WAVE,TYPE=AIRY
2.83,234.5,270.0,1.0
**********************************************************************
**--------------HISTORY DATA INPUT-------------------------------------
**********************************************************************
**                A. PROCEDURES
**********************************************************************
*STEP,NLGEOM,CYCLE=15,INC=20
Loading of submerged pile
*STATIC,PTOL=100,MTOL=14500
0.25,1.0
*DLOAD
PILE,GRAV,9.81,0.0,0.0,-1.0
BELOW,PZ,35964.3
BELOW,PD,1.0,2.134,0.53,0.0,1.47
************************** PRINTING
*NODE PRINT,NSET=PRINT,FREQUENCY=100
U
*NODE PRINT,NSET=BOTTOM,FREQUENCY=100
RF
*ELPRINT,ELSET=PRINT,FREQUENCY=100
S,E
*ENDSTEP
```

```
**********************************************************************
**                A. PROCEDURES
**********************************************************************
*STEP,NLGEOM,CYCLE=15,INC=4000
Single Airy wave on submerged pile
*DYNAMIC,PTOL=500,MTOL=70000,HAFTOL=1.E7
0.1,200.0,,0.2
********************** PRINTING
*NODE PRINT,NSET=PRINT,FREQUENCY=0
U
*NODE PRINT,NSET=BOTTOM,FREQUENCY=0
RF
*EL PRINT,ELSET=PRINT,FREQUENCY=0
S
*PRINT,RESIDUAL=NO
********************** POST-PROC.
*NODE FILE,NSET=PLOT
U
*NODE FILE,NSET=BOTTOM
RF
*EL FILE,ELSET=PLOT1
S
*EL FILE,ELSET=PLOT2
S,E
*ENDSTEP
```

APPENDIX B : DERIVATION OF EQUATIONS FOR PFEM

The formulation of the probabilistic finite element method, as discussed below, is documented mainly in ref [18,21,23,26]. In the following, the q-dimensional vector of random parameters, **b**, is given by

$$\mathbf{b} = \begin{bmatrix} C_D \\ C_M \end{bmatrix}$$

where q = 2.

The random process, $\varphi(\mathbf{b})$, which is a function of the random vector, can be expanded in the Taylor series:

$$\varphi(\mathbf{b}) = \varphi(\mu_\mathbf{b}) + \frac{\partial \varphi}{\partial \mathbf{b}}\bigg|_{\mu_\mathbf{b}} (\mathbf{b} - \mu_\mathbf{b}) + \frac{\partial^2 \varphi}{2!\partial \mathbf{b}^2}\bigg|_{\mu_\mathbf{b}} (\mathbf{b} - \mu_\mathbf{b})^2 + \ldots \qquad (\mathcal{B}1)$$

where $\mu_\mathbf{b}$ is the mean value of **b**, also referred to as the first statistical moment of **b**. The expectancy operator, E[ ], is a linear operator and can be applied to both sides of eqn ($\mathcal{B}1$), yielding:

$$E[\varphi(\mathbf{b})] = E[\varphi(\mu_\mathbf{b})] + E\left[\frac{\partial \varphi}{\partial \mathbf{b}}\bigg|_{\mu_\mathbf{b}} (\mathbf{b} - \mu_\mathbf{b})\right] + E\left[\frac{\partial^2 \varphi}{2!\partial \mathbf{b}^2}\bigg|_{\mu_\mathbf{b}} (\mathbf{b} - \mu_\mathbf{b})^2\right] + \ldots \qquad (\mathcal{B}2)$$

The values of $\mu_\mathbf{b}$, $\varphi(\mu_\mathbf{b})$, $\frac{\partial \varphi}{\partial \mathbf{b}}\Big|_{\mu_\mathbf{b}}$, and $\frac{\partial^2 \varphi}{2!\partial \mathbf{b}^2}\Big|_{\mu_\mathbf{b}}$ are deterministic and the expected values of these are therefore the values themselves. Approximating $E[\varphi(\mathbf{b})]$ to the 2nd order term of the Taylor series, eqn ($\mathcal{B}2$) becomes:

$$E[\varphi(\mathbf{b})] \simeq \varphi(\mu_\mathbf{b}) + \frac{\partial \varphi}{\partial \mathbf{b}}\bigg|_{\mu_\mathbf{b}} \left(E[\mathbf{b}] - \mu_\mathbf{b}\right) + \frac{\partial^2 \varphi}{2!\partial \mathbf{b}^2}\bigg|_{\mu_\mathbf{b}} E\left[(\mathbf{b} - \mu_\mathbf{b})^2\right] \qquad (\mathcal{B}3)$$

From the standard texts on probability theory[20,29,30], the expected value of a random function X, the mean function, is defined as:

$$E[X] = \int_{-\infty}^{\infty} x p_X(x)\, dx = \mu_X$$

This value is often also referred to as the ensemble average, the statistical mean, mathematical expectation, or first moment. ($p_X(\alpha)$ is the probability density function of X.) Hence, $E[\mathbf{b}] = \mu_{\mathbf{b}}$, and the second term on the right hand side of eqn ($\mathcal{B}3$) vanishes.

If X_1 and X_2 are two random variables, the covariance of X_1 and X_2 is defined as:

$$E\left[(X_1 - \mu_{X_1})(X_2 - \mu_{X_2})\right] = \kappa_{X_1X_2} \qquad (\mathcal{B}4)$$

If these two random variables are uncorrelated, their covariance is zero, and eqn ($\mathcal{B}4$) can be rewritten as:

$$E\left[(X - \mu_X)^2\right] = \mathrm{Var}(X),$$

which is known as the variance of X. It is now assumed that C_D and C_M are uncorrelated, and the third term on the right hand side of eqn ($\mathcal{B}3$) becomes:

$$\frac{\partial^2 \varphi}{2!\partial \mathbf{b}^2}\bigg|_{\mu_{\mathbf{b}}} \mathrm{Var}(\mathbf{b}).$$

The 2^{nd} order approximation of the expected value of $\varphi(\mathbf{b})$ is then rewritten as:

$$E[\varphi(\mathbf{b})] \simeq \varphi(\mu_{\mathbf{b}}) + \frac{\partial^2 \varphi}{2!\partial \mathbf{b}^2}\bigg|_{\mu_{\mathbf{b}}} \mathrm{Var}(\mathbf{b}) = \varphi(\mu_{\mathbf{b}}) + \frac{1}{2}\sum_{j=1}^{q} \frac{\partial^2 \varphi}{\partial b_j^2}\bigg|_{\mu_{\mathbf{b}}} \mathrm{Var}(b_j) \qquad (\mathcal{B}5)$$

Applying the expectancy operator to eqn (3.2) gives:

$$E[\mathbf{Ma}] + E[\mathbf{Cv}] + E[\mathbf{Kd}] = E[\mathbf{f}].$$

Using the result of eqn ($\mathcal{B}5$), the first term on the left hand side of the above equation reduces to:

$$E[\mathbf{Ma}] = (\mathbf{Ma})\Big|_{\mu_{\mathbf{b}}} + \frac{1}{2}\sum_{j=1}^{q} \frac{\partial^2 (\mathbf{Ma})}{\partial b_j^2}\bigg|_{\mu_{\mathbf{b}}} \mathrm{Var}(b_j).$$

Noting that a bar above an arbitrary function of **b**, say $\phi(\mathbf{b})$, indicates that the function is evaluated at the mean value of the parameter **b** (i.e. $\bar{\phi}(\mathbf{b}) = \phi(\mu_{\mathbf{b}})$),

$$E[\mathbf{Ma}] = \overline{\mathbf{M}}\,\overline{\mathbf{a}} + \frac{1}{2}\sum_{j=1}^{q}\left(\overline{\frac{\partial^2(\mathbf{Ma})}{\partial b_j^2}}\right)\mathrm{Var}(b_j)$$

$$= \overline{\mathbf{M}}\,\overline{\mathbf{a}} + \frac{1}{2}\sum_{j=1}^{q}\left[\frac{\partial}{\partial b_j}\left(\frac{\overline{\partial \mathbf{M}}}{\partial b_j}\,\overline{\mathbf{a}} + \overline{\mathbf{M}}\,\frac{\overline{\partial \mathbf{a}}}{\partial b_j}\right)\right]\mathrm{Var}(b_j)$$

$$= \overline{\mathbf{M}}\,\overline{\mathbf{a}} + \frac{1}{2}\sum_{j=1}^{q}\left[\left(\overline{\frac{\partial^2 \mathbf{M}}{\partial b_j^2}}\right)\overline{\mathbf{a}} + \frac{\overline{\partial \mathbf{M}}}{\partial b_j}\frac{\overline{\partial \mathbf{a}}}{\partial b_j} + \frac{\overline{\partial \mathbf{M}}}{\partial b_j}\frac{\overline{\partial \mathbf{a}}}{\partial b_j} + \overline{\mathbf{M}}\left(\overline{\frac{\partial^2 \mathbf{a}}{\partial b_j^2}}\right)\right]\mathrm{Var}(b_j)$$

Since $\left(\overline{\frac{\partial^2 \mathbf{M}}{\partial \mathbf{b}^2}}\right) = 0$,

$$E[\mathbf{Ma}] = \overline{\mathbf{M}}\,\overline{\mathbf{a}} + \frac{1}{2}\sum_{j=1}^{q}\left[2\,\frac{\overline{\partial \mathbf{M}}}{\partial b_j}\frac{\overline{\partial \mathbf{a}}}{\partial b_j} + \overline{\mathbf{M}}\left(\overline{\frac{\partial^2 \mathbf{a}}{\partial b_j^2}}\right)\right]\mathrm{Var}(b_j) \qquad (\mathcal{B}6)$$

Along similar reasoning,

$$E[\mathbf{Cv}] = \overline{\mathbf{C}}\,\overline{\mathbf{v}} + \frac{1}{2}\sum_{j=1}^{q}\left[\overline{\mathbf{C}}\left(\overline{\frac{\partial^2 \mathbf{v}}{\partial b_j^2}}\right)\right]\mathrm{Var}(b_j) \qquad (\mathcal{B}7)$$

and

$$E[\mathbf{Kd}] = \overline{\mathbf{K}}\,\overline{\mathbf{d}} + \frac{1}{2}\sum_{j=1}^{q}\left[\overline{\mathbf{K}}\left(\overline{\frac{\partial^2 \mathbf{d}}{\partial b_j^2}}\right)\right]\mathrm{Var}(b_j) \qquad (\mathcal{B}8)$$

since both **C** and **K** are independent of **b**.

Using eqn (4.1),

$$E[\mathbf{f}] = \overline{\mathbf{f}} + \frac{1}{2}\sum_{j=1}^{q}\left(\overline{\frac{\partial^2 \mathbf{f}}{\partial b_j^2}}\right)\mathrm{Var}(b_j)$$

$$= \overline{\mathbf{f}} + \frac{1}{2}\sum_{j=1}^{q}\left\{\frac{1}{2}\rho_f D_0 s\left[\frac{\partial}{\partial b_j}\left(\frac{\overline{\partial C_D}}{\partial b_j}\overline{\mathbf{V}}^2 + 2\overline{\mathbf{V}}\,\frac{\overline{\partial \mathbf{V}}}{\partial b_j}\,\overline{C}_D\right)\right] + \rho_f A_0 \dot{u}\mathbf{I}_x\left[\frac{\partial}{\partial b_j}\left(\frac{\overline{\partial C_M}}{\partial b_j}\right)\right]\right\}\mathrm{Var}(b_j)$$

$$= \bar{f} + \frac{1}{2}\sum_{j=1}^{q}\left[\rho_f D_0 s\left(\frac{1}{2}\frac{\overline{\partial^2 C_D}}{\partial b_j^2}\bar{V}^2 + \bar{V}\frac{\overline{\partial V}}{\partial b_j}\frac{\overline{\partial C_D}}{\partial b_j} + \frac{\overline{\partial V}}{\partial b_j}\frac{\overline{\partial V}}{\partial b_j}\bar{C}_D + \bar{V}\frac{\overline{\partial^2 V}}{\partial b_j^2}\bar{C}_D + \bar{V}\frac{\overline{\partial V}}{\partial b_j}\frac{\overline{\partial C_D}}{\partial b_j}\right) + \rho_f A_0 \dot{u} I_x\left(\frac{\overline{\partial^2 C_M}}{\partial b_j^2}\right)\right]\mathrm{Var}(b_j)$$

Since $\dfrac{\overline{\partial^2 C_D}}{\partial b^2} = \dfrac{\overline{\partial^2 C_M}}{\partial b^2} = 0$,

$$E[f] = \bar{f} + \frac{1}{2}\sum_{j=1}^{q}\left\{\rho_f D_0 s\left[2\bar{V}\frac{\overline{\partial V}}{\partial b_j}\frac{\overline{\partial C_D}}{\partial b_j} + \left(\frac{\overline{\partial V}}{\partial b_j}\right)^2\bar{C}_D + \bar{V}\frac{\overline{\partial^2 V}}{\partial b_j^2}\bar{C}_D\right]\right\}\mathrm{Var}(b_j)$$

Now, $V = (u_c + u_w - v_x)$,

$$\therefore \frac{\overline{\partial V}}{\partial b} = -\frac{\overline{\partial v_x}}{\partial b} \text{ and } \frac{\overline{\partial^2 V}}{\partial b^2} = -\frac{\overline{\partial^2 v_x}}{\partial b^2}, \text{ and}$$

$$E[f] = \bar{f} + \frac{1}{2}\sum_{j=1}^{q}\left\{\rho_f D_0 s\left[2\bar{V}\left(-\frac{\overline{\partial v_x}}{\partial b_j}\right)\frac{\overline{\partial C_D}}{\partial b_j} + \left(-\frac{\overline{\partial v_x}}{\partial b_j}\right)^2\bar{C}_D + \bar{V}\left(-\frac{\overline{\partial^2 v_x}}{\partial b_j^2}\right)\bar{C}_D\right]\right\}\mathrm{Var}(b_j) \qquad (\mathcal{B}9)$$

It is again stressed that a term in the above equations that carries a bar refers to that term evaluated at μ_b, the mean value of **b**. Using the equations ($\mathcal{B}6$) to $\mathcal{B}(9)$, the probabilistic response of the structure can be given by:

$$E[d] \simeq \bar{d} + \overline{\Delta d} \qquad (\mathcal{B}10a)$$

$$E[v] \simeq \bar{v} + \overline{\Delta v} \qquad (\mathcal{B}10b)$$

$$E[a] \simeq \bar{a} + \overline{\Delta a} \qquad (\mathcal{B}10c)$$

The zeroth order components of the response are calculated from:

$$\bar{M}\,\bar{a} + \bar{C}\,\bar{v} + \bar{K}\,\bar{d} = \bar{f} \qquad (\mathcal{B}11)$$

while the 2nd order components may be evaluated from:

$$\bar{M}\,\overline{\Delta a} + \bar{C}\,\overline{\Delta v} + \bar{K}\,\overline{\Delta d} = \overline{\Delta f} \qquad (\mathcal{B}12)$$

where $\overline{\Delta f}$ consists of the right hand side of eqn ($\mathcal{B}9$) excepting the $\bar{f}$-term, and the second term on the right hand side of eqn ($\mathcal{B}6$). This latter term remains

in the force vector for elements not submerged and thus not subjected to Morison's forces:

$$\overline{\Delta \mathbf{f}} = \frac{1}{2}\sum_{j=1}^{q}\left\{ \rho_f D_0 s \left[2\overline{\mathbf{V}} \left(-\frac{\overline{\partial \mathbf{v}_x}}{\partial b_j} \right) \frac{\overline{\partial C_D}}{\partial b_j} + \left(-\frac{\overline{\partial \mathbf{v}_x}}{\partial b_j} \right)^2 \overline{C}_D + \overline{\mathbf{V}} \left(-\frac{\overline{\partial^2 \mathbf{v}_x}}{\partial b_j^2} \right) \overline{C}_D \right] - 2\frac{\overline{\partial \mathbf{M}}}{\partial b_j}\frac{\overline{\partial \mathbf{a}}}{\partial b_j} \right\} \mathrm{Var}(b_j) \qquad (\mathcal{B}13)$$

The 2nd order components of the response are given by:

$$\overline{\Delta \mathbf{d}} = \frac{1}{2}\sum_{j=1}^{q}\left(\frac{\overline{\partial^2 \mathbf{d}}}{\partial b_j^2} \right) \mathrm{Var}(b_j) \qquad (\mathcal{B}14a)$$

$$\overline{\Delta \mathbf{v}} = \frac{1}{2}\sum_{j=1}^{q}\left(\frac{\overline{\partial^2 \mathbf{v}}}{\partial b_j^2} \right) \mathrm{Var}(b_j) \qquad (\mathcal{B}14b)$$

$$\overline{\Delta \mathbf{a}} = \frac{1}{2}\sum_{j=1}^{q}\left(\frac{\overline{\partial^2 \mathbf{a}}}{\partial b_j^2} \right) \mathrm{Var}(b_j) \qquad (\mathcal{B}14c)$$

The 1st order approximation of the response variances are given by:

$$\mathrm{Var}(\mathbf{d}) \simeq \sum_{i,j=1}^{q}\left(\frac{\overline{\partial \mathbf{d}}}{\partial b_i} \right)\left(\frac{\overline{\partial \mathbf{d}}}{\partial b_j} \right) \mathrm{Cov}(b_i, b_j)$$

$$\mathrm{Var}(\mathbf{v}) \simeq \sum_{i,j=1}^{q}\left(\frac{\overline{\partial \mathbf{v}}}{\partial b_i} \right)\left(\frac{\overline{\partial \mathbf{v}}}{\partial b_j} \right) \mathrm{Cov}(b_i, b_j)$$

$$\mathrm{Var}(\mathbf{a}) \simeq \sum_{i,j=1}^{q}\left(\frac{\overline{\partial \mathbf{a}}}{\partial b_i} \right)\left(\frac{\overline{\partial \mathbf{a}}}{\partial b_j} \right) \mathrm{Cov}(b_i, b_j)$$

If the components of the random vector are assumed uncorrelated, the above equations reduce to:

$$\mathrm{Var}(\mathbf{d}) \simeq \sum_{j=1}^{q}\left(\frac{\overline{\partial \mathbf{d}}}{\partial b_j} \right)^2 \mathrm{Var}(b_j) \qquad (\mathcal{B}15a)$$

$$\mathrm{Var}(\mathbf{v}) \simeq \sum_{j=1}^{q}\left(\frac{\overline{\partial \mathbf{v}}}{\partial b_j} \right)^2 \mathrm{Var}(b_j) \qquad (\mathcal{B}15b)$$

$$\mathrm{Var}(a) \simeq \sum_{j=1}^{q} \left(\frac{\overline{\partial a}}{\partial b_j} \right)^2 \mathrm{Var}(b_j) \qquad (\mathcal{B}15c)$$

In order to evaluate eqn ($\mathcal{B}$15), the first order sensitivity vectors, $\frac{\overline{\partial d}}{\partial b}$, $\frac{\overline{\partial v}}{\partial b}$ and $\frac{\overline{\partial a}}{\partial b}$, are obtained by differentiating eqn (3.2) with respect to **b**:

$$\left(\frac{\overline{\partial (\mathbf{M}a)}}{\partial b} \right) + \left(\frac{\overline{\partial (\mathbf{C}v)}}{\partial b} \right) + \left(\frac{\overline{\partial (\mathbf{K}d)}}{\partial b} \right) = \left(\frac{\overline{\partial f}}{\partial b} \right)$$

$$\frac{\overline{\partial M}}{\partial b}\,\bar{a} + \bar{M}\frac{\overline{\partial a}}{\partial b} + \frac{\overline{\partial C}}{\partial b}\,\bar{v} + \bar{C}\frac{\overline{\partial v}}{\partial b} + \frac{\overline{\partial K}}{\partial b}\,\bar{d} + \bar{K}\frac{\overline{\partial d}}{\partial b} = \frac{\overline{\partial f}}{\partial b}$$

The stiffness **K** (and therefore the stiffness proportional damping, **C**) is independent of **b**, so:

$$\bar{M}\frac{\overline{\partial a}}{\partial b} + \bar{C}\frac{\overline{\partial v}}{\partial b} + \bar{K}\frac{\overline{\partial d}}{\partial b} = \frac{\overline{\partial f}}{\partial b} - \frac{\overline{\partial M}}{\partial b}\,\bar{a} \text{ , where}$$

$$\frac{\overline{\partial f}}{\partial b} = \frac{\partial}{\partial b}\left(\tfrac{1}{2}\rho_f \bar{C}_D D_0 s \bar{V}^2 + \rho_f \bar{C}_M A_0 \dot{u} I_x \right)$$

$$= \tfrac{1}{2}\rho_f D_0 s \left(\frac{\overline{\partial C}_D}{\partial b}\bar{V}^2 + 2\bar{V}\frac{\overline{\partial V}}{\partial b}\bar{C}_D \right) + \rho_f A_0 \dot{u} I_x \frac{\overline{\partial C}_M}{\partial b}$$

Hence,

$$\bar{M}\frac{\overline{\partial a}}{\partial b} + \bar{C}\frac{\overline{\partial v}}{\partial b} + \bar{K}\frac{\overline{\partial d}}{\partial b} = \tfrac{1}{2}\rho_f D_0 s \left[\frac{\overline{\partial C}_D}{\partial b}\bar{V}^2 + 2\bar{V}\left(-\frac{\overline{\partial v}_x}{\partial b} \right)\bar{C}_D \right] + \rho_f A_0 \dot{u} I_x \frac{\overline{\partial C}_M}{\partial b} - \frac{\overline{\partial M}}{\partial b}\,\bar{a} \qquad (\mathcal{B}16)$$

The last term on the right hand side of eqn ($\mathcal{B}$16) applies to both submerged and exposed elements, whereas the other terms apply only to elements experiencing Morison's forces.

These first order sensitivity vectors are evaluated from eqn ($\mathcal{B}$16) using the same global mass, damping and stiffness matrices formulated for solving eqn (3.2). The current values of $\bar{V}$, $\dot{u}$, and $\bar{a}$ are used to evaluate the forcing vector and an iterative approach is necessary to converge to the required value of $\frac{\overline{\partial v}}{\partial b}$.

To evaluate the 2nd order components of the probabilistic response from eqn ($\mathcal{B}$14), requires a differentiation of eqn ($\mathcal{B}$16) with respect to **b** to find the second order sensitivity vectors:

$$\frac{\overline{\partial M}}{\partial b}\frac{\overline{\partial a}}{\partial b} + \overline{M}\left(\frac{\overline{\partial^2 a}}{\partial b^2}\right) + \frac{\overline{\partial C}}{\partial b}\frac{\overline{\partial v}}{\partial b} + \overline{C}\left(\frac{\overline{\partial^2 v}}{\partial b^2}\right) + \frac{\overline{\partial K}}{\partial b}\frac{\overline{\partial d}}{\partial b} + \overline{K}\left(\frac{\overline{\partial^2 d}}{\partial b^2}\right) =$$

$$\frac{\partial}{\partial b}\left\{\tfrac{1}{2}\rho_f D_0 s\left[\frac{\overline{\partial C}_D}{\partial b}\overline{V}^2 + 2\overline{V}\left(-\frac{\overline{\partial v}_x}{\partial b}\right)\overline{C}_D\right] + \rho_f A_0 \dot{u} I_x \frac{\overline{\partial C}_M}{\partial b} - \frac{\overline{\partial M}}{\partial b}\,\overline{a}\right\}$$

Since $\frac{\overline{\partial C}}{\partial b} = \frac{\overline{\partial K}}{\partial b} = 0$,

$$\overline{M}\left(\frac{\overline{\partial^2 a}}{\partial b^2}\right) + \overline{C}\left(\frac{\overline{\partial^2 v}}{\partial b^2}\right) + \overline{K}\left(\frac{\overline{\partial^2 d}}{\partial b^2}\right) =$$

$$\tfrac{1}{2}\rho_f D_0 s\left[\left(\frac{\overline{\partial^2 C_D}}{\partial b^2}\right)\overline{V}^2 + 2\overline{V}\frac{\overline{\partial V}}{\partial b}\frac{\overline{\partial C}_D}{\partial b} + 2\frac{\overline{\partial V}}{\partial b}\left(-\frac{\overline{\partial v}_x}{\partial b}\right)\overline{C}_D + 2\overline{V}\left(-\frac{\overline{\partial^2 v}_x}{\partial b^2}\right)\overline{C}_D + 2\overline{V}\left(-\frac{\overline{\partial v}_x}{\partial b}\right)\frac{\overline{\partial C}_D}{\partial b}\right] + \rho_f A_0 \dot{u} I_x\left(\frac{\overline{\partial^2 C_M}}{\partial b^2}\right) - \left(\frac{\overline{\partial^2 M}}{\partial b^2}\right)\overline{a} - \frac{\overline{\partial M}}{\partial b}\frac{\overline{\partial a}}{\partial b} - \frac{\overline{\partial M}}{\partial b}\frac{\overline{\partial a}}{\partial b}$$

Now, $\left(\frac{\overline{\partial^2 C_D}}{\partial b^2}\right) = \left(\frac{\overline{\partial^2 C_M}}{\partial b^2}\right) = \left(\frac{\overline{\partial^2 M}}{\partial b^2}\right) = 0$ and $\frac{\overline{\partial V}}{\partial b} = -\frac{\overline{\partial v}_x}{\partial b}$, so finally

$$\overline{M}\left(\frac{\overline{\partial^2 a}}{\partial b^2}\right) + \overline{C}\left(\frac{\overline{\partial^2 v}}{\partial b^2}\right) + \overline{K}\left(\frac{\overline{\partial^2 d}}{\partial b^2}\right) = \tfrac{1}{2}\rho_f D_0 s\left[4\overline{V}\left(-\frac{\overline{\partial v}_x}{\partial b}\right)\frac{\overline{\partial C}_D}{\partial b} + 2\left(-\frac{\overline{\partial v}_x}{\partial b}\right)^2\overline{C}_D + 2\overline{V}\left(-\frac{\overline{\partial^2 v}_x}{\partial b^2}\right)\overline{C}_D\right] - 2\frac{\overline{\partial M}}{\partial b}\frac{\overline{\partial a}}{\partial b} \qquad (\mathcal{B}17)$$

Again $\left(\frac{\overline{\partial^2 v}}{\partial b^2}\right)$ appears on both sides of eqn ($\mathcal{B}17$) and the equation should be solved with an iterative scheme, using the current value of **V**, the original global matrices **M**, **C** and **K**, and the first order sensitivity vectors $\frac{\overline{\partial v}_x}{\partial b}$ and $\frac{\overline{\partial a}}{\partial b}$ found from eqn ($\mathcal{B}16$).

It should be appreciated that by calculating the second order components of the response from eqn ($\mathcal{B}14$) will require q integrations in time of eqn ($\mathcal{B}17$) to find the second order sensitivy vectors needed. Ignoring for the moment the fact that several iterations (and therefore integrations) will be necessary to converge to the solution of all the above-mentioned equations, the minimum number of time integrations necessary to solve eqn ($\mathcal{B}10$) will be 2q+1: 1

integration for the solution of the zeroth order components of the response from eqn (B11), q integrations to solve for the first order sensitivity vectors from eqn (B16), and q integrations more will be required to find the second order sensitivity vectors (from eqn (B17)) needed to calculate the second order component of the response given by eqn (B14). If, on the other hand, eqn (B12) is used to find the second order components of the response, the need to calculate the second order sensitivity vectors is obviated by rewriting eqn (B13):

$$\overline{\Delta f} = \frac{1}{2}\sum_{j=1}^{q}\left\{ \rho_f D_0 s \left[2\overline{V}\left(-\frac{\overline{\partial v}_x}{\partial b_j}\right)\frac{\overline{\partial C}_D}{\partial b_j} + \left(-\frac{\overline{\partial v}_x}{\partial b_j}\right)^2 \overline{C}_D \right] \right\} \mathrm{Var}(b_j) -$$

$$\frac{1}{2}\sum_{j=1}^{q}\left[2\,\frac{\overline{\partial M}\,\overline{\partial a}}{\partial b_j \partial b_j}\right] \mathrm{Var}(b_j) + \frac{1}{2}\sum_{j=1}^{q}\left\{ \rho_f D_0 s \left[\overline{V}\left(-\frac{\overline{\partial^2 v}_x}{\partial b_j^2}\right)\overline{C}_D \right] \right\} \mathrm{Var}(b_j)$$

Using the relation in eqn (B14&), the last term in the above equation can be rewritten as $\rho_f D_0 s \overline{V}\ \overline{C}_D(-\overline{\Delta v}_x)$.

Consider next the term:

$$\frac{1}{2}\sum_{j=1}^{q}\left[2\,\frac{\overline{\partial M}}{\partial b_j}\frac{\overline{\partial a}}{\partial b_j}\right] \mathrm{Var}(b_j), \text{ which can be expanded as:}$$

$$\frac{1}{2}\left[\left(2\,\frac{\overline{\partial M}}{\partial C_D}\frac{\overline{\partial a}}{\partial C_D}\right) \mathrm{Var}(C_D) + \left(2\,\frac{\overline{\partial M}}{\partial C_M}\frac{\overline{\partial a}}{\partial C_M}\right) \mathrm{Var}(C_M) \right]$$

Since $\frac{\overline{\partial M}}{\partial C_D} = 0$, the above reduces to $\frac{\overline{\partial M}}{\partial C_M}\frac{\overline{\partial a}}{\partial C_M}\ \mathrm{Var}(C_M)$.

So, the forcing function, $\overline{\Delta f}$, is now given by:

$$\overline{\Delta f} = \frac{1}{2}\sum_{j=1}^{q}\left\{ \rho_f D_0 s \left[2\overline{V}\left(-\frac{\overline{\partial v}_x}{\partial b_j}\right)\frac{\overline{\partial C}_D}{\partial b_j} + \left(-\frac{\overline{\partial v}_x}{\partial b_j}\right)^2 \overline{C}_D \right] \right\} \mathrm{Var}(b_j) +$$

$$\rho_f D_0 s \overline{V}\ \overline{C}_D(-\overline{\Delta v}_x) - \frac{\overline{\partial M}}{\partial b_2}\frac{\overline{\partial a}}{\partial b_2}\ \mathrm{Var}(b_2) \qquad (B18)$$

The minimum number of time integrations is now q+2: 1 integration for the solution of the zeroth order component of the response (which is the same as the deterministic solution), q integrations to solve the first order sensitivity vectors, and one more to solve eqn (B12) using the forcing vector $\overline{\Delta f}$, as shown in eqn (B18) above. The reduction in computational effort is obvious when q is large.

Symbols and their corresponding variable names in the computer program PILE.

A_0	AREAO
$\mathbf{a}$	DYNACC
b_j	for j=1: DRAGCO; for j=2: AMASCO
$\mathbf{C}$	ADAMP
C_D	DRAGCO
C_M	AMASCO
D_0	DIAMO
$\mathbf{d}$	DYNDISP
$\frac{\partial \mathbf{a}}{\partial \mathbf{b}}$	DADB
$\Delta\mathbf{a}$	DA
$\frac{\partial \mathbf{d}}{\partial \mathbf{b}}$	DDDB
$\Delta\mathbf{d}$	DD
$\frac{\partial \mathbf{M}}{\partial b_2}$	DMDB2
$\frac{\partial \mathbf{v}}{\partial \mathbf{b}}$	DVDB
$\frac{\partial v_x}{\partial \mathbf{b}}$	DVxDB
Δv_x	DVx
$\Delta\mathbf{v}$	DV
E[a]	PRBACC
E[d]	PRBDISP
E[v]	PRBVEL
$\mathbf{K}$	ASTIF
$\mathbf{M}$	AMASS
q	NSVAL
ρ_f	ROSEA
s	SIGN
u_c	VELC
u_w	WVEVEL

$\dot{u}$	ACCI
$\overline{v}$	SPEED
$Var(b_j)$	for j=1: VARCD; for j=2: VARCM
Var(**a**)	VARA
Var(**d**)	VARD
Var(**v**)	VARV
v	DYNVEL
$\mathbf{v}_x$	STRVEL

Subscripts:

j	jsval

APPENIDIX C : ALGORITHM FOR THE COMPUTER PROGRAM PILE

Apart from the usual notation used in this work, the following nomenclature applies (in addition) to this section:

d	general displacement vector.
v	general velocity vector.
a	general acceleration vector.
m	slope of the Secant line in the iterative procedure shown in Figure 3.2.1.
k	intercept of the Secant line in the iterative procedure shown in Figure 3.2.1.
flag	condition of iteration: flag = 1 indicates more iterations should be performed; flag = 0 indicates a converged solution.
toler	prescribed tolerance for the iteration loop.

Pre-superscripts: (e.g. ${}^{e}x$)

e	of the degrees of freedom at the midpoint of an element.
n	of the degrees of freedom of each node.
1	of the first node of an element, e .
2	of the second node of an element, e .

Post-superscripts: (e.g. x^{f})

f	final, converged value.
p	predicted value according to the Secant iterative scheme.
c	corrected value.
(i)	pertaining to the previous iteration.
(i+1)	pertaining to the current iteration.

Post-subscripts: (e.g. $x_{(t)}$)

(t)	pertaining to the previous time increment.
(t+Δt)	pertaining to the current time increment.
x	of the degree of freedom in the direction parallel to that of the free stream velocity, u.

At the end of this appendix is a list of symbols used here and their corresponding variable names in the computer program.

The solution procedure for the deterministic dynamic response (or the zero order probabilistic mean response), that for the first order sensitivity vectors , and the second order component of the mean response are very similar. In what follows, the following italic keys in a step indicate that the action pertains only to the solution of that part of the response:

DD: deterministic dynamic response;
SV: solution of the first order sensitivity vectors;
ΔR: solution of the second order component of the mean response.

Where no italic keys appear, it means that the step applies to all three of the above solutions.

1. Initialise: ${}^{n}\mathbf{d}^{f}_{(t=0)}$, ${}^{n}\mathbf{v}^{f}_{(t=0)}$, and ${}^{n}\mathbf{a}^{f}_{(t=0)}$

$${}^{n}\left(\frac{\partial \mathbf{d}}{\partial b_j}\right)^{f}_{(t=0)}, {}^{n}\left(\frac{\partial \mathbf{v}}{\partial b_j}\right)^{f}_{(t=0)}, \text{ and } {}^{n}\left(\frac{\partial \mathbf{a}}{\partial b_j}\right)^{f}_{(t=0)}$$

$${}^{n}(\Delta\mathbf{d})^{f}_{(t=0)}, {}^{n}(\Delta\mathbf{v})^{f}_{(t=0)}, \text{ and } {}^{n}(\Delta\mathbf{a})^{f}_{(t=0)}$$

2. Increment in time: t=t+Δt; i=0; flag=1

3. *SV:* Initialise: ${}^{n}\mathrm{Var}(\mathbf{d})$, ${}^{n}\mathrm{Var}(\mathbf{v})$, and ${}^{n}\mathrm{Var}(\mathbf{a})$

4. *SV:* for j = 1,2

5. For next iteration: i=i+1 if flag=1

6. *DD:*
$${}^{n}d^{p(i)}_{(t+\Delta t)} = {}^{n}\mathbf{d}^{f(i)}_{(t)}$$
$${}^{n}v^{p(i)}_{(t+\Delta t)} = {}^{n}\mathbf{v}^{f(i)}_{(t)}$$
$${}^{n}a^{p(i)}_{(t+\Delta t)} = {}^{n}\mathbf{a}^{f(i)}_{(t)}$$

SV: Same as for *DD*, but replace **d**, **v**, and **a** on the right hand side of the equal sign with $\left(\frac{\partial \mathbf{d}}{\partial b_j}\right)$, $\left(\frac{\partial \mathbf{v}}{\partial b_j}\right)$, and $\left(\frac{\partial \mathbf{a}}{\partial b_j}\right)$ respectively.

ΔR: Same as for *DD*, but replace **d**, **v**, and **a** on the right hand side of the equal sign with **Δd**, **Δv**, and **Δa** respectively.

7. For i=1:

$$ {}^{e}v^{p(i+1)}_{x(t+\Delta t)} = \frac{1}{2}\left({}^{1}v^{p(i)}_{x(t+\Delta t)} + {}^{2}v^{p(i)}_{x(t+\Delta t)} \right) $$

$$ {}^{e}v^{p(i)}_{x(t+\Delta t)} = {}^{e}v^{p(i+1)}_{x(t+\Delta t)} $$

8. For i=2:

$$ {}^{e}v^{p(i+1)}_{x(t+\Delta t)} = \text{factor} \times {}^{e}v^{c(i)}_{x(t+\Delta t)} $$

9. For i>2:

$$ m = \frac{\left({}^{e}v^{c(i)}_{x(t+\Delta t)} - {}^{e}v^{c(i+1)}_{x(t+\Delta t)} \right)}{\left({}^{e}v^{p(i)}_{x(t+\Delta t)} - {}^{e}v^{p(i+1)}_{x(t+\Delta t)} \right)} $$

$$ k = {}^{e}v^{c(i)}_{x(t+\Delta t)} - m \times {}^{e}v^{p(i)}_{x(t+\Delta t)} $$

$$ {}^{e}v^{p(i)}_{x(t+\Delta t)} = {}^{e}v^{p(i+1)}_{x(t+\Delta t)} $$

$$ {}^{e}v^{c(i)}_{x(t+\Delta t)} = {}^{e}v^{c(i+1)}_{x(t+\Delta t)} $$

$$ {}^{e}v^{p(i+1)}_{x(t+\Delta t)} = k \;/\; (1.0 - m) $$

10. *DD:* calculate element drag forces using ${}^{e}v^{p(i+1)}_{x(t+\Delta t)}$

SV: calculate element 'load' vectors according to the first 3 terms of the load vector of eqn (ℬ16).

ΔR: calculate element 'load' vectors according to the first 3 terms of eqn (ℬ18).

11. *DD:* add inertia forces due to fluid acceleration.

12. Assemble new global load vector.

13. *SV:* adjust global load vector by subtracting the last term of the load vetor of eqn (ℬ16) from it.

ΔR: adjust global load vector by subtracting the last term of eqn (ℬ18) from it.

14. Solve for ${}^{n}d^{c(i+1)}_{(t+\Delta t)}$, ${}^{n}v^{c(i+1)}_{(t+\Delta t)}$, and ${}^{n}a^{c(i+1)}_{(t+\Delta t)}$ using the implicit Newmark integration scheme.

15. For i=1:

$$ {}^{e}v^{c(i)}_{x(t+\Delta t)} = \frac{1}{2}\left({}^{1}v^{c(i+1)}_{x(t+\Delta t)} + {}^{2}v^{c(i+1)}_{x(t+\Delta t)} \right) $$

16. For i>1:

a. $${}^{e}v^{c(i+1)}_{x(t+\Delta t)} = \frac{1}{2}\left({}^{1}v^{c(i+1)}_{x(t+\Delta t)} + {}^{2}v^{c(i+1)}_{x(t+\Delta t)} \right)$$

b. Convergence check:

$$\text{If } \frac{\left({}^{e}v^{c(i+1)}_{x(t+\Delta t)} - {}^{e}v^{p(i+1)}_{x(t+\Delta t)} \right)}{{}^{e}v^{p(i+1)}_{x(t+\Delta t)}} < \text{toler, flag=0}$$

17. If flag=0, proceed to step 18.
If flag=1, repeat from step 5.

18. Assign final values of this increment to be used as start-up values for the next increment:

DD:
$${}^{n}\mathbf{d}^{f(i)}_{(t+\Delta t)} = {}^{n}d^{c(i+1)}_{(t+\Delta t)}$$
$${}^{n}\mathbf{v}^{f(i)}_{(t+\Delta t)} = {}^{n}v^{c(i+1)}_{(t+\Delta t)}$$
$${}^{n}\mathbf{a}^{f(i)}_{(t+\Delta t)} = {}^{n}a^{c(i+1)}_{(t+\Delta t)}$$

SV: Same as for *DD* above, but replace **d**, **v**, and **a** on the left hand side of the equal sign with $\left(\frac{\partial \mathbf{d}}{\partial b_j}\right)$, $\left(\frac{\partial \mathbf{v}}{\partial b_j}\right)$, and $\left(\frac{\partial \mathbf{a}}{\partial b_j}\right)$ respectively.

ΔR: Same as for *DD* above, but replace **d**, **v**, and **a** on the left hand side of the equal sign with **Δd**, **Δv**, and **Δa** respectively.

19. *SV:* accumulate variances:

$${}^{n}\text{Var}(\mathbf{d}) = {}^{n}\text{Var}(\mathbf{d}) + \left[{}^{n}\left(\frac{\partial \mathbf{d}}{\partial b_j} \right)^{f(i)}_{(t+\Delta t)} \right]^2 \text{Var}(b_j)$$

$${}^{n}\text{Var}(\mathbf{v}) = {}^{n}\text{Var}(\mathbf{v}) + \left[{}^{n}\left(\frac{\partial \mathbf{v}}{\partial b_j} \right)^{f(i)}_{(t+\Delta t)} \right]^2 \text{Var}(b_j)$$

$${}^{n}\text{Var}(\mathbf{a}) = {}^{n}\text{Var}(\mathbf{a}) + \left[{}^{n}\left(\frac{\partial \mathbf{a}}{\partial b_j} \right)^{f(i)}_{(t+\Delta t)} \right]^2 \text{Var}(b_j)$$

20. *SV:* Repeat for next j from step 4.

21. $${}^{n}E[\mathbf{d}]^{f(i)}_{(t+\Delta t)} = {}^{n}\mathbf{d}^{f(i)}_{(t+\Delta t)} + {}^{n}(\Delta \mathbf{d})^{f(i)}_{(t+\Delta t)}$$

$${}^{n}E[\mathbf{v}]^{f(i)}_{(t+\Delta t)} = {}^{n}\mathbf{v}^{f(i)}_{(t+\Delta t)} + {}^{n}(\Delta \mathbf{v})^{f(i)}_{(t+\Delta t)}$$

$${}^{n}E[\mathbf{a}]^{f(i)}_{(t+\Delta t)} = {}^{n}\mathbf{a}^{f(i)}_{(t+\Delta t)} + {}^{n}(\Delta \mathbf{a})^{f(i)}_{(t+\Delta t)}$$

Symbols and their corresponding variable names in the computer program PILE.

d	XDISP
v	TVELO
a	TACCE
d	DYNDISP
v	DYNVEL
a	DYNACC
factor	VITFAC
m	SLOPE
k	CONST
flag	IFLAG
toler	TOLER
$e_{v_{x(t+\Delta t)}}^{p(i+1)}$	*DD:* STRVEL(ielem); *SV:* DVxDB(ielem); *ΔR:* Vx(ielem)
$e_{v_{x(t+\Delta t)}}^{p(i)}$	OLDVEL(ielem)
$e_{v_{x(t+\Delta t)}}^{c(i)}$	GSVEL1(ielem)
$e_{v_{x(t+\Delta t)}}^{c(i+1)}$	GSVEL2(ielem)
$^{n}\left(\frac{\partial d}{\partial b_j} \right)$	DDDB(isvab,jsval)
$^{n}\left(\frac{\partial v}{\partial b_j} \right)$	DVDB(isvab,jsval)
$^{n}\left(\frac{\partial a}{\partial b_j} \right)$	DADB(isvab,jsval)
Δd	DD
Δv	DV
Δa	DA
E[d]	PRBDISP
E[v]	PRBVEL
E[a]	PRBACC
Var(d)	VARD
Var(v)	VARV
Var(a)	VARA
Var(b_j)	for j=1: VARCD; for j=2: VARCM

Pre-superscripts:

^{e}	ielem
^{n}	isvab

Post-superscripts:

^{l}	icount

Post-subscripts:

$_{t}$	TOTLT
$_{\Delta t}$	DELTI
$_{j}$	jsval

APPENDIX D : VARIABLE NAMES USED IN PROGRAM PILE

(The variable names that do not appear in the lists given at the end of Appendices B and C are given here.)

AREAI	inner area of a section
ASLOD	global load vector (**f** - p 25)
BEETA	β - p 29
CFDAMP	χ - p 26
CNEWM#	see ref.[38], eqn 11.8.7, p 322
CONLOAD	concentrated applied load
COORD	cartesian coordinates of a node
DIAMI	inner diameter of a section
DMASS	element mass matrix (**m** - p 26)
DUMSTIF	original version of ASTIF
ELENG	e - p 25
ELOAD	element load vector ($\mathbf{f}_e$ - p 29)
ESTIF	element stiffness matrix (**k** - p 27)
FIXED	see VALUE
GAAMA	γ - p 29
ICODE	prescribed degree of freedom
IELOD	the number of the first submerged element
IFLGDY	flag for static/dynamic analysis
IFPRE	see ICODE
LNODS	nodes of an element
MATNO	material number
NBOUN	number of prescribed boundary conditions
NDIME	number of dimensions (2D or 3D)
NDOFN	number of degrees of freedom of node
NDYNA	flag for deterministic/probabilistic analysis
NELEM	number of elements in model
NELOD	the number of the last submerged element
NEVAB	number of degrees of freedom of element
NINCS	maximum number of time increments
NITER	maximum number of iterations
NMATS	number of different materials
NNODE	number of nodes per element

NODFX	the number of a node with prescribed boundary conditions
NPLOT	frequency to write data for plotting
NPOIN	number of nodes in model
NPRINT	frequency to print results
NPROP	number of material properties
NSIM	N - p 45,46
NSVAB	number of degrees of freedom of model
PERIOD	T - p 9,11,23
PMASS	element equivalent of DMDB2
PRBLT	starting time of probabilistic analysis
PROPS	material properties of element
RAMP	parameter to prescribe initial velocity of structure
RLOAD	element load vector due to drag and concentrated loads
ROPIPE	density of material of element
SEADPTH	ℓ - p 5,9
VALUE	magnitude of prescribed degree of freedom
WVEAMP	eqn 2.4, p 5
WVEFRQ	eqn 2.4, p 5; p 23; eqn 3.6, p 26
WVELEN	eqn 2.2, p 4; p 9
WVENUM	k - eqn 2.4, p 5
YHALF	y - eqn 2.4, p 5

REFERENCES

1. NEWLAND, D.E. *An Introduction to Random Vibrations and Spectral Analysis* 2nd ed., Longman,' 1984, Essex.
2. BATHE, K. *Finite Element Procedures in Engineering Analysis* Prentice-Hall, 1982, New Jersey.
3. WILSON, J.F. *Dynamics of Offshore Structures* John Wiley & Sons, 1984, New York.
4. LIVESLEY, R.K. *Finite Elements: An Introduction for Engineers* Cambridge University Press, 1983, Cambridge.
5. DU PREEZ, R.J. *Fundamentals of Dynamic Analysis* FEMSA Post-symposium seminar, 13.1.1983.
6. DHATT, G. & TOUZOT, G. *The Finite Element Method Displayed* John Wiley & Sons, 1984, New York.
7. BREBBIA, C.A. & WALKER, S. *Dynamic Analysis of Offshore Structures* Newnes-Butterworths, London.
8. HIBBITT, KARLSSON & SORENSEN *ABAQUS Example Problems Manual* version 4-8, 1989
9. HIBBITT, KARLSSON & SORENSEN *ABAQUS Theory Manual* version 4-8, 1989
10. HIBBITT, KARLSSON & SORENSEN *ABAQUS Users' Manual* version 4-8, 1989
11. YOUNG, R.D., FOWLER, J.R., FISHER, E.A. & LUKE, R.R. *Dynamic Analysis as an Aid to the Design of Marine Risers* Transactions, ASME, Vol.100, pp 200-205, May 1978.
12. MORRISON, D.G. *Simple Models to Evaluate Dynamic Guyed Tower Response* Journal of Energy Resources Technology, ASME, Vol.105, Sept. 1983
13. YOUNG, B.C. *Offshore Pile Installation* UCT final year thesis, 1988, Cape Town.
14. SNYMAN, M.F., MERCER, C.D. & PEARCE, H.T. *Numerical Modelling of an Offshore Pipeline* Applied Mechanics Research Unit, No. 124, Nov.1988, University of Cape Town.
15. CHAKRABARTI, S.K. & FRAMPTON, R.E. *Review of Riser Analysis Techniques* Applied Ocean Research, Vol.4, No.2, pp 73-90.
16. KIRK, C.L. *Dynamic Response of Marine Risers by Single Wave and Spectral Analysis Methods* Applied Ocean Research, Vol.7, No.1, 1985.
17. AHMAD, S. & DATTA, T.K. *Dynamic Response of Marine Risers* Engineering Structures, Vol.11, July 1989.
18. LIU, W.K., BELYTSCHKO, T. & MANI, A. *Probabilistic Finite Elements for Non-linear Structural Dynamics* Computer Methods in Applied Mechanics and Engineering, Vol.56, pp 61-81, 1986.

19. PHAAL, R. *Computational and Modelling Aspects of Marine Riser Analysis* UCT MSc Thesis, 1987, Cape Town.

20. LIN, Y.K. *Probability Theory of Structural Dynamics* McGraw-Hill, 1967, New York.

21. LIU, W.K., BELYTSCHKO, T. & MANI, A. *Random Field Finite Elements* International Journal for Numerical Methods in Engineering, Vol.23, pp 1831-1845, 1986.

22. THOMSON, W.T. *Theory of Vibration with Applications* 2nd ed., Prentice-Hall, 1981, London.

23. LIU, W.K. & BELYTSCHKO, T. *Computational Mechanics of Probabilistic and Reliability Analysis* Elmepress International, 1989, Lausanne.

24. HINTON, E. & OWEN, D.R.J. *An Introduction to Finite Element Computations* Pineridge Press Ltd, 1979, Swansea.

25. BENAROYA, H. & REHAK, M. *Finite Element Methods in Probabilistic Structural Analysis: a Selective Review* Applied Mechanics Review, ASME, Vol.41, No.5, May 1988.

26. LIU, W.K., BESTERFIELD, G. & BELYTSCHKO, T. *Transient Probabilistic Systems* Computer Methods in Applied Mechanics and Engineering, Vol.67, pp 27-54, 1988, North-Holland.

27. HOGBEN, N.,MILLER, B.L., SEARLE, J.N. & WARD, G. *Estimation of Fluid Loading on Offshore Structures* Proceedings of the Institution of Civil Engineers, Vol.63, No.2, pp 517-561, 1977.

28. DITLEVSEN, O. *Uncertainty Modeling* McGraw-Hill, 1981, New York.

29. AUGUSTI, G.,BARATTA, A. & CASCIATI, F. *Probabilistic Methods in Structural Engineering* Chapman and Hall, 1984, London.

30. ANG, A.H-S. & TANG, W.H. *Probabiltic Concepts in Engineering Planning and Design - Volume 1* John Wiley & Sons, 1975, New York.

31. THE NUMERICAL ALGORITHMS GROUP LIMITED *The NAG Fortran Library Manual - Mark 14*, 1st edition, April 1990, Oxford.

32. KNUTH, D.E. *The Art of Computer Programming* 2nd ed., Addison-Wesley, 1989.

33. SARPKAYA, T. & ISAACSON, M. *Mechanics of Wave Forces on Offshore Structures* Van Nostrand Rheinhold, 1981, New York.

34. ZIENKIEWICZ, O.C. *Numerical Methods in Offshore Engineering* John Wiley & Sons, 1978, New York — Chapter 8: *Dynamic Response of Framed and Gravity Stuctures to Waves* by SIGBJÖRNSSON, R., BELL, K. & HOLAND, I., pp 245-279

35. EVERY, M.J., KING, R. & GRIFFIN, O.M. *Hydro-dynamic Loads on Flexible Marine Structures Due to Vortex Shedding* Journal of Energy Resources Technology, ASME, Vol.104, pp 330-336, Dec.1982.

36. SARPKAYA, T. *Vortex-Induced Oscillations* Journal of Applied Mechanics, ASME, Vol.46, No.2, pp 241-258, June 1979.

37. O'BRIEN, P.J. & McNAMARA, J.F. *Benchmark Solutions for Nonlinear Two and Three Dimensional Rigid and Flexible Marine Riser Problems* Proceedings of the ABAQUS Users' Conference, pp 317-332, June 1988, New Port.

38. COOK, R.D. *Concepts and Applications of Finite Element Analysis* 2nd ed., John Wiley & Sons, 1981, New York.

39. OWEN, D.R.J. & HINTON, E. *Finite Elements in Plasticity: Theory and Practice* Pineridge Press Ltd, Swansea, 1980

40. WILSON, C. *Applied Statistics for Engineers* Applied Science Publishers, 1972, London.

41. FREEDMAN, D., PISANI, R. & PURVES, R. *Statistics* 1st ed., WWNorton & Company, 1988, New York.

42. GUTTMAN, I., WILKS, S.S. & HUNTER, J.S. *Introductory Engineering Statistics* 3rd ed., John Wiley & Sons, 1982, New York.

43. HAGGENMACHER, G.W. & LAHEY, R.S. *Practical Aspects of the Finite Element Method* Finite Elements in the Commercial Environment, Vol.1, 1978, Dorset

44. VUGTS, J.H. & HAYES, D.J. *Dynamic Analysis of Fixed Offshore Structures* Engineering Structures, Vol.1, pp 114-120, April 1979

45. McNAMARA, J.F. & HIBBITT, H.D. *Numerical Analysis of Flexible Pipes and Risers in Offshore Applications* Paper presented at the OMAE Specialty Symposium on 'Offshore and Arctic Frontiers', Feb. 1986, New Orleans

46. LEONARD, J.W., GARRISON, C.J. & HUDSPETH, R.T. *Deterministic Fluid Forces on Structures: A Review* Journal of the Structural Division, Proceedings of the ASCE, Vol.107, No.ST6, pp 1041-1057, June 1981

47. IBRAHIM, R.A. *Structural Dynamics with Parameter Uncertainties* Applied Mechanics Review, ASME, Vol.40, No.3, pp 309-328, March 1987